Draft version 1.0.2

ATLAS NOTE

September 9, 2015

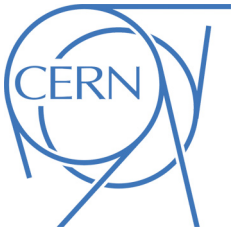

Search for strongly produced superpartners in final states with same-sign leptons or three leptons and jets: preparing for 2015 analyses

B. Abbott[10], J.-F. Arguin[1], S. Berlendis[2], F. Cardillo[3], A. Di Simone[3], O. Ducu[4,5], D. Gerbaudo[6], G. Herten[3], F. Hubaut[5], S. Kahn[5], A. Lleres[2], J. Maurer[4], T. Nguyen[1], A. Olariu[4], M. Pagacova[3], A. Paramonov[7], J. Poveda[8], P. Pralavorio[5], H. Ren[9,5], O. Rifki[10], Y.-T. Shen[10], P. Skubic[10], A. Taffard[6], H. Trepanier[1], S. Upadhyay[6], X. Zhuang[9]

[1]*Université de Montréal*
[2]*Laboratoire de Physique Subatomique et de Cosmologie de Grenoble (LPSC)*
[3]*Albert-Ludwigs-Universität Freiburg*
[4]*Horia Hulubei National Institute for R&D in Physics and Nuclear Engineering (IFIN-HH) Bucharest*
[5]*Centre de Physique des Particules de Marseille (CPPM)*
[6]*University of California, Irvine*
[7]*Argonne National Laboratory*
[8]*European Laboratory for Particle Physics, CERN*
[9]*Institute of High Energy Physics, Chinese Academy of Sciences, Beijing*
[10]*University of Oklahoma*

Abstract

This note contains the documentation of the studies performed with DC14 Monte Carlo samples in preparation for Run-2 for the search for strongly produced supersymmetric particles using signatures involving multiple energetic jets and either two isolated leptons (e or μ) with the same electric charge, or at least three isolated leptons. The analysis also utilises jets originating from b-quarks, missing transverse momentum and other observables to extend its sensitivity.

Contents

1 Introduction **3**

2 Signal models **3**
2.1 Models already considered in Run-1 . . . 3
2.2 New models . . . 6
2.2.1 RPV inspired . . . 6

3 MC samples **8**
3.1 Derivation versions and analysis model . . . 8
3.2 Signal Samples . . . 8
3.3 Background Samples . . . 8
3.4 Detector simulation . . . 9

4 Object definition **14**
4.1 Jets . . . 14
4.1.1 Jet Vertex Fraction . . . 14
4.1.2 *b*-tagging . . . 14
4.2 Leptons . . . 15
4.2.1 Electrons . . . 15
4.2.2 Muons . . . 15
4.2.3 Lepton isolation . . . 16
4.2.4 Electron acceptance . . . 22
4.3 Overlap removal . . . 22
4.4 Missing transverse energy . . . 23

5 Event selection **23**
5.1 Trigger studies . . . 23
5.1.1 Monte Carlo samples and software framework . . . 23
5.1.2 Total event yields . . . 24
5.1.3 Efficiencies . . . 24
5.2 Event pre-selection . . . 24

6 Signal region definition **27**
6.1 Models already considered in Run-1 . . . 27
6.2 Softer selection with 3*b*-jets . . . 28
6.3 3L3b . . . 30
6.4 RPV models . . . 34

7 Background estimation **35**
7.1 Backgrounds with prompt SS dilepton or three leptons . . . 35
7.2 Charge flip leptons . . . 35
7.3 Backgrounds with fake leptons . . . 37
7.3.1 The matrix method . . . 37
7.3.2 The Monte-Carlo template method . . . 38
7.3.3 Statistical tools improving robustness in low statistics regime . . . 39
7.4 Backgrounds with fake *b*-jets . . . 39
7.5 Neglected backgrounds . . . 39
7.6 Validation regions . . . 39

8 Systematic Uncertainties **42**
8.1 Experimental systematics 42
8.2 Theoretical systematics 43

9 Simultaneous fit method and results **44**

10 Conclusion **46**

A Details on the isolation optimization **53**

B Trigger efficiencies **55**

C Generated Samples for the Above the Diagonal Study **57**

1 Introduction

Supersymmetry (SUSY) [1, 2, 3, 4, 5, 6, 7, 8, 9] is a theoretically favoured extension of the Standard Model (SM), which for each degree of freedom of the SM predicts another degree of freedom with a different spin. These degrees of freedom combine into physical superpartners of the SM particles: scalar partners of quarks and leptons (squarks ($\tilde{q}$) and sleptons), fermionic partners of gauge and Higgs bosons (gluinos ($\tilde{g}$), charginos ($\tilde{\chi}_i^{\pm}$, with i = 1,2) and neutralinos ($\tilde{\chi}_i^0$ with i = 1,2,3,4)), all with identical quantum numbers to their SM partners, except spin. Since no superpartner of any of the SM particles has been observed, SUSY must be a broken symmetry at some higher energy scale.

The discovery (or exclusion) of weak-scale SUSY is one of the highest physics priorities for the LHC. The primary target for early supersymmetry searches in proton-proton (pp) collisions at a centre-of-mass energy of 13 TeV at the LHC, given their large expected cross-section, is the strong production of gluinos and squarks. In order for supersymmetry to provide a solution to the hierarchy problem of the SM, the supersymmetric partners of the top and bottom quarks are expected to be light and within reach of the LHC.

Under the hypothesis of R-parity conservation [10, 11, 12, 13], SUSY partners are produced in pairs and decay to the Lightest Supersymmetric Particle (LSP) which is stable and, in large variety of models, is assumed to be the lightest neutralino ($\tilde{\chi}_1^0$) which escapes detection. The undetected $\tilde{\chi}_1^0$ would result in substantial missing transverse momentum ($E_{\mathrm{T}}^{\mathrm{miss}}$), while the rest of the cascade, originating from the decays of squarks and gluinos, would yield final states with multiple jets and possibly leptons.

In this analysis, events containing multiple jets and either two leptons (electrons or muons) of the same electric charge (same-sign leptons, SS) or at least three leptons (3L) are used to search for strongly produced supersymmetric particles. Signatures with SS or 3L are predicted in many SUSY scenarios. Gluinos produced in pairs or in association with a squark can lead to SS signatures when decaying to any final state that includes leptons because gluinos are Majorana fermions. Squark production, directly in pairs or through $\tilde{g}\tilde{g}$ or $\tilde{g}\tilde{q}$ production with subsequent $\tilde{g} \to q\tilde{q}$ decay, can also lead to SS or 3L signatures when the squarks decay in cascades involving top quarks (t), charginos, neutralinos or sleptons, which subsequently decay as $t \to bW$, $\tilde{\chi}_i^{\pm} \to W^{\pm(*)}\tilde{\chi}_j^0$, $\tilde{\chi}_i^0 \to h/Z^{(*)}\tilde{\chi}_j^0$, or $\tilde{\ell} \to \ell\tilde{\chi}_1^0$, respectively. Since this search benefits from low SM backgrounds, it allows the use of relatively loose kinematic requirements on $E_{\mathrm{T}}^{\mathrm{miss}}$, increasing the sensitivity to scenarios with small mass differences between SUSY particles (compressed scenarios) or where R-parity is violated. This search is thus sensitive to a wide variety of models based on very different assumptions.

This note summarizes the studies performed by the analysis team with DC14 Monte Carlo samples in preparation for Run-2. The Run-1 search for strongly produced SUSY particles with SS/3L was conducted using data from the full 2012 data-taking period (20.3 fb^{-1} at $\sqrt{s}$=8 TeV) [14, 15]. In that result, exclusion limits were placed on 15 different models. Gluino-mediated top squark scenarios, favoured by naturalness arguments, were excluded for $m_{\tilde{g}}$ < [600–1000] GeV, largely independently of the top squark mass and decay mode. Similar limits were placed on gluino-mediated production of first- and second-generation quarks for $m_{\tilde{\chi}_1^0}$ < [300–600] GeV. Limits were also placed on pair-production of bottom squarks and squarks of the first and second generations decaying in long cascades.

2 Signal models

2.1 Models already considered in Run-1

Final states with two same-sign leptons and multiple jets are sensitive to a variety of new physics scenarios. In supersymmetric models in particular, such final states can be produced in the decays of heavy superpartners involving massive gauge bosons, sleptons or top quarks. We list in this section the different

simplified models which we use as benchmarks for the choice of signal regions.

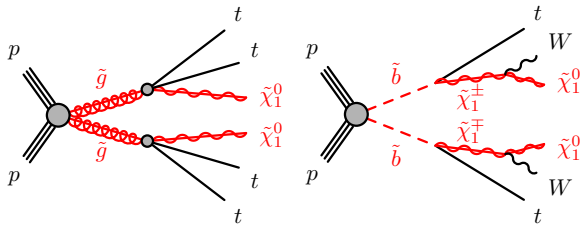

Figure 1: Gluino decay via offshell stop (left), and direct sbottom pair production (right).

Gluino-stop offshell $\tilde{g} \to t\bar{t}\tilde{\chi}_1^0$

In this model inspired by naturalness arguments, gluinos are coupling preferentially to stops which are lighter than the other squarks. Gluinos are however considered lighter than stops, and decay directly into a $t\bar{t}\tilde{\chi}_1^0$ triplet via a virtual stop (Fig. 1). The pair production of gluinos leads to a final state containing four top quarks and two neutralinos. This characteristic final state is accessible through various experimental signatures, which is why this model is commonly used as a benchmark to estimate analyses sensitivities. The searches performed with run-1 data [16], summarized in Fig. 2, showed that the same-sign leptons final state is competitive mainly at large neutralino mass. This region of the phase space is consequently given a particular attention in the choice of signal regions described further on. In the signal samples referenced in this document, the lightest stop mass is fixed to 10 TeV and is mostly a $\widetilde{t_R}$ state. Only gluino pair production is considered, followed by an exclusive decay in the aforementioned channel.

Direct sbottom $\tilde{b}_1 \to t\tilde{\chi}_1^{\pm}$

In this model, bottom squarks are rather lights and assumed to decay in a top quark and a chargino $\tilde{\chi}_1^{\pm}$ (Fig. 1), providing complementarity to the mainstream search which focuses on the channel $\tilde{b}_1 \to b\tilde{\chi}_1^0$. The final state resulting from the production of a sbottom pair contains pairs of top quarks, of W bosons and of neutralinos. While this final state may lead to various experimental signatures, the model was considered in run-1 [16] only by the same-sign leptons and jets search, leading to the exclusion limits presented in Fig. 2. In the signal samples used by the analysis, the neutralino mass is fixed to 60 GeV, and the chargino mass to 150 GeV, while the sbottom mass is varied. Only pair production of the lightest sbottom is considered, followed by an exclusive decay in the aforementioned channel.

Gluinos and squarks 2-step decays via gauginos

These scenarios feature a less oriented search for gluinos or squarks (save third generation) where gluinos couple preferentially to the latter, and squarks decay to charginos (Fig. 3 left) with the subsequent cascade $\tilde{\chi}_1^{\pm} \to W\tilde{\chi}_2^0 \to WZ\tilde{\chi}_1^0$. This leads to final states of two light quarks, two W and Z bosons, and two neutralinos (with two additional light quarks in the case of gluino pair production). Fig. 4 left shows the exclusion limits obtained with the 2012 dataset [16]; in the gluino scenario, the same-sign leptons + jets search provided complementarity at large neutralino mass, while its sensitivity in the squark scenario dominated completely. In the signal samples used here, the chargino mass is set halfway between the neutralino and squark (or gluino) masses, while the neutralino $\tilde{\chi}_2^0$ mass is set halfway between the chargino and neutralino masses. Gluino and squark-antisquark pair production are considered separately in distinct scenarios.

Gluinos and squarks 2-step decays via sleptons

In these scenarios, gluinos couple preferentially to the squarks of the first two generations, and the latter decay either to a chargino $\tilde{\chi}_1^{\pm}$ or a neutralino $\tilde{\chi}_2^0$, which are assumed to be mass-degenerate, and decay in

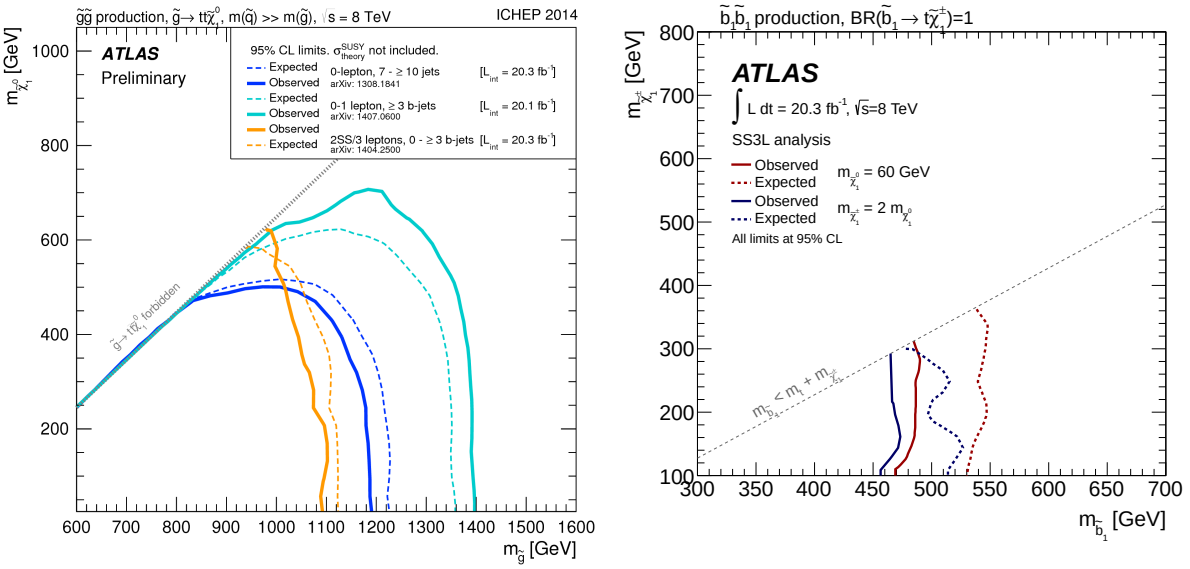

Figure 2: Exclusion limits on the gluino-stop offshell (left) and direct sbottom (right) scenarios set by ATLAS with the 2012 dataset [16].

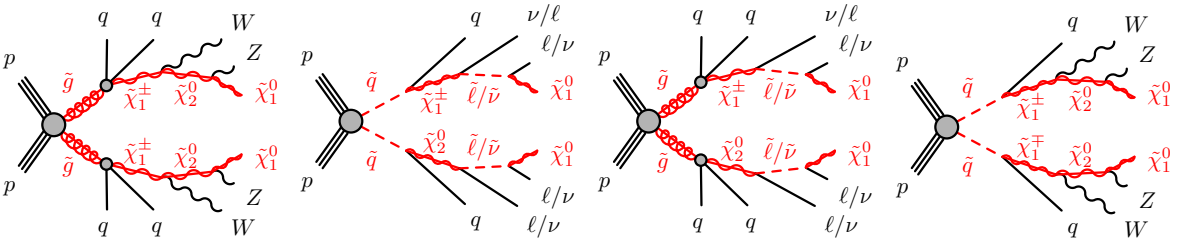

Figure 3: Two-step decays of gluinos and squarks, mediated by gauginos (left) or sleptons (right).

turn to sleptons (Fig. 3 right) with $\mathcal{BR}(\tilde{\chi}_1^\pm \to \nu\tilde{\ell}) = \mathcal{BR}(\tilde{\chi}_1^\pm \to \ell\tilde{\nu}) = \mathcal{BR}(\tilde{\chi}_2^0 \to \nu\tilde{\nu}) = \mathcal{BR}(\tilde{\chi}_2^0 \to \ell\tilde{\ell}) = 50\%$. The corresponding final state may contain zero to four charged leptons, neutrinos, two light quarks and two neutralinos (with two additional light quarks in the case of gluino pair production). Because of the sleptons replacing the gauge bosons featured in the scenarios presented in the previous paragraph, these scenarios have comparatively a lower jet multiplicity but a significantly enhanced acceptance in multi-lepton experimental signatures. As can be seen on Fig. 4 right, which presents the exclusion limits obtained with the 2012 dataset [16], the same-sign leptons and jets signature is again very competitive. In the signal samples used here, the chargino $\tilde{\chi}_1^\pm$ and neutralino $\tilde{\chi}_2^0$ masses are set equal, halfway between the neutralino and squark (or gluino) masses, while the degenerate sleptons masses are set halfway between these gauginos and the lightest neutralino masses. Furthermore, gauginos decay to any slepton flavor with equal probability. Gluino and squark-antisquark pair production are considered separately in distinct scenarios.

Models not considered for the moment

In the publications [14, 16] of the analysis results obtained with run-1 data, exclusion limits were also provided for other signal models, often These scenarios included the $\tilde{g} \to tbW\tilde{\chi}_1^0$ and $\tilde{g} \to tcW\tilde{\chi}_1^0$ simplified models, as well as minimal models featuring R-parity violation through bilinear terms, gauge-mediated SUSY breaking, or universal extra dimensions. These models are not considered here, although

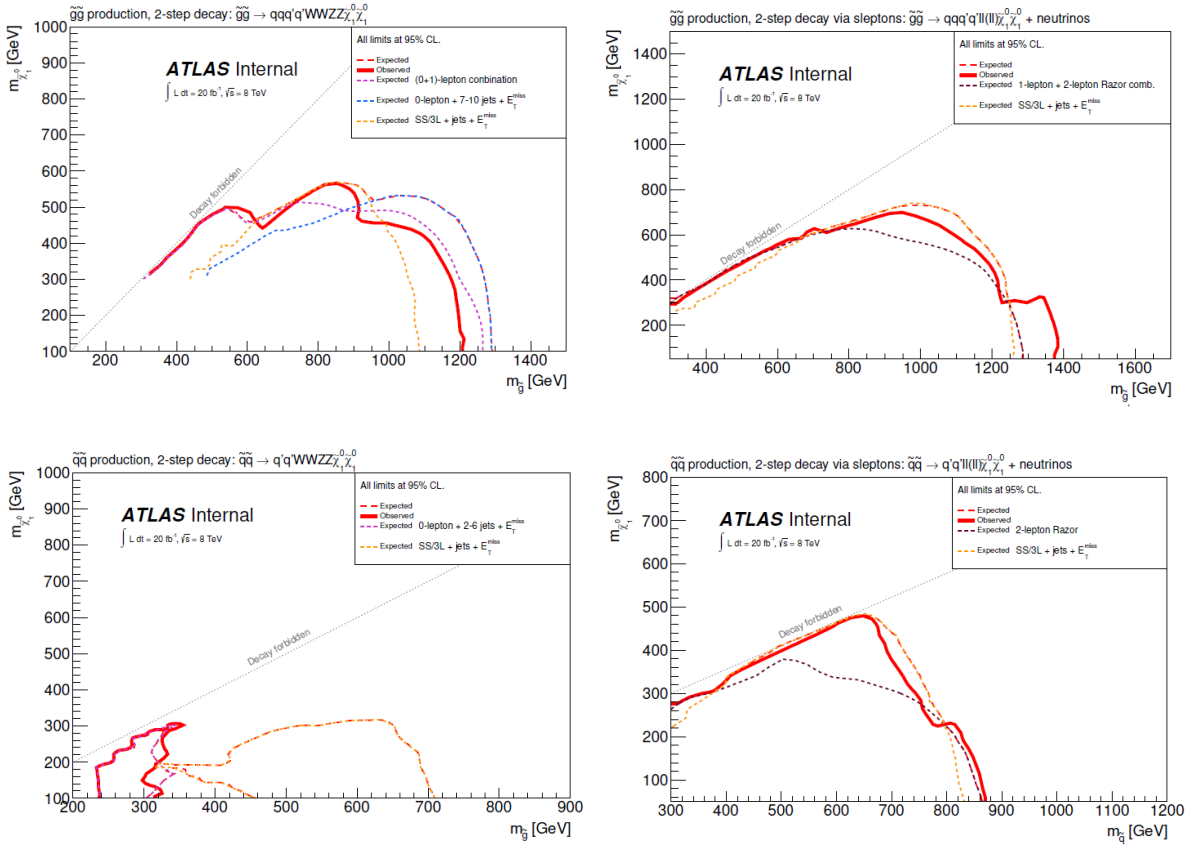

Figure 4: Exclusion limits on scenarios featuring gluino (top) and squarks (bottom) two-steps decays via gauginos (left) or sleptons (right) set by ATLAS with the 2012 dataset [16].

interpretations might be proposed for them again in the future.

2.2 New models

2.2.1 RPV inspired

In supersymmetry, the following superpotential is present :

$$W = \mu HL + \frac{1}{2}\lambda_{ijk}L_iL_jE_k + \lambda'_{ijk}L_iQ_jD_k + \frac{1}{2}\lambda''_{ijk}U_iD_jD_k \quad (1)$$

where H, L, Q, E, U and D are respectively the superpotential associated to the Higgs doublet, the lepton-neutrino doublet, the quark up-down doublet, the right-handed electron, the right-handed up quark and the right-handed down quark. The indices i, j and k are the flavor indices and μ , λ_{ijk} , λ'_{ijk} , λ''_{ijk} are the coupling constants.

The leptonic number violation and the baryonic number violation implied by this potential have an important impact in the physic at low energy and do not respect some low energy constraints like the proton decay time limit. In R-parity conserving (RPC) SUSY models, the R-parity is added in order to remove these terms and keep the proton stable. However, one can play with the couplings μ , λ_{ijk} , λ'_{ijk} and λ''_{ijk} in order to violate R-parity while respecting the low energy constraints. This is called the

191 R-parity violation (RPV) SUSY models.
192
193 In this note, we will only consider the case where the coupling constants μ, λ_{ijk}, λ'_{ijk} and $\lambda''_{(i\neq 3)jk}$ are
194 suppressed. Therefore, the only non-negligible terms are $\lambda''_{321}TSD$, $\lambda''_{331}TBD$ and $\lambda''_{323}TSB$ where T,
195 B, D and S are the superfields associated to the top, bottom, down and strange quark. This scenario is
196 predicted by some RPV models like the Minimal Flavor Violation (MFV) scenarios [17, 18] and leads to
197 the production of same-sign top quarks [19] (see Fig. 5).

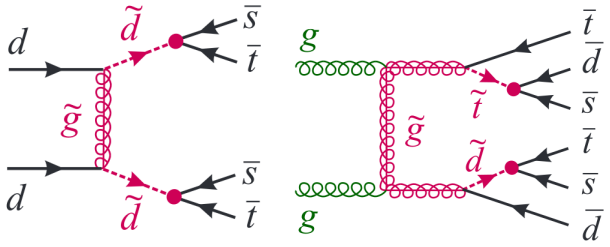

Figure 5: Example of diagrams for RPV model for the *d-quark fusion* topology (left), and the *gluon fusion* topology (right) involving the λ''_{321} coupling. In both cases, the baryonic number is violated by two units.

198 In these scenarios, the R-parity is not conserved and the LSP is not stable (and therefore cannot be
199 a good dark matter candidate). However, the interesting part of this model is that it allows B-violating
200 processes (see Fig. 5). Actually, the baryonic asymmetry in the universe and the fact that the standard
201 model does not respect this symmetry provides a good motivation for the search for B-violation pro-
202 cesses at high energy. In addition, it was also proved that the violation of the baryonic number by two
203 units involving top quarks could respect the low denergy constraints like the proton decay time limit [20].
204
205 In this analysis, two kind of topologies will be considered:

- **d-quark fusion**: Production of two on-shell d-squarks with a gluino in t-channel and the d-squarks decay to an anti-top quark and to one extra jet. The squarks will lighter than the gluino and the cross section will mostly depend on the mass of the squark (see Fig. 5).

$$dd \rightarrow \tilde{d}\tilde{d}\ ,\ \tilde{d} \rightarrow \bar{t}q \tag{2}$$

- **gluon fusion**: Production of two on-shell gluinos which decay to a top or an anti-top quark and to two extra jets. The gluino will be lighter than the squarks and the cross section will only depend on the mass of the gluino (see Fig. 5).

$$gg \rightarrow \tilde{g}\tilde{g}\ ,\ \tilde{g} \rightarrow tqq\ /\ \tilde{g} \rightarrow \bar{t}qq' \tag{3}$$

206 The extra jets could be either b-jet or light jets, depending on the coupling being considered. In order to
207 have access to the charge of the top quark, we will only consider the case where the top quark decays
208 leptonically. At the end, the final states will be composed of two same-sign leptons, at least two b-jets,
209 low missing transverse energy (coming from the neutrinos) and extra jets.
210
211 This model was already constrained by ATLAS [21] and CMS [22] in Run-1, but those analyses only
212 considered the coupling λ''_{323} and the topology of *gluon fusion*. A limit of around 900 GeV was found on
213 the mass of the gluino. The full hadronic final state was also exploited in ATLAS [23].

3 MC samples

This section summarizes the signal and background samples used for the studies presented in this note, as well some details about the Monte Carlo production and analysis framework. All samples used in this note are part of the DC14 Monte-Carlo campaign which exhibits a number of deficiencies [24], most notably the inaccessibility of detailed trigger information.

3.1 Derivation versions and analysis model

In all cases, the SUSY1 DxAOD derivations are used. Derivation tag p1872 (19.1.4.9 cache) is used for most of the samples used in this note, although some signal samples were not initially available in that tag and p1863 (19.1.4.8 cache) was used instead. Both derivation tags included the fix of lepton isolation variables (see Section 4.2.3 for more details).

Most of the studies shown in this note were performed using flat ROOT ntuples produced on the grid using code based on the `SUSYAnalysiExample` EventLoop package and SUSYTools-00-05-00-26 tag. They contained basic object information, although no overlap removal or isolation cuts were applied to allow flexibility for optimization studies. No event skimming or systematic uncertainties were included. The total size of these ntuples is 70 GB (both background and signal samples). These files were shared among the groups participating in the analysis, although some of the groups developed their own framework for xAOD analysis.

In addition, dedicated flat ROOT ntuples with all the systematic variations included in the SUSYTools `getSystInfoList()` method were also produced for the samples containing prompt SS/3L ($t\bar{t}+V$, $t\bar{t}+h$, diboson, signals). To reduce the size of the output files, only events that contained in any of the systematic variations at least 2 leptons with $p_{\mathrm{T}} > 10$ GeV, and either $E_{\mathrm{T}} > 100$ GeV or at least 3 b-tagged jets ($p_{\mathrm{T}} > 20$ GeV) or $H_{\mathrm{T}} > 300$ GeV were kept. In order to benefit from the recently implemented grouping of the Egamma systematics, the SUSYTools-00-05-00-29 tag was used for this production, which contains only other minor updates with respect to SUSYTools-00-05-00-26. The total size of these ntuples is below 50 GB.

3.2 Signal Samples

This section describes the signal samples used for in this note. The baseline signal models used are the ones described in Section 2, and all the signal samples used are listed in Table 1.

The gluino-stop offshell ($\tilde{g} \rightarrow t\bar{t}\tilde{\chi}_1^0$) and direct sbottom ($\tilde{b}_1 \rightarrow t\tilde{\chi}_1^{\pm}$ with $\tilde{b}_1 \rightarrow t\tilde{\chi}_1^{\pm}$) samples are produced with Herwig++ [25]. The UE-EE-4 Herwig++ tune [26] is used to describe the underlying event. The other signal samples used in this note (gluinos and squarks 2-step decays via gauginos or sleptons) are produced using the Madgraph v5 generator [27] using leading-order (LO) matrix elements with up to two additional partons. Pythia 6.425 [28] with the AUET2B tune [29, 30] is used for hadronisation and to describe the underlying event. In all the signal samples, the CTEQ6L1 [31] set of parton distribution functions is used in all the signal samples. The signal samples are normalised to the next-to-next-to-leading order cross-section including the resummation of soft gluon emission at next-to-next-to-leading-logarithmic accuracy (NLO+NLL), as detailed in Ref. [32].

3.3 Background Samples

All the background samples used are listed in Tables 2-4.

Simulated $t\bar{t}$ events are generated using the Powheg generator version r2330.2 [33, 34, 35], which implements the next-to-leading order matrix element for inclusive $t\bar{t}$ production and uses the CT10 PDF set [36]. Powheg is interfaced to Pythia 6.427 [28] with the CTEQ6L1 PDF set using the Perugia2012

tune [37]. The $t\bar{t}$ samples are normalised to their next-to-next-to-leading order cross-section including the resummation of soft gluon emission at next-to-next-to-leading-logarithmic accuracy using Top++2.0 [38].

Simulated W/Z+jets samples are produced using Sherpa 1.4.5 [39] with massive b-, c-quarks with up to four additional partons in the matrix element and parton shower and are normalised to their next-to-next-to-leading order QCD theoretical cross sections [40].

Samples of single top quark backgrounds corresponding to the t-, s- and Wt production mechanisms are generated with Powheg version r2330.2 using the CT10 PDF set. All single-top samples are interfaced to Pythia 6.427 with the CTEQ6L1 set of parton distribution functions using the Perugia2012 tune. The leading-order cross-sections obtained from the generator is used for these samples.

The processes of $t\bar{t}+V$ production are generated with MadGraph 5 2.1.1 [27] + Pythia 6.427 using the CTEQ6L1 set of parton distribution functions and the AUET2B underlying event tune [30]. The samples are normalised to their next-to-leading order cross-sections using the k-factors computed for $\sqrt{s} = 14$ TeV [41, 42].

Simulated samples for diboson processes are simulated with Sherpa 1.4.5 ($WZ/ZZ \to \ell\ell\nu\nu$ and $W^{\pm}W^{\pm}jj \to \ell^{\pm}\ell^{\pm}\nu\nu jj$ electroweak production), Powheg r2330.3 + Pythia 8 (WW, WZ and ZZ) and `gg2VV` [43, 44] in Powheg r2330.3 + Pythia 8 ($gg \to h \to WW$).

QCD multijets are not included in this study since these backgrounds are expected to be very small. Note that some background processes that had a non-negligible (despite small) contribution to the analysis in Run-1, such as tri-boson or $t+Z$ production, were not included in the DC14 productions.

3.4 Detector simulation

The detector simulation is performed with a full ATLAS detector simulation [45] based on Geant4 [46]. All simulated samples are generated with a range of minimum-bias interactions using Pythia 8 [47] with the MSTW2008LO PDF set [48] and the AUET2B tune overlaid on the hard-scattering event to account for the multiple pp interactions in the same bunch crossing (in-time pileup) and neighbouring bunch crossing (out-of-time pileup). A bunch spacing of 25 ns is assumed, and for the bulk of the events a flat probability distribution for the average number of interactions per bunch crossing is assumed with values ranging from 20 to 40 at most [24].

datasetID	Sample name	σ [pb]	k-Factor	ϵ_{filter}	N_{gen}	L_{equiv}
	Gluino-stop offshell ($\tilde{g} \to t\tilde{\chi}_1^0$)					
204533	mc14_13TeV.204533.Herwigpp_UEEE4_CTEQ6L1_Gtt_G1000_T5000_L100.merge.DAOD_SUSY1.e3094_s1982_s2008_r5787_r5853_p1872/	0.3254	1.00	1.000	20000	61.5
204534	mc14_13TeV.204534.Herwigpp_UEEE4_CTEQ6L1_Gtt_G1300_T5000_L100.merge.DAOD_SUSY1.e3094_s1982_s2008_r5787_r5853_p1872/	0.0461	1.00	1.000	19500	423.0
204535	mc14_13TeV.204535.Herwigpp_UEEE4_CTEQ6L1_Gtt_G1600_T5000_L100.merge.DAOD_SUSY1.e3094_s1982_s2008_r5787_r5853_p1872/	0.0081	1.00	1.000	20000	2469.1
204536	mc14_13TeV.204536.Herwigpp_UEEE4_CTEQ6L1_Gtt_G1900_T5000_L100.merge.DAOD_SUSY1.e3094_s1982_s2008_r5787_r5853_p1872/	0.0016	1.00	1.000	20000	12500.0
204537	mc14_13TeV.204537.Herwigpp_UEEE4_CTEQ6L1_Gtt_G2200_T5000_L100.merge.DAOD_SUSY1.e3094_s1982_s2008_r5787_r5853_p1872/	0.0004	1.00	1.000	20000	50000.0
204539	mc14_13TeV.204539.Herwigpp_UEEE4_CTEQ6L1_Gtt_G1300_T5000_L400.merge.DAOD_SUSY1.e3094_s1982_s2008_r5787_r5853_p1872/	0.0461	1.00	1.000	15000	325.4
204540	mc14_13TeV.204540.Herwigpp_UEEE4_CTEQ6L1_Gtt_G1300_T5000_L700.merge.DAOD_SUSY1.e3094_s1982_s2008_r5787_r5853_p1872/	0.0461	1.00	1.000	20000	433.8
204541	mc14_13TeV.204541.Herwigpp_UEEE4_CTEQ6L1_Gtt_G1300_T5000_L900.merge.DAOD_SUSY1.e3094_s1982_s2008_r5787_r5853_p1872/	0.0461	1.00	1.000	20000	433.8
204912	mc14_13TeV.204912.Herwigpp_UEEE4_CTEQ6L1_Gtt_G1500_T5000_L200.merge.DAOD_SUSY1.e3328_s1982_s2008_r5787_r5853_p1872/	0.0142	1.00	1.000	20000	1408.5
204913	mc14_13TeV.204913.Herwigpp_UEEE4_CTEQ6L1_Gtt_G1500_T5000_L400.merge.DAOD_SUSY1.e3328_s1982_s2008_r5787_r5853_p1872/	0.0142	1.00	1.000	20000	1408.5
204914	mc14_13TeV.204914.Herwigpp_UEEE4_CTEQ6L1_Gtt_G1500_T5000_L600.merge.DAOD_SUSY1.e3328_s1982_s2008_r5787_r5853_p1872/	0.0142	1.00	1.000	20000	1408.5
204915	mc14_13TeV.204915.Herwigpp_UEEE4_CTEQ6L1_Gtt_G1500_T5000_L800.merge.DAOD_SUSY1.e3328_s1982_s2008_r5787_r5853_p1872/	0.0142	1.00	1.000	20000	1408.5
204916	mc14_13TeV.204916.Herwigpp_UEEE4_CTEQ6L1_Gtt_G1500_T5000_L1000.merge.DAOD_SUSY1.e3328_s1982_s2008_r5787_r5853_p1872/	0.0142	1.00	1.000	20000	1408.5
	Direct sbottom ($\tilde{b}_1 \to t\tilde{\chi}_1^{\pm}$ with $\tilde{b}_1 \to t\tilde{\chi}_1^{\pm}$)					
204973	mc14_13TeV.204973.Herwigpp_UEEE4_CTEQ6L1_sbottom_tchr_2lep_B450_C150_N60.merge.DAOD_SUSY1.e3356_s1982_s2008_r5787_r5853_p1863/	0.9483	0.41	0.409	20000	125.8
204974	mc14_13TeV.204974.Herwigpp_UEEE4_CTEQ6L1_sbottom_tchr_2lep_B550_C150_N60.merge.DAOD_SUSY1.e3356_s1982_s2008_r5787_r5853_p1863/	0.2961	0.43	0.432	11000	200.0
204975	mc14_13TeV.204975.Herwigpp_UEEE4_CTEQ6L1_sbottom_tchr_2lep_B650_C150_N60.merge.DAOD_SUSY1.e3356_s1982_s2008_r5787_r5853_p1863/	0.1070	0.45	0.451	20000	921.0
204976	mc14_13TeV.204976.Herwigpp_UEEE4_CTEQ6L1_sbottom_tchr_2lep_B750_C150_N60.merge.DAOD_SUSY1.e3356_s1982_s2008_r5787_r5853_p1863/	0.0431	0.47	0.472	20000	2091.8
204977	mc14_13TeV.204977.Herwigpp_UEEE4_CTEQ6L1_sbottom_tchr_2lep_B850_C150_N60.merge.DAOD_SUSY1.e3356_s1982_s2008_r5787_r5853_p1863/	0.0190	0.48	0.483	20000	4540.3
	gluino 2-step decays via gauginos					
204952	mc14_13TeV.204952.MadGraphPythia_AUET2BCTEQ6L1_SMGG2WWZZ_1100_600_100.merge.DAOD_SUSY1.e3345_s1982_s2008_r5787_r5853_p1872/	0.1635	1.00	1.000	19500	119.3
204953	mc14_13TeV.204953.MadGraphPythia_AUET2BCTEQ6L1_SMGG2WWZZ_1300_700_100.merge.DAOD_SUSY1.e3345_s1982_s2008_r5787_r5853_p1872/	0.0461	1.00	1.000	5000	108.5
204954	mc14_13TeV.204954.MadGraphPythia_AUET2BCTEQ6L1_SMGG2WWZZ_1500_800_100.merge.DAOD_SUSY1.e3345_s1982_s2008_r5787_r5853_p1872/	0.0142	1.00	1.000	20000	1408.5
204955	mc14_13TeV.204955.MadGraphPythia_AUET2BCTEQ6L1_SMGG2WWZZ_1700_900_100.merge.DAOD_SUSY1.e3345_s1982_s2008_r5787_r5853_p1872/	0.0047	1.00	1.000	15000	3191.5
204956	mc14_13TeV.204956.MadGraphPythia_AUET2BCTEQ6L1_SMGG2WWZZ_1900_1000_100.merge.DAOD_SUSY1.e3345_s1982_s2008_r5787_r5853_p1872/	0.0016	1.00	1.000	15500	9687.5
204957	mc14_13TeV.204957.MadGraphPythia_AUET2BCTEQ6L1_SMGG2WWZZ_2100_1100_100.merge.DAOD_SUSY1.e3345_s1982_s2008_r5787_r5853_p1872/	0.0006	1.00	1.000	5000	8333.3
204958	mc14_13TeV.204958.MadGraphPythia_AUET2BCTEQ6L1_SMGG2WWZZ_2300_1200_100.merge.DAOD_SUSY1.e3345_s1982_s2008_r5787_r5853_p1872/	0.0002	1.00	1.000	13500	67500.0
204959	mc14_13TeV.204959.MadGraphPythia_AUET2BCTEQ6L1_SMGG2WWZZ_1000_700_400.merge.DAOD_SUSY1.e3345_s1982_s2008_r5787_r5853_p1872/	0.3254	1.00	1.000	5000	15.4
204960	mc14_13TeV.204960.MadGraphPythia_AUET2BCTEQ6L1_SMGG2WWZZ_1000_750_500.merge.DAOD_SUSY1.e3345_s1982_s2008_r5787_r5853_p1872/	0.3254	1.00	1.000	7500	23.0
204961	mc14_13TeV.204961.MadGraphPythia_AUET2BCTEQ6L1_SMGG2WWZZ_1000_800_600.merge.DAOD_SUSY1.e3345_s1982_s2008_r5787_r5853_p1872/	0.3254	1.00	1.000	20000	61.5
204962	mc14_13TeV.204962.MadGraphPythia_AUET2BCTEQ6L1_SMGG2WWZZ_1000_850_700.merge.DAOD_SUSY1.e3345_s1982_s2008_r5787_r5853_p1872/	0.3254	1.00	1.000	20000	61.5
204963	mc14_13TeV.204963.MadGraphPythia_AUET2BCTEQ6L1_SMGG2WWZZ_1000_900_800.merge.DAOD_SUSY1.e3345_s1982_s2008_r5787_r5853_p1872/	0.3254	1.00	1.000	20000	61.5
204964	mc14_13TeV.204964.MadGraphPythia_AUET2BCTEQ6L1_SMGG2WWZZ_1000_950_900.merge.DAOD_SUSY1.e3345_s1982_s2008_r5787_r5853_p1872/	0.3254	1.00	1.000	10000	30.7
	squark 2-step decays via gauginos					
204965	mc14_13TeV.204965.MadGraphPythia_AUET2BCTEQ6L1_SMSS2WWZZ_650_375_100.merge.DAOD_SUSY1.e3345_s1982_s2008_r5787_r5853_p1872/	0.0695	1.00	1.000	5000	71.9
204966	mc14_13TeV.204966.MadGraphPythia_AUET2BCTEQ6L1_SMSS2WWZZ_750_425_100.merge.DAOD_SUSY1.e3345_s1982_s2008_r5787_r5853_p1872/	0.0219	1.00	1.000	20000	913.2
204967	mc14_13TeV.204967.MadGraphPythia_AUET2BCTEQ6L1_SMSS2WWZZ_850_475_100.merge.DAOD_SUSY1.e3345_s1982_s2008_r5787_r5853_p1872/	0.0075	1.00	1.000	17500	2333.3
204968	mc14_13TeV.204968.MadGraphPythia_AUET2BCTEQ6L1_SMSS2WWZZ_950_525_100.merge.DAOD_SUSY1.e3345_s1982_s2008_r5787_r5853_p1872/	0.0027	1.00	1.000	19000	7037.0
204969	mc14_13TeV.204969.MadGraphPythia_AUET2BCTEQ6L1_SMSS2WWZZ_650_475_300.merge.DAOD_SUSY1.e3345_s1982_s2008_r5787_r5853_p1872/	0.0695	1.00	1.000	20000	287.8
204970	mc14_13TeV.204970.MadGraphPythia_AUET2BCTEQ6L1_SMSS2WWZZ_650_525_400.merge.DAOD_SUSY1.e3345_s1982_s2008_r5787_r5853_p1872/	0.0695	1.00	1.000	20000	287.8
204971	mc14_13TeV.204971.MadGraphPythia_AUET2BCTEQ6L1_SMSS2WWZZ_650_575_500.merge.DAOD_SUSY1.e3345_s1982_s2008_r5787_r5853_p1872/	0.0695	1.00	1.000	20000	287.8
204972	mc14_13TeV.204972.MadGraphPythia_AUET2BCTEQ6L1_SMSS2WWZZ_650_625_600.merge.DAOD_SUSY1.e3345_s1982_s2008_r5787_r5853_p1872/	0.0695	1.00	1.000	20000	287.8

Table 1: List of simulated samples for the signal models used in this note. The dataset ID, the cross-section σ, the k-Factor, the generator filter efficiency ϵ_{filter}, the total number of generated events N_{gen} and the equivalent luminosity (L_{equiv}) are shown.

datasetID	Sample name	σ [pb]	k-Factor	ϵ_{filter}	N_{gen}	L_{equiv}
110401	mc14_13TeV.110401.PowhegPythia_P2012_ttbar_nonallhad.merge.DAOD_SUSY1.e2928_s1982_s2008_r5787_r5853_p1872/	831.7600	1.00	0.543	9970500	22.1
119353	mc14_13TeV.119353.MadGraphPythia_AUET2BCTEQ6L1_ttbarW.merge.DAOD_SUSY1.e3214_s1982_s2008_r5787_r5853_p1872/	0.2014	1.22	1.000	399500	1625.9
119355	mc14_13TeV.119355.MadGraphPythia_AUET2BCTEQ6L1_ttbarZ.merge.DAOD_SUSY1.e3214_s1982_s2008_r5787_r5853_p1872/	0.1857	1.56	1.000	400000	1380.8
119583	mc14_13TeV.119583.MadgraphPythia_AUET2B_CTEQ6L1_ttbarWW.merge.DAOD_SUSY1.e3214_s1982_s2008_r5787_r5853_p1872/	0.0030	1.00	1.000	10000	3333.3
174830	mc14_13TeV.174830.MadGraphPythia_AUET2BCTEQ6L1_ttbarWjExcl.merge.DAOD_SUSY1.e3214_s1982_s2008_r5787_r5853_p1872/	0.1313	1.22	1.000	399500	2494.0
174831	mc14_13TeV.174831.MadGraphPythia_AUET2BCTEQ6L1_ttbarWjjIncl.merge.DAOD_SUSY1.e3214_s1982_s2008_r5787_r5853_p1872/	0.1627	1.22	1.000	395000	1990.0
174832	mc14_13TeV.174832.MadGraphPythia_AUET2BCTEQ6L1_ttbarZjExcl.merge.DAOD_SUSY1.e3214_s1982_s2008_r5787_r5853_p1872/	0.1663	1.56	1.000	399500	1539.9
174833	mc14_13TeV.174833.MadGraphPythia_AUET2BCTEQ6L1_ttbarZjjIncl.merge.DAOD_SUSY1.e3214_s1982_s2008_r5787_r5853_p1872/	0.2076	1.56	1.000	399500	1233.6
110070	mc14_13TeV.110070.PowhegPythia_P2012_singletop_tchan_lept_top.merge.DAOD_SUSY1.e3049_s1982_s2008_r5787_r5853_p1872/	43.7550	1.00	1.000	999000	22.8
110071	mc14_13TeV.110071.PowhegPythia_P2012_singletop_tchan_lept_antitop.merge.DAOD_SUSY1.e3049_s1982_s2008_r5787_r5853_p1872/	25.7780	1.00	1.000	1000000	38.8
110302	mc14_13TeV.110302.PowhegPythia_P2012_st_schan_lep.merge.DAOD_SUSY1.e3049_s1982_s2008_r5787_r5853_p1872/	3.3514	1.00	1.000	999500	298.2
110305	mc14_13TeV.110305.PowhegPythia_P2012_st_Wtchan_incl_DR.merge.DAOD_SUSY1.e3049_s1982_s2008_r5787_r5853_p1872/	68.4590	1.00	1.000	958500	14.0
167740	mc14_13TeV.167740.Sherpa_CT10_WenuMassiveCBPt0_BFilter.merge.DAOD_SUSY1.e2822_s1982_s2008_r5787_r5853_p1872/	18795.0000	1.07	0.018	497000	1.4
167741	mc14_13TeV.167741.Sherpa_CT10_WenuMassiveCBPt0_CJetFilterBVeto.merge.DAOD_SUSY1.e2822_s1982_s2008_r5787_r5853_p1872/	18804.0000	1.07	0.063	494500	0.4
167742	mc14_13TeV.167742.Sherpa_CT10_WenuMassiveCBPt0_CJetVetoBVeto.merge.DAOD_SUSY1.e2822_s1982_s2008_r5787_r5853_p1872/	18843.0000	1.07	0.919	1000000	0.1
167743	mc14_13TeV.167743.Sherpa_CT10_WmunuMassiveCBPt0_BFilter.merge.DAOD_SUSY1.e2822_s1982_s2008_r5787_r5853_p1872/	18793.0000	1.07	0.018	499500	1.4
167744	mc14_13TeV.167744.Sherpa_CT10_WmunuMassiveCBPt0_CJetFilterBVeto.merge.DAOD_SUSY1.e2822_s1982_s2008_r5787_r5853_p1872/	18788.0000	1.07	0.056	498000	0.4
167745	mc14_13TeV.167745.Sherpa_CT10_WmunuMassiveCBPt0_CJetVetoBVeto.merge.DAOD_SUSY1.e2822_s1982_s2008_r5787_r5853_p1872/	18797.0000	1.07	0.926	989500	0.1
167746	mc14_13TeV.167746.Sherpa_CT10_WtaunuMassiveCBPt0_BFilter.merge.DAOD_SUSY1.e2822_s1982_s2008_r5787_r5853_p1872/	18795.0000	1.07	0.018	500000	1.4
167747	mc14_13TeV.167747.Sherpa_CT10_WtaunuMassiveCBPt0_CJetFilterBVeto.merge.DAOD_SUSY1.e2822_s1982_s2008_r5787_r5853_p1872/	18808.0000	1.07	0.060	500000	0.4
167748	mc14_13TeV.167748.Sherpa_CT10_WtaunuMassiveCBPt0_CJetVetoBVeto.merge.DAOD_SUSY1.e2822_s1982_s2008_r5787_r5853_p1872/	18800.0000	1.07	0.923	499500	0.0
167761	mc14_13TeV.167761.Sherpa_CT10_WenuMassiveCBPt70_140_BFilter.merge.DAOD_SUSY1.e2822_s1982_s2008_r5787_r5853_p1872/	557.8700	1.07	0.055	349500	10.6
167762	mc14_13TeV.167762.Sherpa_CT10_WenuMassiveCBPt70_140_CJetFilterBVeto.merge.DAOD_SUSY1.e2822_s1982_s2008_r5787_r5853_p1872/	557.9200	1.07	0.227	350000	2.6
167763	mc14_13TeV.167763.Sherpa_CT10_WenuMassiveCBPt70_140_CJetVetoBVeto.merge.DAOD_SUSY1.e2822_s1982_s2008_r5787_r5853_p1872/	558.3700	1.07	0.718	985500	2.3
167764	mc14_13TeV.167764.Sherpa_CT10_WmunuMassiveCBPt70_140_BFilter.merge.DAOD_SUSY1.e2822_s1982_s2008_r5787_r5853_p1872/	557.8700	1.07	0.055	345500	10.5
167765	mc14_13TeV.167765.Sherpa_CT10_WmunuMassiveCBPt70_140_CJetFilterBVeto.merge.DAOD_SUSY1.e2822_s1982_s2008_r5787_r5853_p1872/	558.2500	1.07	0.220	350000	2.7
167766	mc14_13TeV.167766.Sherpa_CT10_WmunuMassiveCBPt70_140_CJetVetoBVeto.merge.DAOD_SUSY1.e2822_s1982_s2008_r5787_r5853_p1872/	557.4800	1.07	0.724	500000	1.2
167767	mc14_13TeV.167767.Sherpa_CT10_WtaunuMassiveCBPt70_140_BFilter.merge.DAOD_SUSY1.e2822_s1982_s2008_r5787_r5853_p1872/	557.9200	1.07	0.055	349500	10.6
167768	mc14_13TeV.167768.Sherpa_CT10_WtaunuMassiveCBPt70_140_CJetFilterBVeto.merge.DAOD_SUSY1.e2822_s1982_s2008_r5787_r5853_p1872/	557.6800	1.07	0.224	349500	2.6
167769	mc14_13TeV.167769.Sherpa_CT10_WtaunuMassiveCBPt70_140_CJetVetoBVeto.merge.DAOD_SUSY1.e2822_s1982_s2008_r5787_r5853_p1872/	558.5900	1.07	0.720	999500	2.3
167770	mc14_13TeV.167770.Sherpa_CT10_WenuMassiveCBPt140_280_BFilter.merge.DAOD_SUSY1.e2822_s1982_s2008_r5787_r5853_p1872/	81.8640	1.07	0.075	198000	30.1
167771	mc14_13TeV.167771.Sherpa_CT10_WenuMassiveCBPt140_280_CJetFilterBVeto.merge.DAOD_SUSY1.e2822_s1982_s2008_r5787_r5853_p1872/	81.9180	1.07	0.255	200000	8.9
167772	mc14_13TeV.167772.Sherpa_CT10_WenuMassiveCBPt140_280_CJetVetoBVeto.merge.DAOD_SUSY1.e2822_s1982_s2008_r5787_r5853_p1872/	81.7640	1.07	0.671	398000	6.8
167773	mc14_13TeV.167773.Sherpa_CT10_WmunuMassiveCBPt140_280_BFilter.merge.DAOD_SUSY1.e2822_s1982_s2008_r5787_r5853_p1872/	81.7750	1.07	0.074	349500	54.0
167774	mc14_13TeV.167774.Sherpa_CT10_WmunuMassiveCBPt140_280_CJetFilterBVeto.merge.DAOD_SUSY1.e2822_s1982_s2008_r5787_r5853_p1872/	81.8130	1.07	0.250	349000	15.9
167775	mc14_13TeV.167775.Sherpa_CT10_WmunuMassiveCBPt140_280_CJetVetoBVeto.merge.DAOD_SUSY1.e2822_s1982_s2008_r5787_r5853_p1872/	81.9250	1.07	0.676	999500	16.9
167776	mc14_13TeV.167776.Sherpa_CT10_WtaunuMassiveCBPt140_280_BFilter.merge.DAOD_SUSY1.e2822_s1982_s2008_r5787_r5853_p1872/	81.8670	1.07	0.075	200000	30.4
167777	mc14_13TeV.167777.Sherpa_CT10_WtaunuMassiveCBPt140_280_CJetFilterBVeto.merge.DAOD_SUSY1.e2822_s1982_s2008_r5787_r5853_p1872/	81.7000	1.07	0.253	199927	9.0
167778	mc14_13TeV.167778.Sherpa_CT10_WtaunuMassiveCBPt140_280_CJetVetoBVeto.merge.DAOD_SUSY1.e2822_s1982_s2008_r5787_r5853_p1872/	81.7680	1.07	0.673	400000	6.8
167779	mc14_13TeV.167779.Sherpa_CT10_WenuMassiveCBPt280_500_BFilter.merge.DAOD_SUSY1.e2822_s1982_s2008_r5787_r5853_p1872/	6.2271	1.00	0.098	399500	654.6
167780	mc14_13TeV.167780.Sherpa_CT10_WenuMassiveCBPt280_500_CJetFilterBVeto.merge.DAOD_SUSY1.e2822_s1982_s2008_r5787_r5853_p1872/	6.2128	1.07	0.273	99500	54.8
167781	mc14_13TeV.167781.Sherpa_CT10_WenuMassiveCBPt280_500_CJetVetoBVeto.merge.DAOD_SUSY1.e2822_s1982_s2008_r5787_r5853_p1872/	6.2357	1.07	0.630	200000	47.6
167782	mc14_13TeV.167782.Sherpa_CT10_WmunuMassiveCBPt280_500_BFilter.merge.DAOD_SUSY1.e2822_s1982_s2008_r5787_r5853_p1872/	6.2188	1.07	0.097	199500	309.1
167783	mc14_13TeV.167783.Sherpa_CT10_WmunuMassiveCBPt280_500_CJetFilterBVeto.merge.DAOD_SUSY1.e2822_s1982_s2008_r5787_r5853_p1872/	6.2277	1.07	0.266	199000	112.3
167784	mc14_13TeV.167784.Sherpa_CT10_WmunuMassiveCBPt280_500_CJetVetoBVeto.merge.DAOD_SUSY1.e2822_s1982_s2008_r5787_r5853_p1872/	6.2271	1.07	0.635	399500	94.4
167785	mc14_13TeV.167785.Sherpa_CT10_WtaunuMassiveCBPt280_500_BFilter.merge.DAOD_SUSY1.e2822_s1982_s2008_r5787_r5853_p1872/	6.2235	1.07	0.097	399500	618.5
167786	mc14_13TeV.167786.Sherpa_CT10_WtaunuMassiveCBPt280_500_CJetFilterBVeto.merge.DAOD_SUSY1.e2822_s1982_s2008_r5787_r5853_p1872/	6.2311	1.07	0.271	100000	55.3
167787	mc14_13TeV.167787.Sherpa_CT10_WtaunuMassiveCBPt280_500_CJetVetoBVeto.merge.DAOD_SUSY1.e2822_s1982_s2008_r5787_r5853_p1872/	6.2060	1.07	0.631	200000	47.7
167788	mc14_13TeV.167788.Sherpa_CT10_WenuMassiveCBPt500_BFilter.merge.DAOD_SUSY1.e2822_s1982_s2008_r5787_r5853_p1872/	0.5143	1.07	0.118	10000	154.0
167789	mc14_13TeV.167789.Sherpa_CT10_WenuMassiveCBPt500_CJetFilterBVeto.merge.DAOD_SUSY1.e2822_s1982_s2008_r5787_r5853_p1872/	0.5208	1.07	0.289	10000	62.1
167790	mc14_13TeV.167790.Sherpa_CT10_WenuMassiveCBPt500_CJetVetoBVeto.merge.DAOD_SUSY1.e2822_s1982_s2008_r5787_r5853_p1872/	0.5131	1.07	0.597	40000	122.0
167791	mc14_13TeV.167791.Sherpa_CT10_WmunuMassiveCBPt500_BFilter.merge.DAOD_SUSY1.e2822_s1982_s2008_r5787_r5853_p1872/	0.5149	1.07	0.118	398000	6122.0
167792	mc14_13TeV.167792.Sherpa_CT10_WmunuMassiveCBPt500_CJetFilterBVeto.merge.DAOD_SUSY1.e2822_s1982_s2008_r5787_r5853_p1872/	0.5132	1.07	0.280	100000	650.4
167793	mc14_13TeV.167793.Sherpa_CT10_WmunuMassiveCBPt500_CJetVetoBVeto.merge.DAOD_SUSY1.e2822_s1982_s2008_r5787_r5853_p1872/	0.5130	1.07	0.603	199000	601.2
167794	mc14_13TeV.167794.Sherpa_CT10_WtaunuMassiveCBPt500_BFilter.merge.DAOD_SUSY1.e2822_s1982_s2008_r5787_r5853_p1872/	0.5169	1.07	0.119	10000	151.9
167795	mc14_13TeV.167795.Sherpa_CT10_WtaunuMassiveCBPt500_CJetFilterBVeto.merge.DAOD_SUSY1.e2822_s1982_s2008_r5787_r5853_p1872/	0.5136	1.07	0.291	10000	62.5
167796	mc14_13TeV.167796.Sherpa_CT10_WtaunuMassiveCBPt500_CJetVetoBVeto.merge.DAOD_SUSY1.e2822_s1982_s2008_r5787_r5853_p1872/	0.5145	1.07	0.600	40000	121.1
180534	mc14_13TeV.180534.Sherpa_CT10_WenuMassiveCBPt40_70_BFilter.merge.DAOD_SUSY1.e2822_s1982_s2008_r5787_r5853_p1872/	1315.7000	1.07	0.041	350000	6.1
180535	mc14_13TeV.180535.Sherpa_CT10_WenuMassiveCBPt40_70_CJetFilterBVeto.merge.DAOD_SUSY1.e2822_s1982_s2008_r5787_r5853_p1872/	1316.8000	1.07	0.191	347500	1.3
180536	mc14_13TeV.180536.Sherpa_CT10_WenuMassiveCBPt40_70_CJetVetoBVeto.merge.DAOD_SUSY1.e2822_s1982_s2008_r5787_r5853_p1872/	1312.7000	1.07	0.767	499000	0.5
180537	mc14_13TeV.180537.Sherpa_CT10_WmunuMassiveCBPt40_70_BFilter.merge.DAOD_SUSY1.e2822_s1982_s2008_r5787_r5853_p1872/	1311.0000	1.07	0.041	10000	0.2
180538	mc14_13TeV.180538.Sherpa_CT10_WmunuMassiveCBPt40_70_CJetFilterBVeto.merge.DAOD_SUSY1.e2822_s1982_s2008_r5787_r5853_p1872/	1302.1000	1.07	0.184	10000	0.0
180539	mc14_13TeV.180539.Sherpa_CT10_WmunuMassiveCBPt40_70_CJetVetoBVeto.merge.DAOD_SUSY1.e2822_s1982_s2008_r5787_r5853_p1872/	1323.8000	1.07	0.772	40000	0.0
180540	mc14_13TeV.180540.Sherpa_CT10_WtaunuMassiveCBPt40_70_BFilter.merge.DAOD_SUSY1.e2822_s1982_s2008_r5787_r5853_p1872/	1316.1000	1.07	0.041	995000	17.2
180541	mc14_13TeV.180541.Sherpa_CT10_WtaunuMassiveCBPt40_70_CJetFilterBVeto.merge.DAOD_SUSY1.e2822_s1982_s2008_r5787_r5853_p1872/	1314.2000	1.07	0.189	349500	1.3
180542	mc14_13TeV.180542.Sherpa_CT10_WtaunuMassiveCBPt40_70_CJetVetoBVeto.merge.DAOD_SUSY1.e2822_s1982_s2008_r5787_r5853_p1872/	1314.4000	1.07	0.769	349000	0.3

Table 2: List of simulated samples for top-related background processes as well as W+jets. The dataset ID, the generator cross-section σ, the k-Factor, the generator filter efficiency ϵ_{filter}, the total number of generated events N_{gen} and the equivalent luminosity (L_{equiv}) are shown.

datasetID	Sample name	σ [pb]	k-Factor	ϵ_{filter}	N_{gen}	L_{equiv}
167749	mc14_13TeV.167749.Sherpa_CT10_ZeeMassiveCBPt0_BFilter.merge.DAOD_SUSY1.e2798_s1982_s2008_r5787_r5853_p1872/	1928.9000	1.09	0.038	500000	6.3
167750	mc14_13TeV.167750.Sherpa_CT10_ZeeMassiveCBPt0_CFilterBVeto.merge.DAOD_SUSY1.e2798_s1982_s2008_r5787_r5853_p1872/	1926.8000	1.09	0.328	149500	0.2
167751	mc14_13TeV.167751.Sherpa_CT10_ZeeMassiveCBPt0_CVetoBVeto.merge.DAOD_SUSY1.e2798_s1982_s2008_r5787_r5853_p1872/	1938.8000	1.09	0.636	150000	0.1
167752	mc14_13TeV.167752.Sherpa_CT10_ZmumuMassiveCBPt0_BFilter.merge.DAOD_SUSY1.e2798_s1982_s2008_r5787_r5853_p1872/	1929.9000	1.09	0.038	499500	6.2
167753	mc14_13TeV.167753.Sherpa_CT10_ZmumuMassiveCBPt0_CFilterBVeto.merge.DAOD_SUSY1.e2798_s1982_s2008_r5787_r5853_p1872/	1927.0000	1.09	0.326	150000	0.2
167754	mc14_13TeV.167754.Sherpa_CT10_ZmumuMassiveCBPt0_CVetoBVeto.merge.DAOD_SUSY1.e2798_s1982_s2008_r5787_r5853_p1872/	1936.4000	1.09	0.636	150000	0.1
167755	mc14_13TeV.167755.Sherpa_CT10_ZtautauMassiveCBPt0_BFilter.merge.DAOD_SUSY1.e2798_s1982_s2008_r5787_r5853_p1872/	1929.7000	1.09	0.038	499500	6.2
167756	mc14_13TeV.167756.Sherpa_CT10_ZtautauMassiveCBPt0_CFilterBVeto.merge.DAOD_SUSY1.e2798_s1982_s2008_r5787_r5853_p1872/	1928.4000	1.09	0.327	150000	0.2
167757	mc14_13TeV.167757.Sherpa_CT10_ZtautauMassiveCBPt0_CVetoBVeto.merge.DAOD_SUSY1.e2798_s1982_s2008_r5787_r5853_p1872/	1925.5000	1.09	0.634	149500	0.1
167797	mc14_13TeV.167797.Sherpa_CT10_ZeeMassiveCBPt70_140_BFilter.merge.DAOD_SUSY1.e2798_s1982_s2008_r5787_r5853_p1872/	66.7490	1.09	0.102	300000	40.4
167798	mc14_13TeV.167798.Sherpa_CT10_ZeeMassiveCBPt70_140_CFilterBVeto.merge.DAOD_SUSY1.e2798_s1982_s2008_r5787_r5853_p1872/	66.8320	1.09	0.394	99500	3.5
167799	mc14_13TeV.167799.Sherpa_CT10_ZeeMassiveCBPt70_140_CVetoBVeto.merge.DAOD_SUSY1.e2798_s1982_s2008_r5787_r5853_p1872/	66.7900	1.09	0.505	100000	2.7
167800	mc14_13TeV.167800.Sherpa_CT10_ZmumuMassiveCBPt70_140_BFilter.merge.DAOD_SUSY1.e2798_s1982_s2008_r5787_r5853_p1872/	66.7440	1.09	0.102	299500	40.4
167801	mc14_13TeV.167801.Sherpa_CT10_ZmumuMassiveCBPt70_140_CFilterBVeto.merge.DAOD_SUSY1.e2798_s1982_s2008_r5787_r5853_p1872/	66.6270	1.09	0.395	100000	3.5
167802	mc14_13TeV.167802.Sherpa_CT10_ZmumuMassiveCBPt70_140_CVetoBVeto.merge.DAOD_SUSY1.e2798_s1982_s2008_r5787_r5853_p1872/	66.9090	1.09	0.506	99500	2.7
167803	mc14_13TeV.167803.Sherpa_CT10_ZtautauMassiveCBPt70_140_BFilter.merge.DAOD_SUSY1.e2798_s1982_s2008_r5787_r5853_p1872/	66.8420	1.09	0.102	299500	40.3
167804	mc14_13TeV.167804.Sherpa_CT10_ZtautauMassiveCBPt70_140_CFilterBVeto.merge.DAOD_SUSY1.e2798_s1982_s2008_r5787_r5853_p1872/	66.8820	1.09	0.393	99500	3.5
167805	mc14_13TeV.167805.Sherpa_CT10_ZtautauMassiveCBPt70_140_CVetoBVeto.merge.DAOD_SUSY1.e2798_s1982_s2008_r5787_r5853_p1872/	66.9950	1.09	0.506	100000	2.7
167809	mc14_13TeV.167809.Sherpa_CT10_ZeeMassiveCBPt140_280_BFilter.merge.DAOD_SUSY1.e2798_s1982_s2008_r5787_r5853_p1872/	10.6360	1.09	0.118	200000	146.2
167810	mc14_13TeV.167810.Sherpa_CT10_ZeeMassiveCBPt140_280_CFilterBVeto.merge.DAOD_SUSY1.e2798_s1982_s2008_r5787_r5853_p1872/	10.6210	1.09	0.407	50000	10.6
167811	mc14_13TeV.167811.Sherpa_CT10_ZeeMassiveCBPt140_280_CVetoBVeto.merge.DAOD_SUSY1.e2798_s1982_s2008_r5787_r5853_p1872/	10.6170	1.09	0.473	50000	9.1
167812	mc14_13TeV.167812.Sherpa_CT10_ZmumuMassiveCBPt140_280_BFilter.merge.DAOD_SUSY1.e2798_s1982_s2008_r5787_r5853_p1872/	10.6290	1.09	0.118	199500	145.9
167813	mc14_13TeV.167813.Sherpa_CT10_ZmumuMassiveCBPt140_280_CFilterBVeto.merge.DAOD_SUSY1.e2798_s1982_s2008_r5787_r5853_p1872/	10.6500	1.09	0.411	50000	10.5
167814	mc14_13TeV.167814.Sherpa_CT10_ZmumuMassiveCBPt140_280_CVetoBVeto.merge.DAOD_SUSY1.e2798_s1982_s2008_r5787_r5853_p1872/	10.6750	1.09	0.476	50000	9.0
167815	mc14_13TeV.167815.Sherpa_CT10_ZtautauMassiveCBPt140_280_BFilter.merge.DAOD_SUSY1.e2798_s1982_s2008_r5787_r5853_p1872/	10.6260	1.09	0.118	200000	146.3
167816	mc14_13TeV.167816.Sherpa_CT10_ZtautauMassiveCBPt140_280_CFilterBVeto.merge.DAOD_SUSY1.e2798_s1982_s2008_r5787_r5853_p1872/	10.6270	1.09	0.409	50000	10.6
167817	mc14_13TeV.167817.Sherpa_CT10_ZtautauMassiveCBPt140_280_CVetoBVeto.merge.DAOD_SUSY1.e2798_s1982_s2008_r5787_r5853_p1872/	10.6690	1.09	0.475	50000	9.1
167821	mc14_13TeV.167821.Sherpa_CT10_ZeeMassiveCBPt280_500_BFilter.merge.DAOD_SUSY1.e2798_s1982_s2008_r5787_r5853_p1872/	0.8306	1.09	0.134	99000	816.0
167822	mc14_13TeV.167822.Sherpa_CT10_ZeeMassiveCBPt280_500_CFilterBVeto.merge.DAOD_SUSY1.e2798_s1982_s2008_r5787_r5853_p1872/	0.8350	1.09	0.423	40000	103.9
167823	mc14_13TeV.167823.Sherpa_CT10_ZeeMassiveCBPt280_500_CVetoBVeto.merge.DAOD_SUSY1.e2798_s1982_s2008_r5787_r5853_p1872/	0.8326	1.09	0.445	40000	99.0
167824	mc14_13TeV.167824.Sherpa_CT10_ZmumuMassiveCBPt280_500_BFilter.merge.DAOD_SUSY1.e2798_s1982_s2008_r5787_r5853_p1872/	0.8309	1.09	0.133	100000	830.2
167825	mc14_13TeV.167825.Sherpa_CT10_ZmumuMassiveCBPt280_500_CFilterBVeto.merge.DAOD_SUSY1.e2798_s1982_s2008_r5787_r5853_p1872/	0.8321	1.09	0.425	40000	103.8
167826	mc14_13TeV.167826.Sherpa_CT10_ZmumuMassiveCBPt280_500_CVetoBVeto.merge.DAOD_SUSY1.e2798_s1982_s2008_r5787_r5853_p1872/	0.8351	1.09	0.445	40000	98.7
167827	mc14_13TeV.167827.Sherpa_CT10_ZtautauMassiveCBPt280_500_BFilter.merge.DAOD_SUSY1.e2798_s1982_s2008_r5787_r5853_p1872/	0.8314	1.09	0.133	99500	825.5
167828	mc14_13TeV.167828.Sherpa_CT10_ZtautauMassiveCBPt280_500_CFilterBVeto.merge.DAOD_SUSY1.e2798_s1982_s2008_r5787_r5853_p1872/	0.8334	1.09	0.424	40000	103.9
167829	mc14_13TeV.167829.Sherpa_CT10_ZtautauMassiveCBPt280_500_CVetoBVeto.merge.DAOD_SUSY1.e2798_s1982_s2008_r5787_r5853_p1872/	0.8301	1.09	0.443	40000	99.8
167833	mc14_13TeV.167833.Sherpa_CT10_ZeeMassiveCBPt500_BFilter.merge.DAOD_SUSY1.e2798_s1982_s2008_r5787_r5853_p1872/	0.0684	1.09	0.146	9500	872.7
167834	mc14_13TeV.167834.Sherpa_CT10_ZeeMassiveCBPt500_CFilterBVeto.merge.DAOD_SUSY1.e2798_s1982_s2008_r5787_r5853_p1872/	0.0684	1.09	0.434	10000	309.0
167835	mc14_13TeV.167835.Sherpa_CT10_ZeeMassiveCBPt500_CVetoBVeto.merge.DAOD_SUSY1.e2798_s1982_s2008_r5787_r5853_p1872/	0.0685	1.09	0.419	40000	1278.6
167836	mc14_13TeV.167836.Sherpa_CT10_ZmumuMassiveCBPt500_BFilter.merge.DAOD_SUSY1.e2798_s1982_s2008_r5787_r5853_p1872/	0.0683	1.09	0.144	10000	932.8
167837	mc14_13TeV.167837.Sherpa_CT10_ZmumuMassiveCBPt500_CFilterBVeto.merge.DAOD_SUSY1.e2798_s1982_s2008_r5787_r5853_p1872/	0.0690	1.09	0.441	10000	301.5
167838	mc14_13TeV.167838.Sherpa_CT10_ZmumuMassiveCBPt500_CVetoBVeto.merge.DAOD_SUSY1.e2798_s1982_s2008_r5787_r5853_p1872/	0.0687	1.09	0.417	40000	1281.0
167839	mc14_13TeV.167839.Sherpa_CT10_ZtautauMassiveCBPt500_BFilter.merge.DAOD_SUSY1.e2798_s1982_s2008_r5787_r5853_p1872/	0.0685	1.09	0.144	10000	930.1
167840	mc14_13TeV.167840.Sherpa_CT10_ZtautauMassiveCBPt500_CFilterBVeto.merge.DAOD_SUSY1.e2798_s1982_s2008_r5787_r5853_p1872/	0.0688	1.09	0.441	10000	302.4
167841	mc14_13TeV.167841.Sherpa_CT10_ZtautauMassiveCBPt500_CVetoBVeto.merge.DAOD_SUSY1.e2798_s1982_s2008_r5787_r5853_p1872/	0.0679	1.09	0.415	40000	1302.3

Table 3: List of simulated samples for $Z \rightarrow \ell\ell$+jets. The dataset ID, the generator cross-section σ, the k-Factor, the generator filter efficiency ϵ_{filter}, the total number of generated events N_{gen} and the equivalent luminosity (L_{equiv}) are shown.

datasetID	Sample name	σ [pb]	k-Factor	ϵ_{filter}	N_{gen}	L_{equiv}
187150	mc14_13TeV.187150.PowhegPythia8_AU2CT10_WpWm_ee.merge.DAOD_SUSY1.e3059_s1982_s2008_r5787_r5853_p1872/	1.1792	1.00	1.000	100000	84.8
187151	mc14_13TeV.187151.PowhegPythia8_AU2CT10_WpWm_mue.merge.DAOD_SUSY1.e3059_s1982_s2008_r5787_r5853_p1872/	1.1790	1.00	1.000	200000	169.6
187152	mc14_13TeV.187152.PowhegPythia8_AU2CT10_WpWm_taue.merge.DAOD_SUSY1.e3059_s1982_s2008_r5787_r5853_p1872/	1.1790	1.00	1.000	199500	169.2
187153	mc14_13TeV.187153.PowhegPythia8_AU2CT10_WpWm_emu.merge.DAOD_SUSY1.e3059_s1982_s2008_r5787_r5853_p1872/	1.1790	1.00	1.000	199500	169.2
187154	mc14_13TeV.187154.PowhegPythia8_AU2CT10_WpWm_mumu.merge.DAOD_SUSY1.e3059_s1982_s2008_r5787_r5853_p1872/	1.1792	1.00	1.000	100000	84.8
187155	mc14_13TeV.187155.PowhegPythia8_AU2CT10_WpWm_taumu.merge.DAOD_SUSY1.e3059_s1982_s2008_r5787_r5853_p1872/	1.1790	1.00	1.000	199500	169.2
187156	mc14_13TeV.187156.PowhegPythia8_AU2CT10_WpWm_etau.merge.DAOD_SUSY1.e3059_s1982_s2008_r5787_r5853_p1872/	1.1790	1.00	1.000	198500	168.4
187157	mc14_13TeV.187157.PowhegPythia8_AU2CT10_WpWm_mutau.merge.DAOD_SUSY1.e3059_s1982_s2008_r5787_r5853_p1872/	1.1790	1.00	1.000	194500	165.0
187158	mc14_13TeV.187158.PowhegPythia8_AU2CT10_WpWm_tautau.merge.DAOD_SUSY1.e3059_s1982_s2008_r5787_r5853_p1872/	1.1792	1.00	1.000	100000	84.8
187401	mc14_13TeV.187401.gg2vvPythia8_AU2CT10_WpWmenuenu.merge.DAOD_SUSY1.e3131_s1982_s2008_r5787_r5853_p1872/	0.3981	1.00	1.000	30000	75.4
187402	mc14_13TeV.187402.gg2vvPythia8_AU2CT10_WpWmenumunu.merge.DAOD_SUSY1.e3131_s1982_s2008_r5787_r5853_p1872/	0.3981	1.00	1.000	29500	74.1
187403	mc14_13TeV.187403.gg2vvPythia8_AU2CT10_WpWmenutaunu.merge.DAOD_SUSY1.e3131_s1982_s2008_r5787_r5853_p1872/	0.3981	1.00	1.000	29500	74.1
187404	mc14_13TeV.187404.gg2vvPythia8_AU2CT10_WpWmmunuenu.merge.DAOD_SUSY1.e3131_s1982_s2008_r5787_r5853_p1872/	0.3981	1.00	1.000	30000	75.4
187405	mc14_13TeV.187405.gg2vvPythia8_AU2CT10_WpWmmunumunu.merge.DAOD_SUSY1.e3131_s1982_s2008_r5787_r5853_p1872/	0.3981	1.00	1.000	30000	75.4
187406	mc14_13TeV.187406.gg2vvPythia8_AU2CT10_WpWmmunutaunu.merge.DAOD_SUSY1.e3131_s1982_s2008_r5787_r5853_p1872/	0.3981	1.00	1.000	30000	75.4
187407	mc14_13TeV.187407.gg2vvPythia8_AU2CT10_WpWmtaunuenu.merge.DAOD_SUSY1.e3131_s1982_s2008_r5787_r5853_p1872/	0.3981	1.00	1.000	30000	75.4
187408	mc14_13TeV.187408.gg2vvPythia8_AU2CT10_WpWmtaunumunu.merge.DAOD_SUSY1.e3131_s1982_s2008_r5787_r5853_p1872/	0.3981	1.00	1.000	30000	75.4
187409	mc14_13TeV.187409.gg2vvPythia8_AU2CT10_WpWmtaunutaunu.merge.DAOD_SUSY1.e3131_s1982_s2008_r5787_r5853_p1872/	0.3981	1.00	1.000	30000	75.4
187160	mc14_13TeV.187160.PowhegPythia8_AU2CT10_WmZ_3e_mll0p25_DiLeptonFilter.merge.DAOD_SUSY1.e3059_s1982_s2008_r5787_r5853_p1872/	1.6880	1.00	0.285	198500	412.6
187161	mc14_13TeV.187161.PowhegPythia8_AU2CT10_WmZ_e2mu_mll0p4614_DiLeptonFilter.merge.DAOD_SUSY1.e3059_s1982_s2008_r5787_r5853_p1872/	1.1680	1.00	0.341	158500	398.0
187162	mc14_13TeV.187162.PowhegPythia8_AU2CT10_WmZ_e2tau_mll3p804_DiLeptonFilter.merge.DAOD_SUSY1.e3059_s1982_s2008_r5787_r5853_p1872/	0.2141	1.00	0.163	100000	2865.5
187163	mc14_13TeV.187163.PowhegPythia8_AU2CT10_WmZ_mu2e_mll0p25_DiLeptonFilter.merge.DAOD_SUSY1.e3059_s1982_s2008_r5787_r5853_p1872/	1.7690	1.00	0.286	197500	390.4
187164	mc14_13TeV.187164.PowhegPythia8_AU2CT10_WmZ_3mu_mll0p4614_DiLeptonFilter.merge.DAOD_SUSY1.e3059_s1982_s2008_r5787_r5853_p1872/	1.1510	1.00	0.342	199500	506.8
187165	mc14_13TeV.187165.PowhegPythia8_AU2CT10_WmZ_mu2tau_mll3p804_DiLeptonFilter.merge.DAOD_SUSY1.e3059_s1982_s2008_r5787_r5853_p1872/	0.2141	1.00	0.164	100000	2848.0
187166	mc14_13TeV.187166.PowhegPythia8_AU2CT10_WmZ_tau2e_mll0p25_DiLeptonFilter.merge.DAOD_SUSY1.e3059_s1982_s2008_r5787_r5853_p1872/	1.7690	1.00	0.147	99500	382.6
187167	mc14_13TeV.187167.PowhegPythia8_AU2CT10_WmZ_tau2mu_mll0p4614_DiLeptonFilter.merge.DAOD_SUSY1.e3059_s1982_s2008_r5787_r5853_p1872/	1.1680	1.00	0.185	98500	455.8
187168	mc14_13TeV.187168.PowhegPythia8_AU2CT10_WmZ_3tau_mll3p804_DiLeptonFilter.merge.DAOD_SUSY1.e3059_s1982_s2008_r5787_r5853_p1872/	0.2104	1.00	0.060	100000	7921.4
187170	mc14_13TeV.187170.PowhegPythia8_AU2CT10_WpZ_3e_mll0p25_DiLeptonFilter.merge.DAOD_SUSY1.e3059_s1982_s2008_r5787_r5853_p1872/	2.3540	1.00	0.272	198500	310.0
187171	mc14_13TeV.187171.PowhegPythia8_AU2CT10_WpZ_e2mu_mll0p4614_DiLeptonFilter.merge.DAOD_SUSY1.e3059_s1982_s2008_r5787_r5853_p1872/	1.5590	1.00	0.326	199500	392.5
187172	mc14_13TeV.187172.PowhegPythia8_AU2CT10_WpZ_e2tau_mll3p804_DiLeptonFilter.merge.DAOD_SUSY1.e3059_s1982_s2008_r5787_r5853_p1872/	0.3129	1.00	0.164	100000	1948.7
187173	mc14_13TeV.187173.PowhegPythia8_AU2CT10_WpZ_mu2e_mll0p25_DiLeptonFilter.merge.DAOD_SUSY1.e3059_s1982_s2008_r5787_r5853_p1872/	2.3710	1.00	0.272	198000	307.0
187174	mc14_13TeV.187174.PowhegPythia8_AU2CT10_WpZ_3mu_mll0p4614_DiLeptonFilter.merge.DAOD_SUSY1.e3059_s1982_s2008_r5787_r5853_p1872/	1.5910	1.00	0.327	199500	383.5
187175	mc14_13TeV.187175.PowhegPythia8_AU2CT10_WpZ_mu2tau_mll3p804_DiLeptonFilter.merge.DAOD_SUSY1.e3059_s1982_s2008_r5787_r5853_p1872/	0.3129	1.00	0.163	99500	1950.9
187176	mc14_13TeV.187176.PowhegPythia8_AU2CT10_WpZ_tau2e_mll0p25_DiLeptonFilter.merge.DAOD_SUSY1.e3059_s1982_s2008_r5787_r5853_p1872/	2.3710	1.00	0.138	100000	305.6
187177	mc14_13TeV.187177.PowhegPythia8_AU2CT10_WpZ_tau2mu_mll0p4614_DiLeptonFilter.merge.DAOD_SUSY1.e3059_s1982_s2008_r5787_r5853_p1872/	1.5590	1.00	0.174	100000	368.6
187178	mc14_13TeV.187178.PowhegPythia8_AU2CT10_WpZ_3tau_mll3p804_DiLeptonFilter.merge.DAOD_SUSY1.e3059_s1982_s2008_r5787_r5853_p1872/	0.3081	1.00	0.060	99500	5382.5
187180	mc14_13TeV.187180.PowhegPythia8_AU2CT10_ZZ_4e_mll4_DiLeptonFilter.merge.DAOD_SUSY1.e3059_s1982_s2008_r5787_r5853_p1872/	0.1324	1.00	0.919	293500	2412.2
187181	mc14_13TeV.187181.PowhegPythia8_AU2CT10_ZZ_2e2mu_mll4_DiLeptonFilter.merge.DAOD_SUSY1.e3059_s1982_s2008_r5787_r5853_p1872/	0.2961	1.00	0.849	294500	1171.5
187182	mc14_13TeV.187182.PowhegPythia8_AU2CT10_ZZ_2e2tau_mll4_DiLeptonFilter.merge.DAOD_SUSY1.e3059_s1982_s2008_r5787_r5853_p1872/	0.2961	1.00	0.609	300000	1663.7
187183	mc14_13TeV.187183.PowhegPythia8_AU2CT10_ZZ_4mu_mll4_DiLeptonFilter.merge.DAOD_SUSY1.e3059_s1982_s2008_r5787_r5853_p1872/	0.1324	1.00	0.923	300000	2454.9
187184	mc14_13TeV.187184.PowhegPythia8_AU2CT10_ZZ_2mu2tau_mll4_DiLeptonFilter.merge.DAOD_SUSY1.e3059_s1982_s2008_r5787_r5853_p1872/	0.2961	1.00	0.616	299500	1642.0
187185	mc14_13TeV.187185.PowhegPythia8_AU2CT10_ZZ_4tau_mll4_DiLeptonFilter.merge.DAOD_SUSY1.e3059_s1982_s2008_r5787_r5853_p1872/	0.1324	1.00	0.113	300000	20051.9
187186	mc14_13TeV.187186.PowhegPythia8_AU2CT10_ZZ_2e2nu_mll4.merge.DAOD_SUSY1.e3059_s1982_s2008_r5787_r5853_p1872/	0.1032	1.00	1.000	100000	969.0
187187	mc14_13TeV.187187.PowhegPythia8_AU2CT10_ZZ_2mu2nu_mll4.merge.DAOD_SUSY1.e3059_s1982_s2008_r5787_r5853_p1872/	0.1032	1.00	1.000	100000	969.0
187188	mc14_13TeV.187188.PowhegPythia8_AU2CT10_ZZ_2tau2nu_mll4.merge.DAOD_SUSY1.e3059_s1982_s2008_r5787_r5853_p1872/	0.1032	1.00	1.000	99500	964.1
200920	mc14_13TeV.200920.Sherpa_CT10_llll.merge.DAOD_SUSY1.e3213_s1982_s2008_r5787_r5853_p1872/	1.0467	1.00	1.000	1000000	955.4
200982	mc14_13TeV.200982.Sherpa_CT10_lllvjj_EW6.merge.DAOD_SUSY1.e3618_s1982_s2008_r5787_r5853_p1872/	0.04184	1.00	1.000	99500	2378.1
200983	mc14_13TeV.200983.Sherpa_CT10_llljj_EW6.merge.DAOD_SUSY1.e3618_s1982_s2008_r5787_r5853_p1872/	0.01307	1.00	1.000	96000	7345.1
200922	mc14_13TeV.200922.Sherpa_CT10_llvv.merge.DAOD_SUSY1.e3213_s1982_s2008_r5787_r5853_p1872/	13.8200	1.00	1.000	4972000	359.8
200980	mc14_13TeV.200980.Sherpa_CT10_llvvjj_ss_EW4.merge.DAOD_SUSY1.e3618_s1982_s2008_r5787_r5853_p1872/	0.02595	1.00	1.000	100000	3853.6
200981	mc14_13TeV.200981.Sherpa_CT10_llvvjj_ss_EW6.merge.DAOD_SUSY1.e3618_s1982_s2008_r5787_r5853_p1872/	0.04295	1.00	1.000	100000	2328.3

Table 4: List of simulated samples for di-boson background processes. The dataset ID, the generator cross-section σ, the k-Factor, the generator filter efficiency ϵ_{filter}, the total number of generated events N_{gen} and the equivalent luminosity (L_{equiv}) are shown.

4 Object definition

This section presents the definition of the objects used in the analysis: jets, electrons, muons and $E_{\mathrm{T}}^{\mathrm{miss}}$. Unless otherwise stated, the recommendations implemented in SUSYTools-00-05-00-26 tag and analysis release Base,2.0.30 are used for all the objects.

4.1 Jets

The jet selection is summarized in Table 5. Jets are reconstructed using the anti-k_t jet algorithm [49] with the distance parameter R set to 0.4 and topological clusters as input. Jets are calibrated with local cluster weighting LCW+JES scheme, which classifies topological clusters as either being of electromagnetic or hadronic origin, and based on this applies energy corrections derived from Monte Carlo simulation.

The jets are kept only if they have $p_{\mathrm{T}} > 20$ GeV and lie within $|\eta| < 2.8$. In order to remove events with fake $E_{\mathrm{T}}^{\mathrm{miss}}$, an event is vetoed when a jet with quality judged as bad in `VeryLoose` criterion is present.

Table 5: Summary of the jet selection criteria. The signal jet requirements are applied on top of the preselection.

Pre-selected jet	
Collection	AntiKt4LCTopoJets
Acceptance	$p_{\mathrm{T}} > 20$ GeV, $\|\eta\| < 2.8$
Overlap	$\Delta R(jet, e) > 0.2$
b-jets	
Acceptance	$p_{\mathrm{T}} > 20$ GeV, $\|\eta\| < 2.5$
b-tagging	MV1 algorithm 70% OP

4.1.1 Jet Vertex Fraction

During Run-1, in many analyses a Jet Vertex Fraction (JVF) cut was applied to jets with $p_{\mathrm{T}} < 50$ GeV and $|\eta| < 2.4$ to mitigate the effects of pileup. JVF is reported to be buggy in DC14 samples due to lacking a proper track selection for the computation of this variable. Figure 6 shows the distribution of JVF as a function of the ΔR between the jet and the nearest truth jet originated from the hard scattering for jets with $p_{\mathrm{T}} < 50$ GeV and $|\eta| < 2.4$ in a DC14 $t\bar{t}+W$ sample. Despite the technical problem mention above, most of the reconstructed jets not originated from the hard scattering have JVF<0.5. Nevertheless, the distribution for jets well matched to truth jets is very flat, and applying a cut on JVF would lead to low efficiency on jets originated from the hard scattering.

4.1.2 *b*-tagging

Tagging of jets is done using the MV1 algorithm as included in DC14 with the 70% efficiency operating point. This algorithm is based on a neural network using the output weights of the JetFitter+IP3D, IP3D and SV1 algorithms as input.

Note that MV1 will be superseded by MV2c in MC15 productions (release 20), with better background rejection and signal efficiency. The Flavor Tagging CP group also recently released 20-like (p_{T},

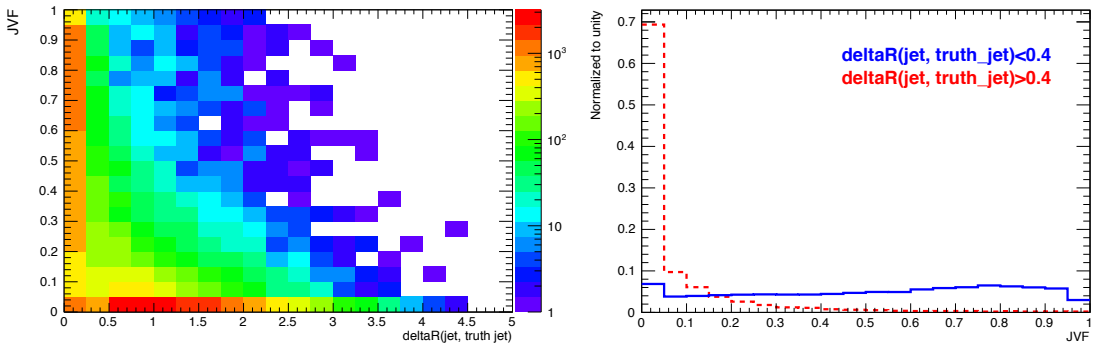

Figure 6: On the left, jet vertex fraction as a function of the distance between the reconstructed jet and the nearest truth jet originated from the hard scattering in a $t\bar{t}+W$ sample. On the right, jet vertex fraction distribution for jets with ΔR values below and above 0.4. Only jets with $p_{\mathrm{T}} < 50$ GeV and $|\eta| < 2.4$ are included in the plots.

η) efficiency and mis-tag maps obtained from $t\bar{t}$ to be used in DC14 samples, which could not be used for this note due to lack of time.

4.2 Leptons

This section summarizes the electron and muon object selection, as well as developments done in the optimization of the lepton isolation and electron acceptance cuts.

4.2.1 Electrons

The electron selection is summarized in Table 6. The Egamma CP group recommends the likelihood-based electron identification [50] for Run-2, since it provides a factor of two better background rejection than the cut-based identification. Four working points (`VeryLooseLLH`, `LooseLLH`, `MediumLLH`, `TightLLH`) are available for LLH electrons.

Pre-selected electrons must satisfy the `LooseLLH` requirements defined by the Egamma group and have $E_{\mathrm{T}} > 10$ GeV and $|\eta| < 2.47$. Signal electrons are additionally required to pass the isolation cuts defined in 4.2.3 as well as the `TightLLH` identification criteria.

A multiplicative event weight is applied for each selected electron to the overall event weight in order to correct for differences in efficiency between data and MC as recommended by the Egamma group.

4.2.2 Muons

The muon selection is summarized in Table 6. The Run-2 muon PID is provided by the so-called *third chain*: this has been designed to provide the best performances from Run-1 STACO and MUID chains. The following working points are supported: `Tight`, `Medium`, `Loose` and `VeryLoose`.

Pre-selected muon candidates must pass the `Medium` muon quality cuts and have $p_{\mathrm{T}} > 10$ GeV and $|\eta| < 2.4$. A smearing procedure is applied to the muon p_{T}. A multiplicative event weight is applied for each selected muon to the overall event weight in order to correct for differences in efficiency between data and MC as recommended by the Muon CP group.

Finally, signal muon candidates have been required to pass the isolation cuts defined in 4.2.3.

Note that events with “cosmic” muons, or “Bad” muon are vetoed as described in Section 5.2.

Table 6: Summary of the electron and muon selection criteria. The signal selection requirements are applied on top of the preselection. The lepton-jet isolation requirement is applied after electron-jet overlap removal.

	Pre-selected Electron	**Pre-selected Muon**
Acceptance	$p_{\mathrm{T}} > 10$ GeV, $\lvert\eta^{\mathrm{clust}}\rvert < 2.47$	$p_{\mathrm{T}} > 10$ GeV, $\lvert\eta\rvert < 2.4$
Quality	`LooseLLH`	`xAOD::Muon::Medium`
Impact parameter	$\lvert d_0/\sigma(d_0)\rvert < 5.0$	-
ℓ-jet Isolation	$\Delta R(e, jet) > 0.4$	$\Delta R(\mu, jet) > 0.4$
	Signal Electron	**Signal Muon**
Quality	`TightLLH`	-
Track Isolation	ptvarcone20/p_{T}<0.06	ptvarcone30/$p_{\mathrm{T}} < 0.06$
Calorimeter Isolation	topoetcone20/p_{T}<0.06	-
Impact parameter	$\lvert z_0 \cdot sin(\theta)\rvert < 0.4$ mm $\lvert d_0/\sigma(d_0)\rvert < 3.0$	$\lvert z_0 \cdot sin(\theta)\rvert < 0.4$ mm $\lvert d_0/\sigma(d_0)\rvert < 3.0$

4.2.3 Lepton isolation

The lepton isolation variables contained a number of bugs/issues in the DC14 xAOD productions, which made them unusable for analysis. In particular, track isolation variables lacked a proper track selection (eg: z_0 selection), and calorimeter isolation variables had missing or wrong p_{T} and pileup corrections. A fix for those problems was provided in the derivation framework cache 19.1.4.5, which made the isolation variables essentially identical to those being developed for release 20.

The isolation variables are provided for three different cone sizes: 0.2 (`cone20`), 0.3 (`cone30`) and 0.4 (`cone40`), and are the following:

- **ptcone**: sum of the p_{T} of tracks in the given cone around the object of interest
- **topoetcone**: sum of transverse energy of the topological energy clusters in the calorimeter in the given cone around the object of interest. Unlike in Run-1, this variable is now available for both electrons and muons.
- **ptvarcone** (known as mini-isolation during Run-1): sum of the p_{T} of tracks in a cone around the object with radius being the smallest between the given cone size or 10 GeV/p_{T}[GeV] (where p_{T} is the p_{T} of the lepton). This definition effectively uses narrower cones for high-p_{T} leptons, for instance ptvarcone30 deviates from ptcone30 only above 33.3 GeV.

Dedicated optimizations were performed about the lepton isolation, exploring track and calorimeter isolation variables with different cone sizes and cut values. Since this analysis is dominated by the non-prompt lepton background, an excellent rejection against this background is needed to keep a good signal sensitivity. This should be balanced with the fact the signal acceptance to SS/3L is typically low due to the leptonic branching ratio of W/Z bosons, and it is therefore also essential to keep the signal efficiency as high as possible.

Optimization procedure For optimization of the isolation variables, the per-lepton efficiency is computed as the ratio of number of leptons passing a given isolation criteria over the total number of leptons. For this ratio, the denominator is defined as all the leptons passing the pre-selection in SS/3L events

defined in Table 6, after applying the same signal lepton impact parameter cuts as in Run-1. The numerator is defined as the number of leptons additionally passing the isolation cuts as well as the electron `MediumLLH`/`TightLLH` identification criteria. The isolation efficiency for non-prompt leptons in a $t\bar{t}$ sample is plotted as function of the efficiency for prompt leptons in signal events for different relative isolation cut values raging from 0 to 0.20 in steps of 0.01.

In addition, a single point corresponding to the Run-1 settings is also shown for comparison. Table 7 shows the details of the isolation criteria used in Run-1. Since some of those variables are not supported anymore, in this study tight++ is replaced by `MediumLLH` for electrons, and etcone by topoetcone in the case of muons.

Table 7: Summary of the signal electron and signal muon selection criteria used in Run-1.

	Run-1 Signal Electron	Run-1 Signal Muon
Quality	`Tight++`	-
Track Isolation	ptcone20/min(p_{T}, 60 GeV) < 0.06	ptcone30/min(p_{T}, 60 GeV) < 0.12
Calorimeter Isolation	topoEtcone20/min(p_{T}, 60 GeV) < 0.06	etcone30/min(p_{T}, 60 GeV) < 0.12
Impact parameter	$\lvert z_0 \cdot sin(\theta)\rvert$ < 0.4 mm $\lvert d_0/\sigma(d_0)\rvert$ < 3.0	$\lvert z_0 \cdot sin(\theta)\rvert$ < 0.4 mm $\lvert d_0/\sigma(d_0)\rvert$ < 3.0

Variable selection for muons Figure 7 shows the isolation efficiency for muons using several variables. As shown, if relying on cone20 variables, both track and calorimeter isolation would be needed to bring the background rejection to levels comparable to those used in Run-1, particularly at muon p_{T} below 40 GeV. On the contrary, using cone30 variables a similar performance as during Run-1 can be achieved even at low p_{T}. In addition, using track isolation can provide larger signal efficiency than a combined track+calo isolation for any given background rejection. Comparing the two possible choices for track isolation, ptvarcone provide about 5% extra signal efficiency for signal at $p_{\mathrm{T}} > 40$ GeV. Therefore, ptvarcone30 is chosen as the only variable to be used for muon isolation due to its good signal efficiency at high p_{T} together with a very good background rejection at low p_{T}.

Variable selection for electrons Figure 8 compares the performances of several isolation cones in the case of electrons. As shown, only combining calorimeter and track isolation and using cone20 variables similar efficiency/rejection performance to that in Run-1 can be achieved.

Figure 9 and 10 compare the performance of the isolation variables including `MediumLLH` and `TightLLH` electron identification. Similar performance is obtained in both cases, although `MediumLLH` (`TightLLH`) offers a slightly larger signal efficiency at the same rejection at $p_{\mathrm{T}} < 60$ GeV ($p_{\mathrm{T}} > 60$ GeV).

Optimization procedure As concluded form the studies above, the variables to use for the optimization of the isolation are ptvarcone30/p_{T} in the case of muons, and ptvarcone20/p_{T} together with topoetcone20/p_{T} and either `MediumLLH` or `TightLLH` for electrons. Appendix A shows the details of the optimization procedure, which takes into account the signal significance for different models for 15 possible isolation definitions. This procedure accounts for many details in background and signal samples: combination of lepton p_{T}, lepton flavour, prompt and non-prompt combinations of leptons, etc. These studies showed that tight isolation criteria were favoured, and therefore the isolation cuts stated in Table 6 will be used for the analysis: ptvarcone30/$p_{\mathrm{T}} < 0.06$ for muons; `TightLLH`, ptvarcone20/p_{T}<0.06 and topoetcone20/p_{T}<0.06 for electrons.

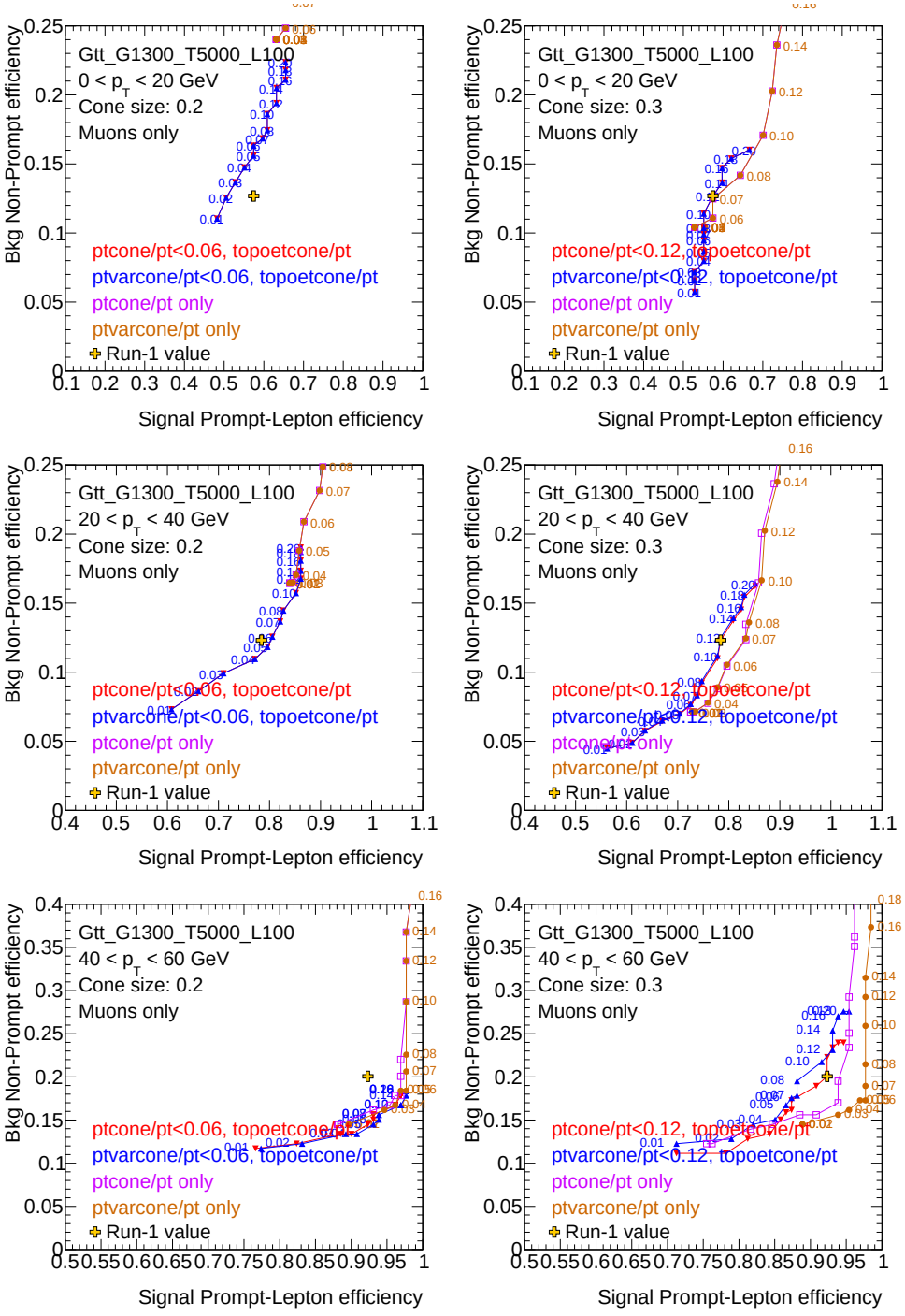

Figure 7: Isolation efficiency for background non-prompt muons as a function of the isolation efficiency for prompt muons in signal events for cone20 variables (left) and cone30 variables (right) in different muon p_{T} bins. Curves are shown for ptcone alone, ptvarcone alone, ptcone combined with topoetcone as well as for ptvarcone combined with topoetcone. In addition, the cross shows the value that would be obtained with settings equivalent to those used during Run-1.

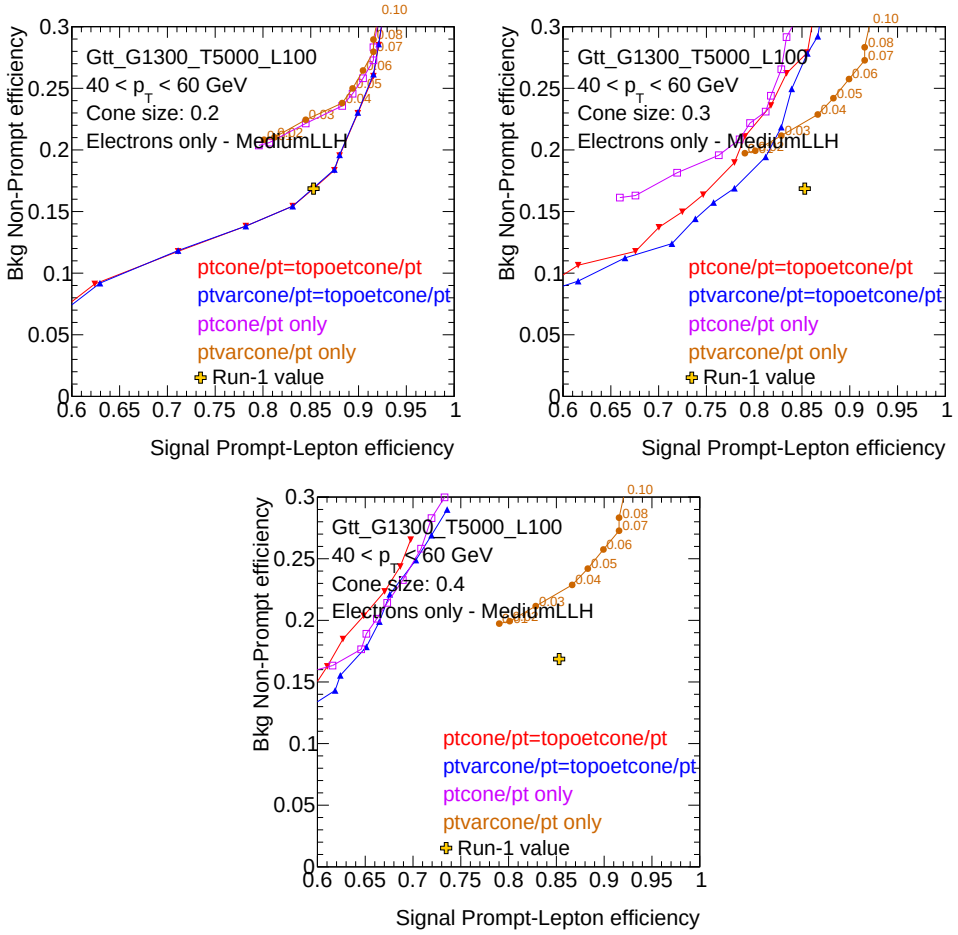

Figure 8: Isolation efficiency for background non-prompt electrons as a function of the isolation efficiency for prompt electrons in signal events for cone20 (left), cone30 variables (center) and cone30 variables (right). Only electrons with $40 < p_{\mathrm{T}} < 60$ GeV are shown. Curves are shown for ptcone alone, ptvarcone alone, ptcone combined with topoetcone as well as for ptvarcone combined with topoetcone. In addition, the cross shows the value that would be obtained with settings equivalent to those used during Run-1.

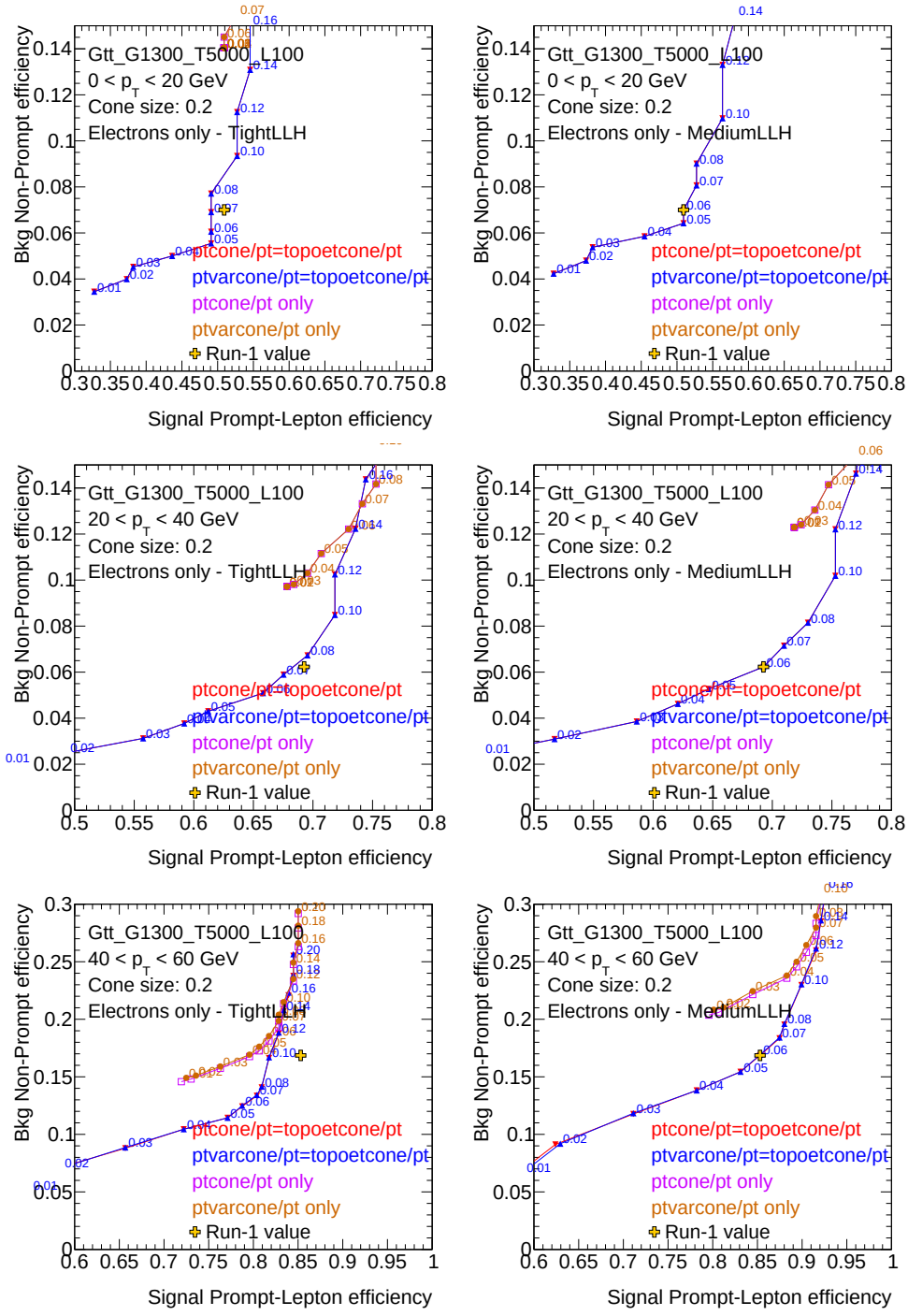

Figure 9: Isolation efficiency for background non-prompt electrons as a function of the isolation efficiency for prompt electrons in signal events for cone20 variables in different electron p_{T} bins. In addition to the isolation cuts, `TightLLH` (left) and `MediumLLH` (right) identification is also applied. Curves are shown for ptcone alone, ptvarcone alone, ptcone combined with topoetcone as well as for ptvarcone combined with topoetcone. In addition, the cross shows the value that would be obtained with settings equivalent to those used during Run-1.

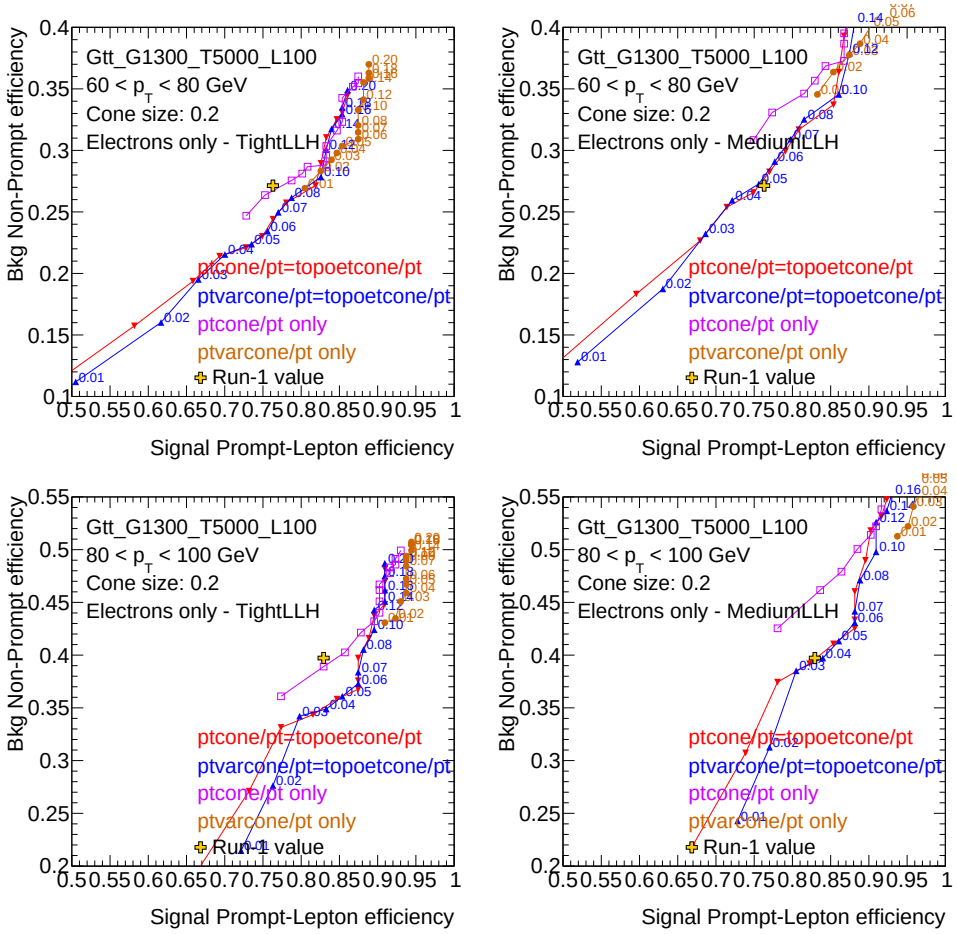

Figure 10: Isolation efficiency for background non-prompt electrons as a function of the isolation efficiency for prompt electrons in signal events for cone20 variables in different electron p_{T} bins. In addition to the isolation cuts, `TightLLH` (left) and `MediumLLH` (right) identification is also applied. Curves are shown for ptcone alone, ptvarcone alone, ptcone combined with topoetcone as well as for ptvarcone combined with topoetcone. In addition, the cross shows the value that would be obtained with settings equivalent to those used during Run-1.

4.2.4 Electron acceptance

Despite not being included in the object selection employed in this note, dedicated studies have been conducted to evaluate the impact of a reduction of the $|\eta|$ coverage for electrons. This is motivated by the fact that the largest contributions from charge-flip and fake-lepton backgrounds are observed at $|\eta| > 2$ and in the LAr crack region ($1.37 < |\eta| < 1.52$).

Table 8 shows the impact on the expected event yields when reducing the electron $|\eta|$ acceptance for the two leading electrons (taking a reference the case of $|\eta| < 2.3$). The event selection applied to compute those numbers requires SS/3L, at least 3 jets with $p_{\mathrm{T}} > 30$ GeV and m_{ee} outside the 84-98 GeV range to reduce the contribution from charge flips.

Table 8: Relative decrease in the event yield when reducing the $|\eta|$ acceptance for the two leading electrons with respect to $|\eta| < 2.3$. The reference is considered to be $|\eta| < 2.47$, and the crack region is excluded in all the cases. Numbers are shown for the event selection described in the text and separately for events with 1 or more b-jets.

	Prompt SS	$t\bar{t} + W$	Gtt (G900_L100)	Non-prompt leptons	Charge flip
$==1b$, $\|\eta\| < 1.37$	14%	16%	12%	28%	69%
$==1b$, $\|\eta\| < 2.0$	5.4%	6%	7%	11%	37%
$==1b$, $\|\eta\| < 2.3$	0.4%	1.5%	4.7%	3.6%	11%
$>1b$, $\|\eta\| < 1.37$	13%	18%	10%	44%	66%
$>1b$, $\|\eta\| < 2.0$	4.3%	6.5%	2.9%	21%	30%
$>1b$, $\|\eta\| < 2.3$	1.3%	1.5%	0.3%	8%	5.8%

As shown, reducing the acceptance to $|\eta| < 2.0$ would reduce the contribution from processes with prompt SS/3L by 6.5% or less, but the reduction in non-prompt leptons (11-21%) and and charge flip (30-37%) is much larger. Also, if reducing the acceptance for the two leading electron to $|\eta| < 1.37$ would reduce the non-prompt and charge flips by 28-44% and ~69%, respectively, with a reduction of only 13-18% in prompt SS/3L processes.

Therefore, this study proves that additional rejection against some of the main backgrounds affecting the analysis can be achieved by reducing the $|\eta|$ acceptance of the electrons, although more work is need to find an optimal selection and minimize the impact on signal efficiency.

4.3 Overlap removal

According to the above definitions, one single final state object can fall in more than one category, being therefore effectively double-counted. For example, one isolated electron is typically reconstructed both as an electron and as a jet. A procedure to remove overlaps between final state objects was therefore put in place, and applied on pre-selected objects. The recommendations by the Harmonization effort [51] have not been applied for this version of the analysis.

First, jets that are angularly close ($\Delta R < 0.2$) to a pre-selected electron are removed from the jet list in the event. Following this, pre-selected electrons (muons) are removed from the electron (muon) list if their distance to the closest jet is $\Delta R < 0.4$. If there are an electron and muon with $\Delta R < 0.1$, it is likely to be the bremsstrahlung of the muon. Such a muon momentum is not measured correctly so that in this case, both an electron and a muon are removed.

4.4 Missing transverse energy

The missing transverse energy ($E_{\mathrm{T}}^{\mathrm{miss}}$) is rebuilt using the xAOD container "MET_RefFinal" as input and using the calibrated electron, muon and jet objects (and baseline taus and photons according to SUSYTools definitions). In this version of the analysis, the calorimeter soft term is used for building the $E_{\mathrm{T}}^{\mathrm{miss}}$ following the defaults in SUSYTools-00-05-00-26.

5 Event selection

5.1 Trigger studies

The trigger strategy for the analysis in Run-2 is similar to the one used in the Run-1 version. There, a combination of $E_{\mathrm{T}}^{\mathrm{miss}}$, single-lepton and di-lepton triggers was used for the selection of events in the signal region and control distributions. The triggers were checked consecutively starting with the $E_{\mathrm{T}}^{\mathrm{miss}}$ trigger, followed by the single lepton trigger and the dilepton triggers, until one of the triggers is passed by the event. Offline cuts on the missing energy and the p_{T} of the triggered objects were applied to ensure to be on the efficiency *plateau* of the corresponding trigger.

For Run-2 the triggers to be used are also missing energy and single- and di-lepton triggers. The lepton trigger menu includes triggers selecting isolated and non-isolated leptons as well as dilepton triggers selecting mixed-flavor lepton events. The following triggers have been regarded as important for this analysis and were used for further studies on performance and efficiency:

- Single-lepton triggers: `HLT_mu26`, `HLT_mu50`, `HLT_mu24_imedium`, `HLT_mu26_imedium`, `HLT_e20_medium`, `HLT_e60_medium`, `HLT_e24_tight_iloose`, `HLT_e26_tight_iloose`
- Di-lepton triggers: `HLT_2m10`, `HLT_2mu14`, `HLT_2e12_loose_L12EM10VH`, `HLT_2e17_loose`, `HLT_e17_loose_mu14`
- Multi-lepton triggers `HLT_3m6`, `HLT_e12_loose_2mu10`
- $E_{\mathrm{T}}^{\mathrm{miss}}$ triggers: `HLT_xe60`, `HLT_xe70`, `HLT_xe100`, `HLT_xe100_cell`

The performance of these triggers has been investigated by running the analysis on dedicated $Z \to \mu\mu$, $Z \to ee$ and $t\bar{t}$ Monte Carlo samples with several trigger applications. For each object triggered, an offline cut on the object p_{T} or the $E_{\mathrm{T}}^{\mathrm{miss}}$ is applied to ensure the full efficiency of the trigger in the selected event. A geometrical ΔR matching between the lepton triggers fired and the signal leptons reconstructed in each event is applied in order to confirm that the according trigger was activated by one of the signal leptons found in the analysis.

5.1.1 Monte Carlo samples and software framework

The trigger studies were performed with the latest available releases of the ATLAS software framework and the latest Monte Carlo productions. The analysis code was setup with the `AnalysisBase` framework (2.3.8 branch for rel.20 ATLAS software). The object selection was done by using the `SUSYTools-00-06-03` package which provides the current recommendations for selection of signal and baseline objetcs.

The Monte Carlo samples used for these studies are validation samples produced with the 20.1.4.3 MC15 ATLAS software release (no pileup).

- $t\bar{t}$ sample:
  `valid3.110401.PowhegPythia_P2012_ttbar_nonallhad.recon.AOD.e3099_s2578_r6540`

- $Z \to \mu\mu$ sample:
  `valid3.167826.Sherpa_CT10_ZmumuMassiveCBPt280_500_CVetoBVeto.recon.AOD.e3099_s2578_r6540`
- $Z \to ee$ sample:
  `valid3.147406.PowhegPythia8_AZNLO_Zee.recon.AOD.e3099_s2578_r6540`

5.1.2 Total event yields

The total event yields for the test MC samples and different trigger configurations was measured. The yields are shown in Fig. 11 for the $t\bar{t}$ Monte Carlo sample and for the $Z \to \mu\mu$, $Z \to ee$ samples respectively. The trigger performance is as expected: while for $Z \to \mu\mu$ Monte Carlo, the muon triggers select most of the events, for $Z \to ee$ the electron triggers do. For $t\bar{t}$ Monte Carlo, the muon- and electron triggers have similar selection rates, and most events are selected by applying $E_{\mathrm{T}}^{\mathrm{miss}}$ triggers.

5.1.3 Efficiencies

The trigger efficiency in Monte Carlo can be obtained by dividing the number of triggered events by the total number of events. The efficiencies have been calculated separately for single-lepton, dilepton triggers and for $E_{\mathrm{T}}^{\mathrm{miss}}$ triggers. The results for some examples are shown in Fig. 12 for single lepton triggers and for dilepton and $E_{\mathrm{T}}^{\mathrm{miss}}$ triggers on Fig. 13. Further efficiency plots can be found in Appendix B. The turn-on curves for the single-lepton and dilepton triggers show the expected evolution. The efficiency at the trigger plateau is between 95% - 98% for single-lepton and around 90% for dilepton triggers. For the $E_{\mathrm{T}}^{\mathrm{miss}}$ trigger, the turn-on is slower with respect to the quoted online threshold. It reaches its efficiency plateau if $E_{\mathrm{T}}^{\mathrm{miss}} > 250$ GeV and the efficiency value in plateau is around 80%.

5.2 Event pre-selection

A sample of two same-sign or three leptons is selected applying the following criteria:

- **Jet Cleaning**: Events are required to pass the `VeryLooseBad` set of cleaning requirements recommended by Jet-$E_{\mathrm{T}}^{\mathrm{miss}}$ group [52] and implemented in the `JetCleaningTool`. An event is rejected if at least one of the pre-selected jets (thus after jet-electron overlap removal) fails the jet quality criteria. The cleaning requirements are intended to remove events where significant energy was deposited in the calorimeters due to instrumental effects such as cosmic rays, beam-induced (non-collision) particles, and noise.
- **Primary Vertex**: events are required to have a primary vertex, that is, one of the reconstructed vertices must be labeled as `xAOD::VxType::PriVtx`. No additional requirements on the number of tracks in the vertex should be applied as recommended by the Tracking CP group [53].
- **Bad Muon Veto**: Events containing at least one pre-selected muon satisfying $\sigma(q/p)/|q/p| > 0.2$ before the overlap removal are rejected.
- **Cosmic Muon Veto**: Events containing a cosmic muon candidate are rejected. Cosmic muon candidates are selected among pre-selected muons, if they fail the requirements $|z_0| < 1.0\,\mathrm{mm}$ and $|d_0| < 0.2\,\mathrm{mm}$, where the longitudinal and transverse impact paramaters z_0 and d_0 are calculated with respect to the primary vertex.
- **At least two leptons**: Events are required to contain at least two signal leptons (see Section 4 and Table 6) with $p_{\mathrm{T}} > 20$ GeV and $p_{\mathrm{T}} > 15$ GeV for the leading and subleading lepton, respectively. If the lepton contains a third lepton with $p_{\mathrm{T}} > 15$ GeV the event is regarded as three-lepton event

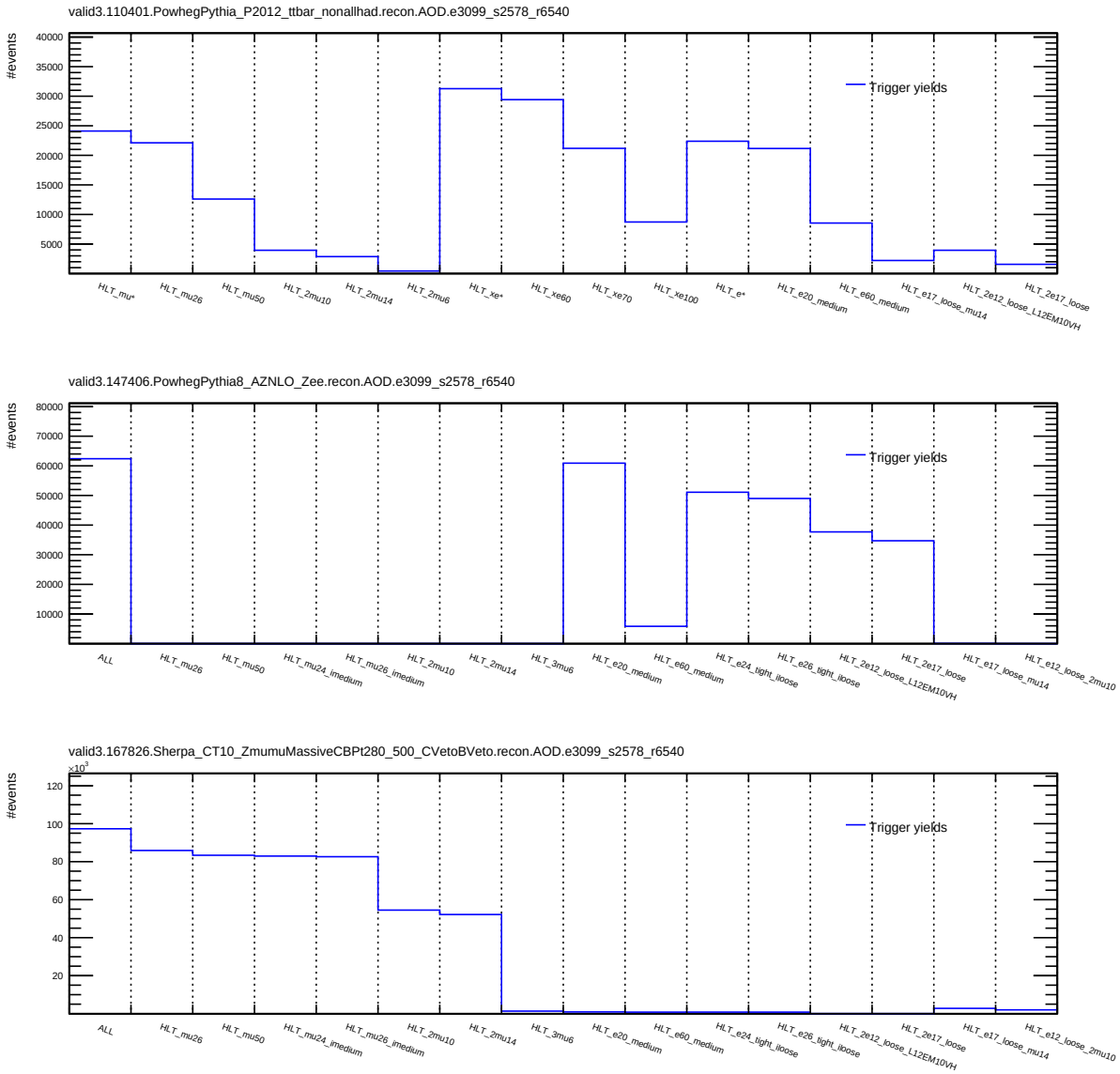

Figure 11: Total event yields for the $t\bar{t}$ sample (top) and for the $Z \to \mu\mu$ (middle), $Z \to ee$ (bottom) samples. On the x-axis the different triggers (or trigger configurations) are shown.

otherwise as a two-lepton event. Once the trigger is fully operative in the MC samples, one or two of the three leptons will be matched to the trigger object if the event is classified as passing a single or dilepton trigger. The data sample obtained is then divided into three channels depending on the flavor of the two leading leptons (ee, $\mu\mu$, $e\mu$).

- **Electron-muon overlap**: For any events containing at least one of each of a signal electron and muon, the event is vetoed if $\Delta R(e,\mu) < 0.1$.

- **Same sign**: If the event is a two-lepton event the two leading leptons have to be of same charge (same-sign).

- **Z-veto**: If the event is a three-lepton event all possible opposite-charge same-flavor lepton combinations are combined to calculate a mass $M_{\ell\ell}$. The event is rejected if one of the calculated mass

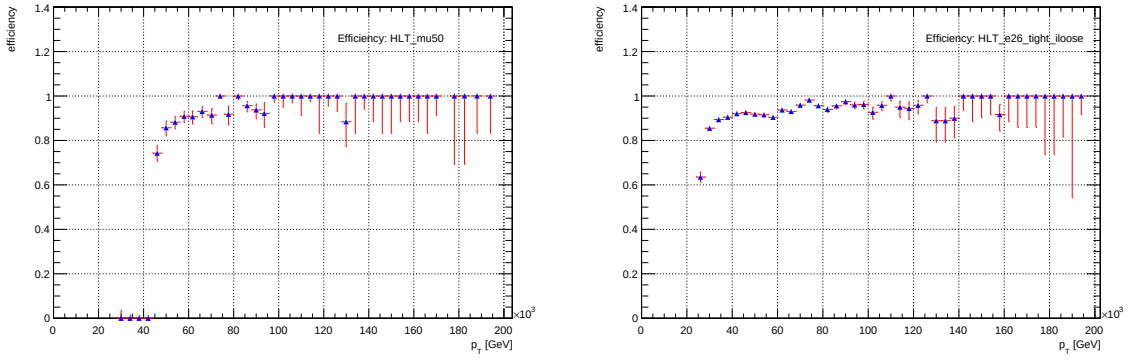

Figure 12: Trigger efficiencies for `HLT_mu50` and `HLT_e26_tight_iloose` versus p_{T} of the leading lepton.

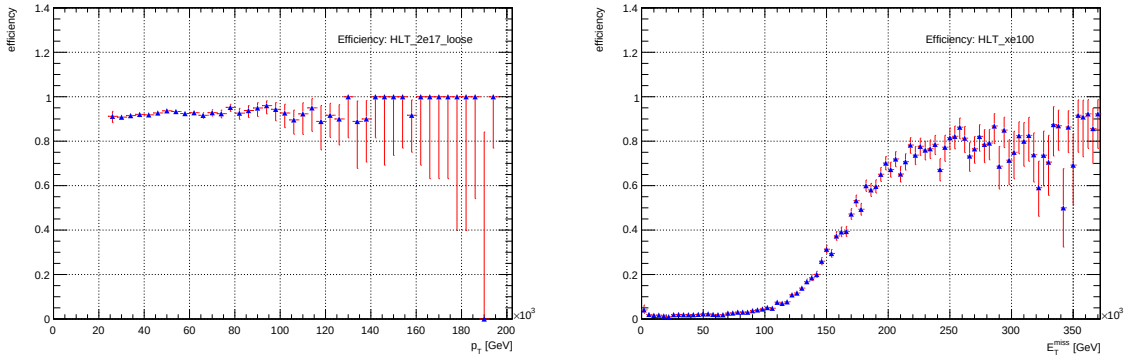

Figure 13: Trigger efficiencies for `HLT_2e17_loose` (left) and `HLT_xe100` (right). The efficiency for the dilepton trigger is plotted against the p_{T} of the leading electron while the efficiency of the $E_{\mathrm{T}}^{\mathrm{miss}}$ trigger is plotted against the corrected missing energy value.

is close to the Z-mass, i.e. $84 < M_{\ell\ell} < 98$ GeV.

- **Invariant mass**: Events with $M_{\ell\ell} < 12$ GeV are rejected to avoid heavy flavor meson resonances. In three-lepton events, the invariant mass $M_{\ell\ell}$ is calculated from the two leading leptons.

The following event variables are also used in the definition of the signal and validation regions in the analysis:

- The inclusive effective mass m_{eff} defined as the scalar sum of the signal leptons p_{T}(see Table 6), all signal jets p_{T} (see Table 5) and $E_{\mathrm{T}}^{\mathrm{miss}}$;
- The transverse mass m_{T} computed from the leading lepton and $E_{\mathrm{T}}^{\mathrm{miss}}$ as $m_{\mathrm{T}} = \sqrt{2 \cdot p_{\mathrm{T}}^{l} \cdot E_{\mathrm{T}}^{\mathrm{miss}} \cdot (1 - cos(\Delta\phi(l, E_{\mathrm{T}}^{\mathrm{miss}})))}$;

6 Signal region definition

6.1 Models already considered in Run-1

Given the high increase in the center of mass energy, and therefore in the background and signal production cross sections, the signal regions used for the Run-1 analysis have to be re-optimized to maximize the sensitivity. Employing a similar methodology as in [15], the optimization is performed for a center-of-mass energy of $\sqrt{s}$ = 13 TeV and a luminosity (L) of 3 fb^{-1}, as a function of the b-jet and lepton multiplicities. The discriminating variables used to separate the signal from the background are $E_{\mathrm{T}}^{\mathrm{miss}}$, m_{eff}, number of jets and leptons, and their p_{T} threshold. In Table 9 the previous defined signal regions are presented, and further used as a benchmark.

Table 9: Definition of the signal regions for the Run-1 two same-sign and three leptons analysis. The cuts for the discovery and exclusion cases are shown separately. For all signal regions, two same-sign or three leptons with p_{T} > [20,15,15] GeV are required. Jets (b-jets) are selected with p_{T} > 40 GeV (20 GeV).

Signal region	N_{lept}	$N^{20}_{b\,jets}$	Signal cuts (exclusion)	Additional cuts (discovery)
SR3b	≥ 2	≥3	$N^{40}_{jets} \geq 5$	m_{eff}>350 GeV
SR1b	==2	≥1	$N^{40}_{jets} \geq 3$, $E_{\mathrm{T}}^{\mathrm{miss}} > 150$ GeV, m_{T}>100 GeV, !SR3b	m_{eff}>700 GeV
SR0b	==2	==0	$N^{40}_{jets} \geq 3$, $E_{\mathrm{T}}^{\mathrm{miss}}$> 150 GeV, m_{T}> 100 GeV	m_{eff}>400 GeV
SR3Lep low $E_{\mathrm{T}}^{\mathrm{miss}}$	≥ 3	-	$N_{jets^{40}} \geq 4$, 50 < $E_{\mathrm{T}}^{\mathrm{miss}}$< 150 GeV, Z $m_{inv m}$ veto, !SR3b	m_{eff}>400 GeV
SR3Lep high $E_{\mathrm{T}}^{\mathrm{miss}}$	≥ 3	-	$N^{40}_{jets} \geq 4$, $E_{\mathrm{T}}^{\mathrm{miss}}$> 150 GeV, !SR3b	m_{eff}>400 GeV

The optimization is performed using as figure of merit the signal discovery significance (Zn). This is calculated with `RooStats::NumberCountingUtils::BinomialObsZ`. This function requires as inputs the observed number of events (equals to SUSY signal plus SM background), the expected SM background events, and the uncertainty on these SM background expectation (40%). For a complete coverage, three different approaches for the lepton selection are considered:

- Inclusive SS leptons: at least two same sign leptons are considered in the event.
- Exclusive SS leptons: exactly two same sign leptons.
- Exclusive three leptons: exactly three leptons.

The cut on number of b-jets in the signal regions is also optimized, and four different cases are studied:

- Inclusive 3 b-jets: at least three b-jets in the event.
- Exclusive 1 b-jet: similarly to Run-1 SR1b. It requires at least one b-jet, and no event with ≥3 b-jets and several jets. The latter cut is considered to mimic a potential SR3b signal region.
- Inclusive 1 b-jet: at least one b-jet and no requirement on the events with three b-jets.
- Exclusive 0 b-jet: no b-jet requirement is considered in the event.

The final signal regions definition is chosen by looking at the signal significance, after comparing the inclusive and exclusive potential signal regions. It is a balance between a high sensitivity and a reduced number of final regions. As a result of the optimization, only four SRs are defined, and presented in Table 10. The signal region with an inclusive lepton selection and at least three b-jets is defined to cover the region of the SUSY phase space with a high gluino mass. For the compressed spectra, an additional

signal region will be defined, as shown in the results section. Compared to the previous signal regions, the combined SR3Lep and the exactly two same sign leptons SR1b or SR0b signal regions are replaced by inclusive same sign leptons SR1b and SR0b. This retains a more simple analysis, suitable to analyze the first data. Two overlapping regions are defined for the selection with no b-jets in the event, and assure a high sensitivity in models with gluino mediated squarks and direct squarks. Sr0b5j is defined for SUSY signatures like gluino pair production via WZ, while SR0b3j for signals like direct squarks via sleptons. If no separation in terms of jet multiplicity is performed, the reached sensitivity is generally decreased by a factor 2 for the studied models. The signal region with at least one b-jet is orthogonal to SR0b5j and SR0b3j, and targets the signatures with 1 or 2 b jets in the cascade decays. When compared to the performance obtained with the Run-1 SRs, an increase in significance is observed (see the results section).

Table 10: Preliminary signal regions definition. The two leading leptons are required to have $p_{\mathrm{T}} > 20$ GeV.

Signal region	N_{lept}	N^{20}_{b-jets}	Other variables
SR3b	≥2	≥3	$N^{40}_{jets} \geq 6$
SR1b	≥2	≥1	$N^{50}_{jets} \geq 4$, $E_{\mathrm{T}}^{\mathrm{miss}} > 150$ GeV, $m_{\mathrm{eff}} > 500$ GeV
SR0b5j	≥2	==0	$N^{50}_{jets} \geq 5$, $E_{\mathrm{T}}^{\mathrm{miss}} > 100$ GeV, $m_{\mathrm{eff}} > 400$ GeV
SR0b3j	≥2	==0	$N^{40}_{jets} \geq 3$, $E_{\mathrm{T}}^{\mathrm{miss}} > 200$ GeV, $m_{\mathrm{eff}} > 400$ GeV

Table 11: Inclusive lepton and b-jets SR1b signal region definition.

Signal region	N_{lept}	N^{20}_{b-jets}	Other variables
SR1b(inclusive)	≥ 2	≥ 1	$N^{40}_{jets} \geq 4$, $E_{\mathrm{T}}^{\mathrm{miss}} > 150$ GeV, $m_{\mathrm{eff}} > 900$ GeV

Inclusive same sign leptons and 1 b-jet signal region

During the optimization, a combined version of Run-1 SR1b and SR3b signal regions was also considered (the inclusive 1 b-jet case presented previously). This study is performed looking at gluino mediated virtual stop and direct sbottom models with RPC and χ^0_1 being the LSP, as generally motivated by *natural SUSY*. The optimization results are pointing to the generally favoured selection presented in Table 11. It requires at least 4 jets, $E_{\mathrm{T}}^{\mathrm{miss}} > 150$ GeV and a tight cut on m_{eff} to reduce the background and increase the sensitivity at high gluino and low LSP masses. The expected fake lepton background is 2.89, while the prompt SS background of 3.38 when considering $L = 3$ fb^{-1}. This region is not suitable in the compressed region of (see Figure 14, where only a significance of 1.4 can be achieved for a mass splitting of 600 GeV between gluino and neutralino), or in the non-excluded region of the direct sbottom model (Figure 15, which is showing one the signal points with larger significance for this model, and it can only reach values of 1.88). The optimization is still work in progress, and the signal region definition might change. Work is ongoing to define a signal region targeting theses regions of the phase space.

6.2 Softer selection with 3b-jets

It was noticed in the 8 TeV signal samples for the gluino stop offshell model with the most compressed mass spectrums, that the signal acceptance could be significantly increased for a similar level of background, by relying on softer jets (20 GeV instead of 40 GeV), but increasing the requirements on the multiplicity (≥ 7 jets was found optimal). We are considering the possibility of implementing such a signal region, which could for example take the form of the jet multiplicity distribution in events with

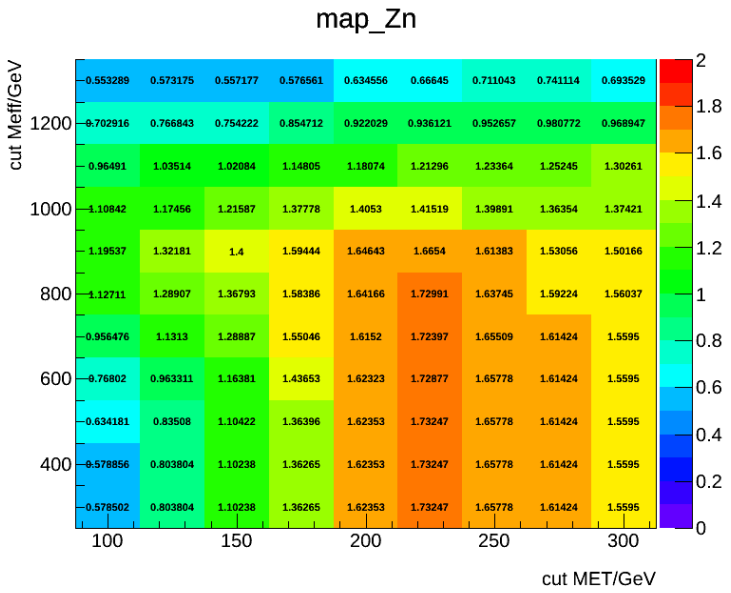

Figure 14: The $E_{\mathrm{T}}^{\mathrm{miss}}$ and m_{eff} cuts optimization. The signal significance (Zn) is calculated for the signal point with a gluino mass of 1300 GeV and LSP mass of 700 GeV (gluino mediated virtual stop model). The event selection requires at least two leptons with p_{T} of [20, 20, 10] GeV, at least 4 jets with $p_{\mathrm{T}} > 40$ GeV and at least one b-jet with $p_{\mathrm{T}} > 20$ GeV. For this point the reached significance with SR1b(inclusive) is 1.4, with a expected signal yield of 5.2 events.

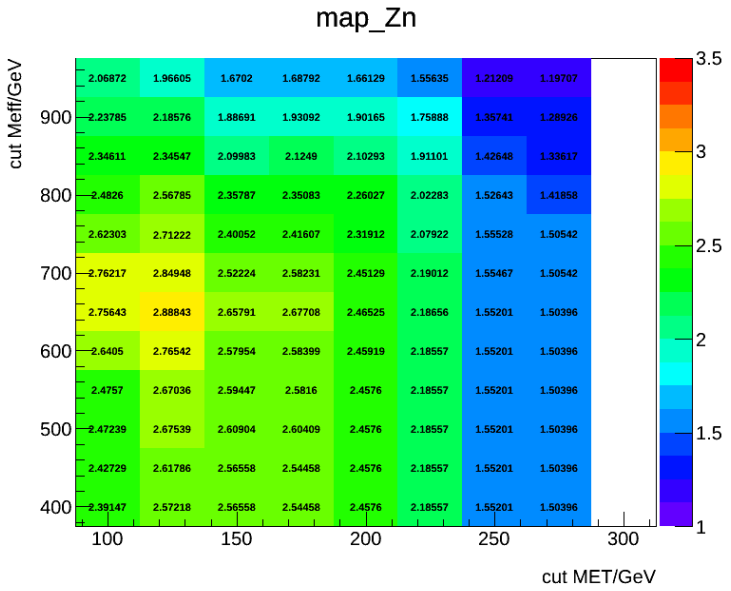

Figure 15: The $E_{\mathrm{T}}^{\mathrm{miss}}$ and m_{eff} cuts optimization. The signal significance (Zn) is calculated for the signal point with a sbottom mass of 550 GeV and $\chi_1^{\pm}$ (χ_1^0) mass of 150 (60) GeV (direct sbottom model). The event selection requires at least two leptons with p_{T} of [20, 20, 10] GeV, at least 4 jets with $p_{\mathrm{T}} > 40$ GeV and at least one b-jet with $p_{\mathrm{T}} > 20$ GeV. For this point the reached significance with SR1b(inclusive) is 1.88, with an expected signal yield of 9.2 events.

two same-sign leptons and three b-jets. The expected number of events for such a distribution can be found in section 9, together with estimates of the sensitivity this signal region would bring.

6.3 3L3b

Given the features observed in events with three leptons and three b-tagged jets (3L3b) int the 20.3 fb^{-1} of 8 TeV data [54], we would like to revisit this region in Run-2 using 13 TeV data. The signal regions on the 2012 search do not cover the kinematic phase space of the 3L3b sample. Therefore, we would like to introduce a signal region so that the entire phase space of the 3L3b sample is considered as a signal region.

We would also like to evaluate the sensitivity of our signal regions to processes that might give rise to the excess observed in the 3L3b sample. A popular simplified compressed SUSY model that might give rise to such signal candidates is gluino-stop offshell $\tilde{g} \rightarrow t\bar{t}\tilde{\chi}_1^0$ model described in Section 2 (Fig. 1). It is assumed that the squarks of the first two generations are much heavier than the gluino and thus decoupled. This decay can be targeted by multiple signatures as seen in Figure Fig 2. One particular process of interest is the n-body decay of $\tilde{g} \rightarrow t\bar{t}\tilde{\chi}_1^0$ mediated by an off-shell top squark where the final state produces four W-bosons and four b quarks. This process has at least two free parameters, the gluino and neutralino masses, and thus it is important to cover all the accessible phase space with the first 13 TeV data. For now, we used signal simulations 8 TeV collisions with $m_{\tilde{g}} - m_{\tilde{\chi}_1^0} \geq 2m_t$. A region of interest that was investigated by ATLAS recently [55] but was not covered in the search is $(m_t + m_W + m_b) < (m_{\tilde{g}} - m_{\tilde{\chi}_1^0}) < 2m_t$ as shown in Fig. 2. However, it was studied by CMS [56]. The gluino decays to a neutralino with one off-shell top which looks at more compressed spectra, the so-called "above the diagonal" region. This region is especially interesting for the same-sign or three leptons analysis since the sensitivity of this channel is better than the other channels based on extrapolating the limits of Fig. 2.

The first case in the gluino decay mode is a 3-body decay with two on-shell top quarks $\tilde{g} \rightarrow t\bar{t}\tilde{\chi}_1^0$. This region was covered by the ATLAS search. When the mass difference between the gluino and neutralino goes below $2m_t$, not all the top quarks that are produced from the gluino decay stay on-shell. The next possible decay modes are the 4-body decay $\tilde{g} \rightarrow \bar{b}W^- t\tilde{\chi}_1^0$ and the 5-body decay $\tilde{g} \rightarrow \bar{b}W^- bW^+\tilde{\chi}_1^0$. The more final particles there are, the smaller the decay width and thus the longer the gluino lifetime. Fig. 16 illustrates these processes where the ratio of the gluino decay width for each n-body decay to the most inclusive mode, 7-body decay, is shown as a function of the neutralino mass.

The gluino might live long enough to decay to leptons that do not originate from the primary vertex, $d_0 > 100$ μm, as illustrated in Fig. 16. Typically, the gluino should live less than about a picosecond in order to decay with prompt leptons. Fig. 17 shows the gluino lifetime as a function of the neutralino mass for different gluino masses that will be considered in this study.

As shown in Fig. 16 and Fig. 17, it is clear that the smaller the mass gap between the gluino and neutralino, the longer the lifetime. More details about the dominant gluino decay modes and lifetimes can be found in [55]. To evaluate the sensitivity of our signal regions to this specific process, we used reconstructed simulations of different mass points to evaluate how many events will pass the standard SS/3L analysis event selection. The grid points were chosen so that for a fixed gluino mass, two neutralino masses were taken to be closer and farther from the diagonal in the region with $m_{\tilde{g}} - m_{\tilde{\chi}_1^0} < 2m_t$ as shown in Table 12.

The event selection of 3L3b follows:

- exactly 3 baseline leptons are required with at least one pair of opposite sign same flavour (OSSF)
- the missing transverse momentum is required to be greater than 50 GeV
- the events are required to have at least three b-jets.

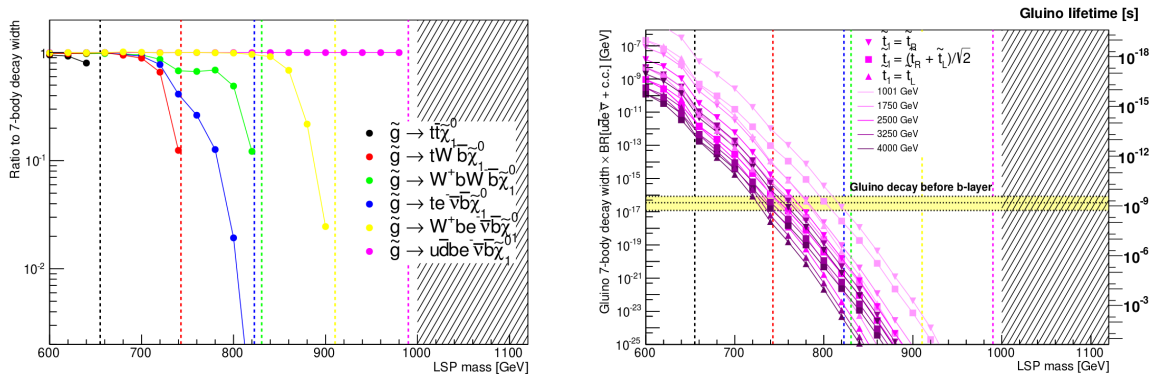

Figure 16: (Left) Virtuality of the top quarks and W bosons in the gluino decay presented as the ratios of decay width between modes forcing on-shell top quarks or W bosons, and the most inclusive mode (7-body decay) with no such constraints as a function of the neutralino mass with the gluino mass fixed at 1 TeV, and stops $\tilde{t}_1$, $\tilde{t}_2$ masses are both set to 2.5 TeV with a mixing angle of 45°. (Right) gluino lifetime as a function of the neutralino mass for different gluino mass points.

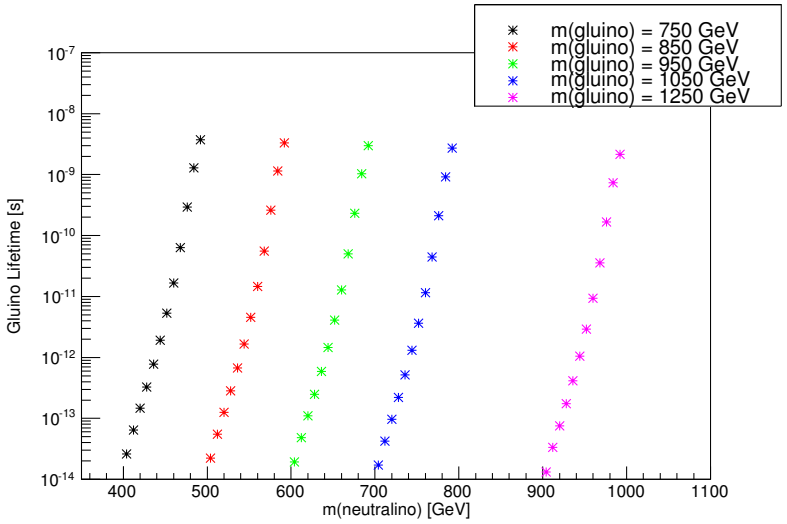

Figure 17: Lifetimes of gluinos with different masses as a function of the neutralino mass considered in the current study. The lightest stop mass is fixed to 2.5 TeV and is a t_L state.

In order to cover the kinematic region of the 3L3b selection, a new signal region is added in the SS/3L analysis that is still orthogonal to rest of the signal regions. This new signal region requires exactly three leptons, at least three b-jets and either at most five jets or $M_{eff} < 350$ GeV and we refer to it as SR3b3L. The final signal regions used in this study are shown in Fig. 9.

Appendix C shows the generated samples used in this study. The event yields for the grid points considered that pass the selection requirements in the different signal regions and normalized to the 13 TeV cross section with 3 fb^{-1} are shown in Table 13.

The kinematic distributions of N_{jets}, N_{b-jets}, $E_{\mathrm{T}}^{\mathrm{miss}}$, and M_{eff} are shown in Fig. 18. The N_{jets} distribution peaks at 2 jets, thus it useful to use the new signal region, SR3b3L, which cover the lower jet multiplicity. The $E_{\mathrm{T}}^{\mathrm{miss}}$ peaks at around 60 GeV and thus motivates the lower cut of 50 GeV in this same signal region. The current cuts in M_{eff} of 350 GeV cover the signal well.

Table 12: Gluino decay width [GeV] and lifetime (s) for $m_{\tilde{t}}$ = 2500 GeV and for different pairs of ($m_{\tilde{g}}$ [GeV] , $m_{\tilde{\chi}_1^0}$ [GeV]).

	$\binom{435}{485}$	$\binom{535}{585}$	$\binom{635}{685}$	$\binom{735}{785}$	(1250, 985)
Gluino Decay Width [eV]	9.4×10^{-4} 4.4×10^{-7}	1.1×10^{-3} 5.1×10^{-7}	1.2×10^{-3} 5.6×10^{-7}	1.4×10^{-3} 6.1×10^{-7}	7.7×10^{-7}
Gluino Lifetime (picoseconds)	0.7 1500	0.6 1300	0.5 1200	0.5 1100	860

Table 13: Number of events passing the selections for $m_{\tilde{t}}$ = 2500 GeV and for different pairs of (m_{gl} [GeV] , $m_{\tilde{\chi}_1^0}$ [GeV]) normalized to 13 TeV with 3 fb^{-1}.

Signal Regions	$\binom{435}{485}$	$\binom{535}{585}$	$\binom{635}{685}$	$\binom{735}{785}$	(1250, 985)
SR3b3L	6.71 3.48	3.44 1.46	2.03 0.57	0.78 0.29	0.07
SR3b	6.03 1.44	2.35 0.45	0.80 0.14	0.46 0.05	0.02
SR1b	1.02 1.61	0.67 1.16	0.42 0.47	0.21 0.22	0.04
SR0b	7.81 5.44	4.30 1.94	1.50 1.01	0.81 0.41	0.12
SR3Llow	1.20 3.07	0.97 0.41	0.43 0.11	0.24 0.07	0.01
SR3Lhigh	1.95 2.46	1.46 0.67	0.52 0.40	0.28 0.24	0.04

633 Our next step is to evaluate the background in these signal regions and determine our sensitivity with
634 13 TeV data.

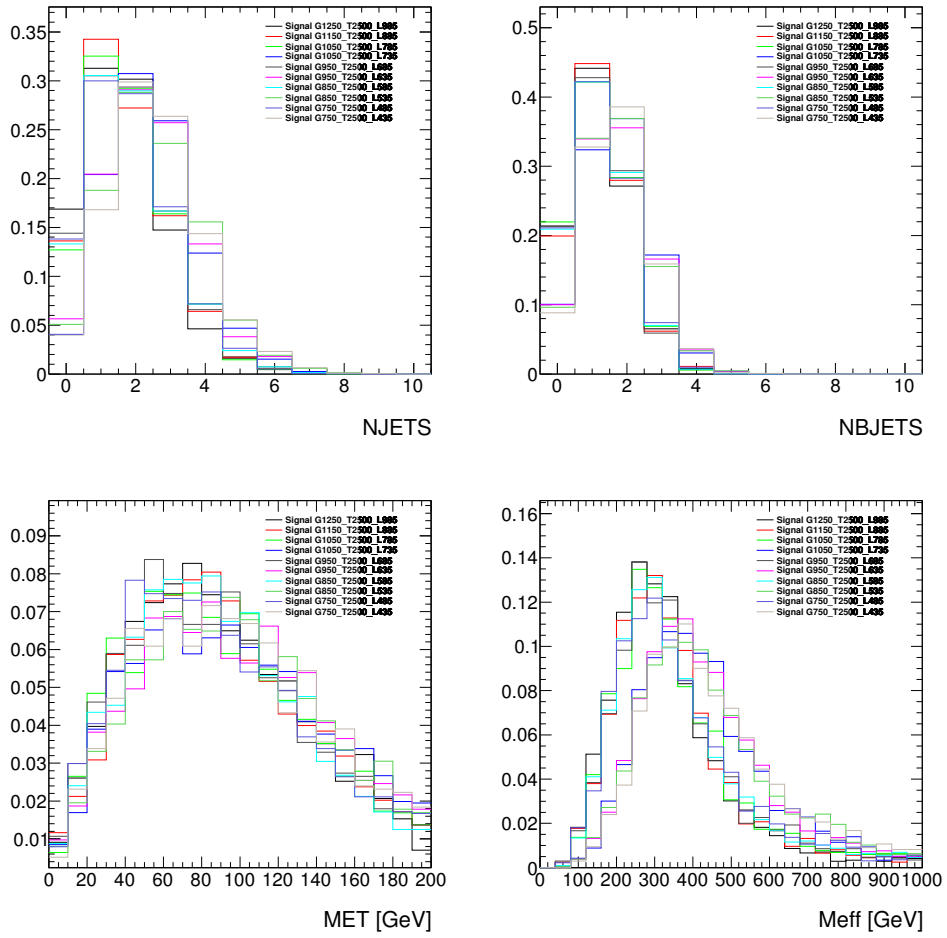

Figure 18: Kinematic distributions for the SS/3L channel with reconstructed samples generated at 8 TeV

6.4 RPV models

The main topologies described in Section 2.2.1 and shown in Fig. 5 lead to the same final state:

$$\ell^{\pm}\ell^{\pm} + b\text{−jets} + \text{jets} + E_{\mathrm{T}}^{\mathrm{miss}} \tag{4}$$

with two leptons and two b-jets coming from the top quarks decay, extra jets and eventually b-jets coming from the decay of the d-squark or the gluino and the $E_{\mathrm{T}}^{\mathrm{miss}}$ coming from the neutrinos from the top quarks decay.

An optimization of signal region for this model was performed and will be soon written out on this note. The main aspects of the optimized signal region are:

- ≥ 2 leptons
- ≥ 1 b-jets
- ≥ 3 jets
- $H_{\mathrm{T}} = \Sigma p_{\mathrm{T}}^{jet} \geq \sim 150$ GeV
- No cut on $E_{\mathrm{T}}^{\mathrm{miss}}$ and M_{T}

The cuts on the number of b-jets and jets are relaxed in order to take into account the boosted region. Indeed, the on-shell gluinos and d-squarks can be so boosted that their decay products are very close and not all the jets and b-jets are reconstructed.

A tight cut on the overall jet activity in the event is the main cut to reject the background. The H_{T} variable was chosen among other variables, such as $H'_{\mathrm{T}} = \Sigma p_{\mathrm{T}}^{jet} + \Sigma p_{\mathrm{T}}^{lep}$ and $M_{\mathrm{eff}} = \Sigma p_{\mathrm{T}}^{jet} + \Sigma p_{\mathrm{T}}^{lep} + E_{\mathrm{T}}^{\mathrm{miss}}$, because it leads to the best results in terms of significance. The exact cut value will be optimized with a future more accurate study.

However, a minimal cut should be applied on $E_{\mathrm{T}}^{\mathrm{miss}}$ and M_{T}. These cuts were originally applied for the search for neutralinos for RPC models and to reject the main background coming from the neutrinos from the decay of W. Since in RPV models our signal is composed of neutrinos, it is necessary that these cuts should be as low as possible in order to avoid the losses in signal acceptance. Table 14 shows the signal acceptance Zn computed assuming a 40% background uncertainty and using the signal samples at truth level. For those numbers, no b-tagging is used, and the b-jets were assigned according to their truth flavor in both background and signal samples.

Table 14: Yields and Significance for each additional cuts at $\sqrt{s} = 13$ TeV for 3 fb^{-1} of luminosity. The signal samples used here are a d-quark fusion (top) and a gluon fusion (bottom) for λ''_{321} coupling for the respective mass points ($m_{\tilde{g}} = 2000$ GeV, $m_{\tilde{q}} = 1400$ GeV) and ($m_{\tilde{g}} = 800$ GeV, $m_{\tilde{q}} = 2000$ GeV).

Cuts	RPV d-quark fusion	Z + jets	$t\bar{t}$	$t\bar{t}$ + V	Significance
$N_\ell \geq 2$	70.02 ± 1.05	66830 ± 2557	14467 ± 44	91.83 ± 0.85	-0.26
+ $N_{jet} \geq 3$, $N_{b-jet} \geq 1$	51.96 ± 0.90	1697 ± 43	11277 ± 39	84.04 ± 0.81	-0.25
+ $H_{\mathrm{T}} > 150$ GeV	37.36 ± 0.76	1.06 ± 0.85	8.29 ± 1.06	0.53 ± 0.05	4.23
Cuts	RPV gluon fusion	Z + jets	$t\bar{t}$	$t\bar{t}$ + V	Significance
$N_\ell \geq 2$	56.73 ± 0.90	66830 ± 2557	14467 ± 44	91.83 ± 0.85	-0.26
+ $N_{jet} \geq 3$, $N_{b-jet} \geq 1$	45.30 ± 0.81	1697 ± 43	11277 ± 39	84.04 ± 0.81	-0.26
+ $H_{\mathrm{T}} > 150$ GeV	14.89 ± 0.46	1.06 ± 0.85	8.29 ± 1.06	0.53 ± 0.05	2.00

7 Background estimation

The main challenge, in this analysis, is to achieve reliable predictions of the low Standard Model background leading to the same-sign leptons + jets final state. This background is composed partly of rare processes such as the associate production of a top quark pair with a massive boson, or the production of multiple bosons. The other contribution consists in experimental backgrounds originating from the imperfect discrimination between prompt leptons and other objects, or the occasional misreconstruction of the electron charge. The following sections provide more details about the nature of these different categories of background, and the foreseen methods that will be used to estimate their contributions to the signal regions.

7.1 Backgrounds with prompt SS dilepton or three leptons

There are two main sources of Standard Model background leading to pairs of same-sign prompt leptons:

- The associate production of top quark(s) and massive bosons, where the same-sign leptons pair is produced from leptonic decays of one of the top quarks and of the boson. These processes are characterized by a large jet multiplicity, the presence of b-jet(s), and always have intrinsic missing momentum. Therefore they generally represent the largest contribution to the signal regions. The dominant processes are $pp \to t\bar{t}W(j)$ and $pp \to t\bar{t}Z(j)$, while there are also minor contributions from $pp \to t\bar{t}H$, $tZbj$, $t\bar{t}WW$, and $pp \to t\bar{t}t\bar{t}$.

- The production of multiple massive bosons. These processes have generally low jet multiplicities. However, due to their larger cross-sections, they contribute in a significant way to the background entering signal regions without b-jets requirements. The dominant processes include $pp \to W^{\pm}W^{\pm}jj$, WZ, ZZ, with minor contributions from $pp \to WH$, ZH, VVV and $pp \to H \to lll$.

We plan to estimate the contributions of these various processes to the signal regions by relying on the Monte-Carlo predictions, normalized with the best known theoretical cross-sections : these processes are too rare to allow use of control regions until a significant integrated luminosity will be collected.

Processes containing top quarks have cross-sections below 1 pb, which have consequently not yet been much constrained experimentally. On the theoretical side, uncertainties on the cross sections are typically large: 30% for $t\bar{t}W$ and 50% for $t\bar{t}Z$ for the same-sign $\sqrt{s} = 7$ TeV analysis [57], 22% for both $t\bar{t}W$ and $t\bar{t}Z$ for the $\sqrt{s} = 8$ TeV analysis [15].

Cross-sections for diboson processes are known with a rather good accuracy, but only for the inclusive processes, while we are mostly interested in processes where several additional partons are produced.

The validation regions described in section 7.6 will help us ensure that our understanding of these processes is sufficiently reliable, and that the systematic uncertainties assigned to the estimated rates are reasonable.

7.2 Charge flip leptons

Electrons are occasionally reconstructed with the wrong charge, generally because an irrelevant track is matched to the electron cluster during reconstruction instead of the real electron track. This may occur for example in the so-called trident process, where an electron emits a hard Brehmsstrahlung photon which further converts into an electron-positron pair, resulting in three close tracks. This confusion is the main reason for lepton charge flip, as errors on the track reconstruction itself are much rarer. Indeed, muon charge flip has been estimated negligible in past studies [15], and we consider only charge flip background originating from electrons.

This type of background is particularly relevant to searches with same-sign leptons, as they may turn a pair of opposite-sign leptons from an abundant Standard Model process ($pp \to Z$, $t\bar{t}$, $W^+W^-\ldots$) into a

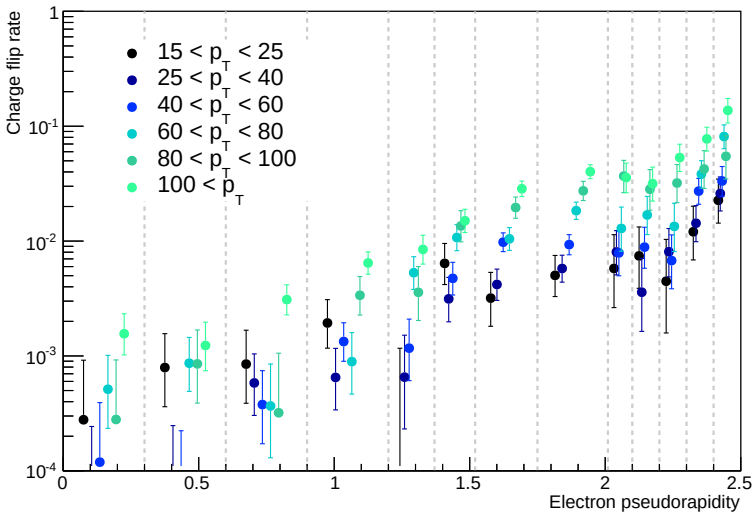

Figure 19: Expected electron charge flip rate determined in simulated $t\bar{t} \to e\mu\nu\nu$ events

much rarer same-sign pair. Because of the jets requirements characteristic of our analysis, the dominant source of charge flip electrons in most of the signal regions arise from leptonic decays of $t\bar{t}$ pairs. This type of background contributes only moderately to the signal regions – for example in the Run-1 analysis it represented at most 10% of the total background yield. But for looser event selections, such as the ones used to validate the background modelling, it can be a major component in electron channels. It is therefore important to be able to predict reliably this background.

Figure 19 shows the expected rate of charge flip for electrons satisfying the requirements listed in sections 4.2.1 and 4.2.3, determined in simulated $t\bar{t} \to e\mu\nu\nu$ events. The rate increases significantly at large pseudorapidity, reflecting the larger amount of material in front of the calorimeter. There is also a significant dependency to the transverse momentum, with larger rates obtained for energetic electrons.

Background estimation methodology

We rely on a purely data-driven method to estimate yields of events with charge flipped electrons. Assuming one knows the electron charge flip rates $\xi(\eta, p_T)$, a simple way to estimate the yields is to select events with pairs of opposite-sign leptons and assign them a weight:

$$w = \xi\left(\eta^1, p_T^1\right)\left[1 - \xi\left(\eta^2, p_T^2\right)\right] + \xi\left(\eta^2, p_T^2\right)\left[1 - \xi\left(\eta^1, p_T^1\right)\right] \tag{5}$$

where $\xi = 0$ for muons.

The advantages of this method are a good statistical precision since the charge flip rate is rather low, and the lack of dependency on the simulation and related uncertainties. Obviously, it requires a precise measurement of the rates, which is described in the next paragraph. Another inconvenient is that the reconstructed electron energy (hence momentum as well) of charge flipped electrons tends to be too low by a few GeV, because of the hard Brehmsstrahlung at the origin of the charge flip. Simply reweighting electrons from opposite-sign lepton pairs therefore does not predict correctly the charge-flip background shape for energy-dependent variables. In the past this effect was simply neglected, as we do not rely on discriminant variables very sensitive to the electron energy. But we are now considering applying energy correction factors, or assign dedicated systematic uncertainties.

Measurement of the charge flip rates

The simulation of the charge flip process is not accurate enough to be relied on (discrepancies up to a factor 2 were seen in Run-1 analyses), therefore the rates have to be measured in data. In Run-2, electron charge flip rate measurements will be centralized by the Egamma performance group (unlike up to now). One of our group members is involved in these activities and will provide the rates according to our customized electron definitions. The standard method which will be employed for these measurements is similar to the one described in the documentation of the Run-1 same-sign leptons + jets search [15]. It relies on the observed numbers of opposite (OS) and same-sign (SS) electrons with an invariant mass close to the Z mass, which provides a clean sample of electrons. Expressing these numbers as function of the electron charge flip rate $\xi(\eta, p_T)$:

$$N_{\mathrm{SS}}\left(\eta^1, p_T^1, \eta^2, p_T^2\right) \approx \left[\xi\left(\eta^1, p_T^1\right) + \xi\left(\eta^2, p_T^2\right)\right] N\left(\eta^1, p_T^1, \eta^2, p_T^2\right), \quad N = N_{\mathrm{OS}} + N_{\mathrm{SS}} \tag{6}$$

the rates are then obtained as the maximum likelihood estimators for the product of Poisson distributions $\mathcal{P}(N_{\mathrm{SS}}|N)$ binned in η and p_T of the two electrons.

Sources of systematic uncertainties on the measured rates account for the background subtraction, and closure tests performed on Monte-Carlo (differences between the computed and true rates) and data (Z lineshape opposite-sign electrons pairs reweighted by the measured rates, compared to the distribution of same-sign pairs).

7.3 Backgrounds with fake leptons

The term ”fake lepton” denotes here any reconstructed lepton not originating from the decay of massive gauge or Higgs bosons, or an electroweak initial/final state radiation. They can be non-prompt leptons produced in heavy flavor meson decays, converted photons, light hadrons faking the electron shower, in-flight decays of kaons or pions to muons, etc. Common properties shared by these objects are a bad response to electron identification cuts, non-zero impact parameters, and the reconstructed leptons are often not well isolated; these properties can be used to discriminate fake leptons against the prompt leptons we are interested in.

In signal regions enriched in b-jets, Monte-Carlo simulations predict that the dominant source of fake leptons originates from semileptonic $t\bar{t}$ events, with a non-prompt lepton in the decay chain of one of the B mesons. Contributions from photon conversions and hadron fakes are not to be neglected though, in particular in b-jet-depleted signal regions where the rate of $t\bar{t}$ events is lower and is competed by processes such as $W\gamma$ + jets.

We will rely on at least two different methods to estimate the fake leptons yields in the signal regions, which are briefly described in the next paragraphs. They have both been employed successfully in the Run-1 analysis [15].

7.3.1 The matrix method

The matrix method is a purely data-driven approach which relies on the different response of prompt and fake leptons to identification, isolation and impact parameters requirements: fake leptons have low probabilities to satisfy these requirements, unlike prompt leptons. No tentative is made to consider the different categories of fake leptons separately – systematic uncertainties are assigned in consequence.

Methodology

A combination of tight requirements on discriminant variables such as electron identification, lepton isolation and impact parameters, is defined (see Tabe 6). Reconstructed leptons are then classified in two categories (”tight” and ”loose”), depending on their success satisfying the tight requirements or not. If ϵ and ζ are respectively the probabilities for a prompt/fake lepton to satisfy the requirements, linear

relationships can be established between the mean values of the rates of prompt/fakes and tight/loose leptons, which for the 1-lepton case are:

$$< N_{\text{tight}} > = \epsilon < N_{\text{prompt}} > + \zeta < N_{\text{fake}} > \quad (7)$$
$$< N_{\text{loose}} > = (1-\epsilon) < N_{\text{prompt}} > + (1-\zeta) < N_{\text{fake}} >$$

This system of equations can be used to evaluate the number of prompt and fake leptons given the observed number of tight and loose leptons. A detailed explanation of the generalization of the method to handle events with arbitrary number of leptons, as used in the Run-1 analysis, can be found in [15, 58].

The method relies of the prior knowledge of the probabilities ϵ and ζ, which need to be measured in dedicated samples enriched in prompt and fake leptons (see next paragraph). The uncertainties on the probabilities for fake leptons constitute the main source of uncertainties in the asymptotic regime. In the low statistics regime, one has to cope with the fact that the loose and tight leptons categories are not enough populated to provide reliable estimates: for example predictions of negative yields are a possible outcome. In general these estimates are accompanied by large statistical uncertainties.

Finally, one should note that the charge flip electron background interferes with the matrix method as charged flipped electrons are notably more prone to fail impact parameter or tight identification requirements, and the related efficiencies are distinct from both those of prompt and fake electrons. They correspond so to speak to a third category of objects, while the matrix method is based on the assumption that only two categories are present. One way to solve the issue is to rely on the linearity of the matrix method estimate with respect to its input number of events; therefore one can simply subtract the estimated charge flip background in the tight and loose leptons categories, from observed data. This requires a dedicated measurement of the charge flip rate for electrons failing the tight requirement.

Measurement of the ϵ, ζ probabilities

These parameters are measured in dedicated samples enriched in prompt or fake leptons. Probabilities for prompt leptons are measured in $Z \to \ell\ell$ tag-and-probe selections, and are assigned systematic uncertainties determined in Monte-Carlo covering the differences between the lepton properties in the measurement regions, and in the signal regions which have much busier event topologies. Other systematic uncertainties should account for the less isolated leptons that can be found in signal scenarios where decay products are particularly boosted (for example the gluino-stop offshell model).

Probabilities for fake leptons are much harder to determine, due to the difficulty to identify an event selection that would provide both a high purity, and enough statistics, especially for leptons with $p_T >$ 40 GeV. In the 8 TeV versions of this analysis, such selections were requiring at least two same-sign leptons together with a jet, and the fake electron probabilities were determined separately for events with or without b-jets. Other analyses have been using inclusive selections with a single lepton, which have the advantage to be much more populated, but on the other hand are less representative of the properties of fake leptons that can be found in our signal regions. In general the probabilities vary largely with p_T (see e.g. the isolation efficiencies in section 4.2.3) thus require binned measurements.

The measurements of fake leptons probabilities are associated to large uncertainties, which cover for the nature of the fake leptons and the events that produce them being different between the measurement and signal regions.

7.3.2 The Monte-Carlo template method

This method is Monte-Carlo based, and makes use of the samples corresponding to the various processes expected to produce fake leptons. Correction factors of the fake lepton modelling in the simulation are determined in a combined fit of several control regions involving shapes of discriminant variables such as the missing transverse momentum or the jet multiplicity. There are five such correction factors (for

fake electrons and muons originating from light or heavy flavor jets, and an additional factor for charge flip), which are applied on an event basis depending on the generator information about the origin of the fake lepton in the event. More details can be found in the documentation of the Run-1 analysis [15].

7.3.3 Statistical tools improving robustness in low statistics regime

Some alternatives to the matrix method have been considered, based on the same principles but with more formal constructions as probabilistic tools (hence a better behaviour in conditions far from the asymptotic regime), and are currently being developed. One of these methods [59] relies on the construction of a likelihood function which translates the equation system (7) in terms of probabilities for single leptons, instead of relationships between mean values; this also allows to treat ϵ and ζ as nuisance parameters (according to their measurements uncertainties) instead of being frozen. One could then simply estimate the rates of prompt and fake leptons as the maximum likelihood estimators of the observations, but the large number of parameters (several leptons per event hence many possible loose/tight combinations, binned probabilities ϵ and $\zeta \ldots$) renders this approach impractical. A simplification is discussed in [59, 58], which preserves some advantages over the standard matrix method.

Another approach has been proposed recently [58], consisting in building confidence intervals on the rate of fake leptons from the associated Bayesian posterior, which may be numerically computed with Gibbs sampling. The claimed advantages are a better assessment of the uncertainties on the final estimate, since the whole posterior distribution is known, as well as the absence of issues with local minima which might affect likelihood-based methods. More details can be found in [58].

We are planning to check if these methods can be applied with all the complexity of a real world analysis, in which case they would bring quite a nice improvement to the current way of predicting fake lepton background in the signal regions.

7.4 Backgrounds with fake b-jets

In the signal regions requiring at least three b-jets, an important part of the background originates from processes with two real b-jets, and a third jet not originating from a b-quark but satisfying the b-tagging requirements. Unlike the case of fake leptons, the b-tagging performance group usually provides scale factors (and associated uncertainties) to correct the simulation for mismodelling both of real and fake b-jets. The fake leptons and charge flip background, being predicted from data, obviously do not need any correction.

An alternative data-driven method was used in Run-1 as cross-check, consisting in the equivalent of the lepton matrix method but applying on jets and replacing lepton tight requirements by the output weight of the b-tagging algorithm. This approach was primarily developed for the ATLAS SUSY search with 0/1 lepton and 3 b-jets [60]. It could be considered again for Run-2.

7.5 Neglected backgrounds

Other sources of background such as cosmic rays or cavern background, as well as pile-up events where two distinct proton-proton pairs may interact and produce leptons, have been evaluated in the past and found to be negligible. Multiple scattering effects are included in the simulations but are also not expected to contribute enough to require in-depth studies.

7.6 Validation regions

The different type of backgrounds will be validated by looking at the agreement between the data observation and the SM expectation in regions dominated by one type of background. As for Run-1, several

validation regions will be considered, and their definition is a balance between high purity, large statistics and low signal contamination. The latter is assured by requiring an upper cut on $E_{\mathrm{T}}^{\mathrm{miss}}$ (< 150 GeV). If no validation region can be designed, the background will be checked by looking at different kinematic variables distributions. For a complete validation, several selections will be considered :

- Loose: requiring at least two signal leptons in the event.
- Intermediate: adding soft cuts i.e. at least one or two signal jets or b jets.
- Hard: increase the number of jets in the event.

It is known that the associated uncertainty on the SM background can be decreased by adding control regions enriched in a certain type of background and orthogonal on the signal regions. However, given the rare SM processes which dominate in the signal regions, the statistics expected with $\sqrt{s} = 13$ TeV and $L \leq 3$ fb^{-1}of data in potential control regions is too small to be included. Hence, only validation regions will be defined for early Run-2.

$t\bar{t} + V$ background

To validate the $t\bar{t} + Z$ and $t\bar{t} + W$ backgrounds estimation, several tentative regions defined with at least 1 or 2 b-jets in the event were considered. To decrease the other type of backgrounds, several jets and a low $E_{\mathrm{T}}^{\mathrm{miss}}$ cut were also required. However, given the low statistics, it was found that a combined $t\bar{t} + V$ region will perform better. The region definition is given in Table 15. The leading and sub-leading leptons are required to be energetic (20 GeV) in order to reduce the fake lepton background, while the veto on the fourth baseline lepton is minimizing the contamination from ZZ processes. Note that it is very hard to obtain a pure validation region in $t\bar{t} + V$, as the difference with the other prompt SS SM processes is mainly the jet multiplicity. The highest purity was found when considering at least four jets in the ee and $e\mu$ channels, and at least three jets in the $\mu\mu$ channel. A high m_{eff} cut is used to further reduce the detector background, wile an upper cut of 900 GeV is used to reduce the signal contamination. Note that this cut can be tighten to further decrease the SUSY contamination from models like direct sbottom. The reached purity for $\sqrt{s} = 13$ TeV and $L \leq 3$ fb^{-1}of data is around 42% if the large eta region is excluded ($|\eta|_e < 1.37$) . The purity can be increased to 60% if the inclusive 1 b jet selection is replaced by inclusive 2 b jet selection (and the 400 GeV cut on m_{eff} is relaxed to 350 GeV). The signal contamination was studied by looking at several available SUSY models studied in this analysis. It can be up to 27% when the direct-sbottom model is considered and the sbottom mass is 550 GeV, or 20% for direct squark (2 step) via sleptons with W/Z bosons in the cascade decay, otherwise it is smaller than 10%.

Table 15: $t\bar{t} + V$ validation region definition. The p_{T} threshold of the leading two leptons is 20 GeV, otherwise 10 GeV.

VR	N_{lept}^{signal}	$N_{lept}^{baseline}$	N_{b-jets}^{20}	Other variables
ttV	≥ 2	< 4	≥ 1	$30 < E_{\mathrm{T}}^{\mathrm{miss}} < 200$ GeV, $400 < m_{\mathrm{eff}} < 900$ GeV, $\|\eta\|_e < 1.37$, $N_{jets}^{30} \geq 4$ in ee and $e\mu$, $N_{jets}^{25} \geq 3$ in $\mu\mu$ channels

ZZ + jets validation region

Even if this type of background is minor in several of the defined signal regions, its contribution can is significant in regions with no b jet requirement and three leptons. Therefore, a validation region was defined as presented in Table 16. It requires at least three signal leptons with $p_{\mathrm{T}} > 20$ GeV, and at least

four baseline leptons. The reached purity for $\sqrt{s}$ = 13 TeV and $L \leq 3$ fb^{-1}of data is up to 97%. In order to be closer to the SRs, another validation region can be defined by asking at least two jets with $p_{\mathrm{T}} > 25$ GeV with a purity of 84%. The signal contamination is at most 20%.

Table 16: ZZ validation region definition. The p_{T} threshold of the two leading leptons is 20 GeV, otherwise 10 GeV. To be closer to the SRs, at least two jets with $p_{\mathrm{T}} > 25$ GeV can be required in the event (and $N^{20}_{b-jets} == 0$ becomes $N^{20}_{b-jets} \geq 0$), without affecting the validation region purity.

VR	N^{signal}_{lept}	$N^{baseline}_{lept}$	N^{20}_{b-jets}	Other variables
ZZ	== 3	≥ 4	==0	$E_{\mathrm{T}}^{\mathrm{miss}} < 150$ GeV, $m_{\mathrm{eff}} > 100$ GeV, $\lvert\eta\rvert_e < 2.$

WZ + jets validation region

Similarly to ZZ type of background, it is negligible in most of signal regions. However, it is expected to populate the regions with 0 b-jets and low jet multiplicity. Therefore, its validation is important and the proposed region definition is presented in Table 17. It requires exactly three leptons and a veto on the fourth-leading baseline lepton in order to reduce the ZZ background contamination. The lower cut on $E_{\mathrm{T}}^{\mathrm{miss}}$ (30 GeV) is mainly reducing the charge flip contamination. The m_{T} cut of 50 GeV, even if is not used to define the signal regions, is assuring a smaller fake lepton contamination. At least one and at most three jets with $p_{\mathrm{T}} > 25$ GeV are required in the event. It assures a purity of 70% for $\sqrt{s}$ = 13 TeV and $L \leq 3$ fb^{-1}of data. The signal contamination is found to be below 1%.

Table 17: WZ validation region definition. The p_{T} threshold of the two leading leptons is 20 GeV, otherwise 10 GeV.

VR	N^{signal}_{lept}	$N^{baseline}_{lept}$	N^{20}_{b-jets}	Other variables
WZ	==3	< 4	==0	$30 < E_{\mathrm{T}}^{\mathrm{miss}} < 300$ GeV, $m_{\mathrm{T}} > 50$ GeV, $1 \leq N^{25}_{jets} \leq 3$, $\lvert\eta\rvert_e < 2.$

WW + jets validation region

Similarly to the other diboson processes, the WW + jets (with a pair of same sign lepton in the final state) events contribute mainly in the signal regions with no b jet requirement. Two validation regions are defined (Table 18). In the first region, a cut on the invariant mass of the first two leading jets in the event is considered. It selects forward jets from VBS processes which are not necessary populating the signal regions defined in the analysis. However it is used as a cross-check as a high purity (50%) can be reached. A second region is defined by selection two energetic jets (50 GeV) and decreasing the electron acceptance to $\lvert\eta\rvert_e < 1.37$. The purity is only 31%. In both validation regions the signal contamination is at most 15%.

Fake lepton validation regions

Beside the usual validation plots shown for the Run-1 analysis, several fake lepton validation regions are defined, in order to increase the confidence on the background estimation methods. Generally, depending on the b-jet multiplicity two categories are considered: low and high m_{eff}, as presented in Table 19. To reduce the charge flip background contamination, a veto on the Z boson mass ($80 < m_{\ell\ell} < 100$ GeV) is imposed only in the ee channel. The background from prompt SS processes

Table 18: *WW* validation region definition. The p_{T} threshold of the two leading leptons is 20 GeV.

VR	N_{lept}^{signal}	$N_{lept}^{baseline}$	N_{b-jets}^{20}	Other variables
WW1	==2	< 3	==0	$40 < E_{\mathrm{T}}^{\mathrm{miss}} < 300$ GeV, Z mass veto, $m_{\mathrm{T}} > 40$ GeV, $N_{jets}^{40} \geq 2$, $m_{jj} > 500$ GeV, $\|\eta\|_e < 2$.
WW1	==2	< 3	==0	$40 < E_{\mathrm{T}}^{\mathrm{miss}} < 300$ GeV, Z mass veto, $m_{\mathrm{T}} > 40$ GeV, $N_{jets}^{50} \geq 2$, $\|\eta\|_e < 1.37$

is reduced by a veto on the third baseline lepton. The leading two leptons are required to have a p_{T} threshold of 15 GeV, and the event should have at least one jet. For the low m_{eff} regions, the highest purity was reached when $E_{\mathrm{T}}^{\mathrm{miss}} < 100$ GeV and $m_{\mathrm{eff}} < 400$ GeV was imposed. A lower cut on m_{eff} will drastically reduce the fake lepton background in the low m_{eff} validation region, while in the high m_{eff} region a higher threshold will increase the level of prompt SS background. Note that, the two validation regions overlap and the reached purity varies between 80 and 90%. The signal contamination is found to be maximum 10%.

Table 19: Fake lepton validation region definition. The p_{T} threshold of the two leading leptons is 15 GeV.

Low meff fake leptons VRs				
VR	N_{lept}^{signal}	$N_{lept}^{baseline}$	N_{b-jets}^{20}	Other variables
FL0b-Lm_{eff}	==2	< 3	==0	$20 < E_{\mathrm{T}}^{\mathrm{miss}} < 100$ GeV, $m_{\mathrm{eff}} < 400$ GeV, $m_{\mathrm{T}} < 60$ GeV, $N_{jets}^{25} \geq 1$
FL1b-Lm_{eff}	==2	< 3	==1	$20 < E_{\mathrm{T}}^{\mathrm{miss}} < 100$ GeV, $m_{\mathrm{eff}} < 400$ GeV, $m_{\mathrm{T}} < 60$ GeV
FL2b-Lm_{eff}	==2	< 3	≥2	$20 < E_{\mathrm{T}}^{\mathrm{miss}} < 100$ GeV, $m_{\mathrm{eff}} < 400$ GeV, $m_{\mathrm{T}} < 80$ GeV
High meff fake leptons VRs				
VR	N_{lept}^{signal}	$N_{lept}^{baseline}$	N_{b-jets}^{20}	Other variables
FL0b-Hm_{eff}	==2	< 3	==0	$20 < E_{\mathrm{T}}^{\mathrm{miss}} < 100$ GeV, $m_{\mathrm{eff}} > 300$ GeV, $m_{\mathrm{T}} < 100$ GeV, $N_{jets}^{25} \geq 1$
FL1b-Hm_{eff}	==2	< 3	==1	$20 < E_{\mathrm{T}}^{\mathrm{miss}} < 50$ GeV, $m_{\mathrm{eff}} > 300$ GeV, $m_{\mathrm{T}} < 80$ GeV
FL2b-Hm_{eff}	==2	< 3	≥2	$20 < E_{\mathrm{T}}^{\mathrm{miss}} < 50$ GeV, $m_{\mathrm{eff}} > 300$ GeV, $m_{\mathrm{T}} < 50$ GeV

8 Systematic Uncertainties

8.1 Experimental systematics

All the experimental systematics provided by the SUSYTools `getSystInfoList()` method have been considered. The list of sources of uncertainty and the corresponding names of the variations are:

Jet energy scale (`JET_GroupedNP_{1-3}__1{up,down}`) One of the strongly reduced uncertainty sets provided by the JetEtMiss group for early Run-2 searches is used in this note. These sets are intended for use by analyses which are not sensitive to jet-by-jet correlations arising from changes to the jet energy scale (as expected for many early SUSY searches). Although the recommendation is to evaluate 4 different reduced sets, only one of them is used for the moment: `InsituJES2012_3NP_Scenario1.config`

(as included in the JetUncertainties-00-09-19 package tag). The jet energy is scaled up and down (in a fully correlated way) by the $\pm 1\sigma$ uncertainty of each nuisance parameter.

Jet energy resolution (`JER__1up`) An extra p_{T} smearing is added to the jets based on their p_{T} and η to account for a possible underestimate of the jet energy resolution in the MC simulation. This is done by the `JERSmearingTool` in the JetResolution-03-00-28 package tag.

Egamma resolution (`EG_RESOLUTION_ALL__1{up,down}`) A nuisance filtering scheme to reduce the ~8 NPs used to electron and photon resolution to only one as implemented in SUSYTools is used.

Egamma scale (`EG_SCALE_ALL__1{up,down}`) A nuisance filtering scheme to reduce the ~16 NPs used to electron and photon resolution to only one as implemented in SUSYTools is used.

Electron efficiency (`EL_EFF_UncorrUncertainty__1{up,down}`) This is uncertainty is associated with the electron efficiency scale factors provided by the Egamma CP group.

Muon efficiency (`MUONSFSTAT__1{up,down}`, `MUONSFSYS__1{up,down}`) This is uncertainty corresponds to the statiscal and systematic uncertainties in the muon efficiency scale factors provided by the Muon CP group.

Muon resolution uncertainty (`MUONS_ID__1{up,down}`, `MUONS_MS__1{up,down}`) This is evaluated as variations in the smearing of the inner detector and muon spectrometer tracks associated to the muon objects by $\pm 1\sigma$ their uncertainty

Muon momentum scale (`MUONS_SCALE__1{up,down}`) This is evaluated as variations in the scale of the momentum of the muon objects

$E_{\mathrm{T}}^{\mathrm{miss}}$ **calorimeter soft term uncertainties** (`MET_SoftCalo_Reso`, `MET_SoftCalo_Scale{Up,Down}`) Note that the effect of the hard object uncertainties (most notably JES and JER) are also propagated to the $E_{\mathrm{T}}^{\mathrm{miss}}$.

Flavor tagging (`FT_Eigen_B_{0-9}__1{up,down}`, `FT_Eigen_C_{0-3}__1{up,down}`, `FT_Eigen_Light_{0-11}__1{up,down}`) The full eigenvector variation approach [61] is used for all jet flavours (B, C and light), while keeping track of uncertainties that are common to multiple jet flavours. Similarly to the case of the JES, a significant reduction in the number of nuisance parameters (currently 52 variations) is expected to be provided by the Flavour Tagging CP group before the start of data taking.

All these experimental systematics have been included in the production of flat ROOT ntuples, as mentioned in Section 3.1, although due to time limitations at the moment of writing this note, its effect was not included in the results shown in Section 9, where flat uncertainty values were used instead.

8.2 Theoretical systematics

In Run-1 [14, 15], the systematic uncertainties associated with the $t\bar{t}+V$ and diboson MC were assessed by using samples where the factorization and renormalization scales have been varied. We plan to follow a similar approach once scale variation samples are available in mc15 productions. Other theoretical uncertainties were evaluated by comparing different generators and samples produced with different

number of partons. A similar approach will be used in 2015, following the recommendations by the Physics Modeling Group.

In addition, the theoretical uncertainties on the cross-sections were 22% for $t\bar{t}W$ [41] and $t\bar{t}Z$ [62] and 7% for diboson production (computed with MCFM [63], considering scales, parton distribution functions and α_s uncertainties). Normalisation uncertainties between 35% and 100% were applied to processes with smaller contributions (triboson production, $t + Z$, etc.).

9 Simultaneous fit method and results

The sensitivity of the signal regions proposed in Section 6 is evaluated with more refined statistical tools in this section, by using the HistFitter framework [64] to perform discovery hypothesis tests for the different signal scenarios of interest. The event yields assumed in these test are the ones predicted by the set of Monte-Carlo samples described in section 3, and the object selections detailed in Sections 4 and 5. All the results in this section are presented for an integrated luminosity of 3 fb^{-1}.

The fit configuration is setup in the *exclusion* mode, i.e. to perform hypothesis testing with a known BSM signal. Of course here the rejected hypothesis is the background-only hypothesis. Only one signal region is fitted at the time; furthermore, there is no control region defined in the analysis. We plan to investigate at a later stage potential benefits of combined fits of several signal regions, which was the setup in use for the Run-1 analysis. Distinct global systematic uncertainties are assigned to each category of background, amounting to 30% for $t\bar{t} + V$ processes, 35% for diboson ,100% for minor processes such as $t\bar{t}H$, and 50% for the reducible background ($t\bar{t}$, V + jets, $W^{\pm}W^{\mp}$).

Event yields in the signal regions

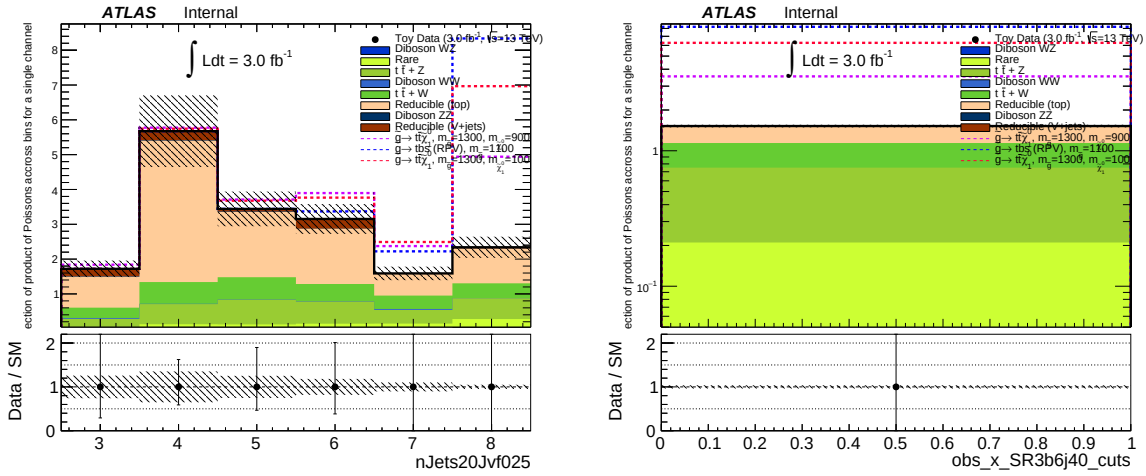

Figure 20: Expected yields for Standard Model processes and a few characteristic signal scenarios, in selections with at least two same-sign leptons and three b-jets. The selection on the right side further requires at least six jets with $p_T > 40$ GeV.

Figures 20 and 21 present the event yields of the background and a few characteristic signal scenarios, in various signal region candidates. The regions that have enough statistics to allow it are binned in the most relevant variable to discriminate between signal and background, either the effective mass or the number of jets (the latter for the 3 b-jets selection). Binnings are chosen such that the background yield in one bin remains at the level of around one event. One should note that they correspond to the

binning used when performing shape fits as described in the next paragraph.

Sensitivity for the gluino stop offshell model

Figure 22 presents the signal significance obtained with several signal region candidates, for the gluino offshell stop model. For some of the regions, a shape fit of the effective mass or jet multiplicity distributions is performed. While it can provide additional benefit over simple cuts, the main reason for its use here was rather simply to avoid tuning cuts for each signal point. One can see indeed on the figure that for each mass, the significance obtained with an effective mass shape fit is rather close to the best of the significances computed with different choices of fixed cuts. As expected, at large neutralino mass signal regions based on ≥ 3 b-jets perform better than the ≥ 1 b-jet signal regions. There is not much difference in significance between the $\geq 3b$ selection requiring 6 hard jets and the one based on softer jets, possibly due to the fact that the mass spectra of the available grid points are not very compressed. One would probably see a larger difference for points lying on the diagonal $m_{\tilde{g}} = 2m_t + m_{\tilde{\chi}_1^0}$.

As only few signal samples have been generated, the projections Figure 22 (right) provides an estimate of the evolution of the sensitivity in a finer way, by simply using the kinematic distributions and yields obtained in a reference sample (gluino mass 1300 GeV, neutralino mass 100 GeV) weighted by the ratio of inclusive cross-sections between the mass to be extrapolated to, and the reference. It has been checked that the significance obtained from the next available sample (at a gluino mass of 1500 GeV) matches rather closely the extrapolated value.

One can conclude from these plots that at low neutralino mass and with such as low integrated luminosity, there is no sensitivity beyond the Run-1 exclusion. At higher neutralino mass however, the analysis would be sensitive to an area not yet excluded.

Sensitivity for the direct sbottom model

Figure 23 (left) shows the signal significance for several sbottom masses and a light neutralino. Here, the advantage of keeping a moderate $E_{\mathrm{T}}^{\mathrm{miss}}$ cut in the definition of the $\geq 1b$ signal region is clear. One can see that 2σ sensitivity up to masses of 650 GeV might be expected, which is quite a nice improvement over the Run-1 reach (450 GeV, although the expected limit was 50 GeV higher).

Sensitivity for the gluino model with RPV stop decay

The expected sensitivity for this model can be found on Fig. 23 (right). The most powerful signal region for this model is as expected the selection with at least 3 b-jets and 6 hard jets. One can notice however that the signal regions with moderate $E_{\mathrm{T}}^{\mathrm{miss}} > 100$ GeV cut are quite sensitive as well : the absence of neutralinos is compensated by the presence of boosted tops decaying leptonically.

Sensitivity for the gluino and squark models with 2-step decays

Finally, the performances of signal region definitions vetoing b-jets are probed with the gluino and squarks models with 2-step decays in gauge bosons. The signal significances for varied masses of gluino/squark or neutralino are provided on Fig 24. The signal region requiring 5 hard jets appears as the best compromise for both models, and in different regions of the phase space. For the gluino model, not much sensitivity beyong the Run-1 exclusion is gained at high gluino mass; at high neutralino mass, however, a significant non-excluded region up to neutralino masses of 650 GeV seems to be at reach. For the squark model, on the other hand, one will be able to probe a new region of the phase space at high squark mass, up to 900 GeV, which was not excluded in Run-1.

10 Conclusion

This note summarized the Run-2 preparation activities for the SUSY search using same-sing dileptons or three leptons, and the current status as of the end of April 2015 for the "SUSY walkthroughs" to be held on April 28th. These studies were conducted with DC14 Monte Carlo samples, and despite the known caveats in these samples (missing samples for some backgrounds, sub-optimal b-tagging, etc.), progress has been reported about object selection, trigger studies, signal region optimization, background estimation strategy and validation regions, as well as first sensitivity results including experimental systematics.

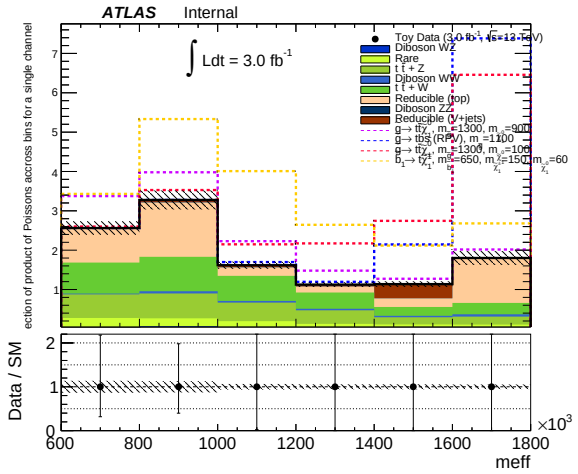

(a)$E_{\mathrm{T}}^{\mathrm{miss}} > 100$, ≥ 4 jets ($p_T > 50$)

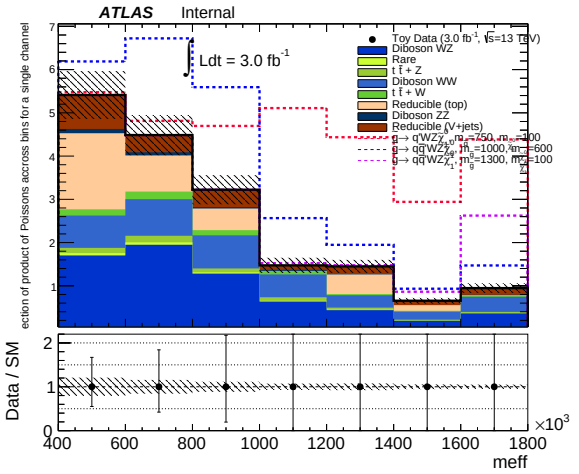

(b)$E_{\mathrm{T}}^{\mathrm{miss}} > 100$, ≥ 3 jets ($p_T > 40$)

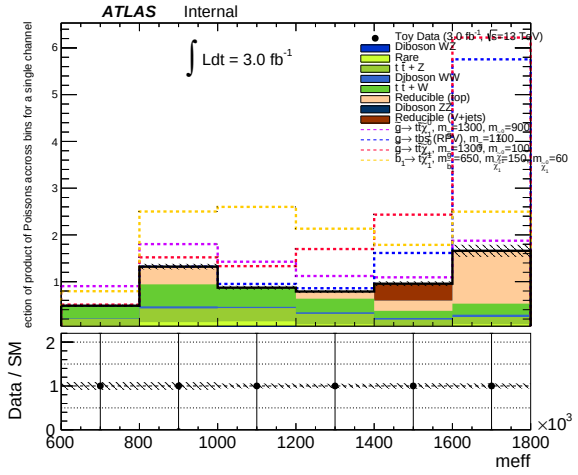

(c)$E_{\mathrm{T}}^{\mathrm{miss}} > 150$, ≥ 4 jets ($p_T > 50$

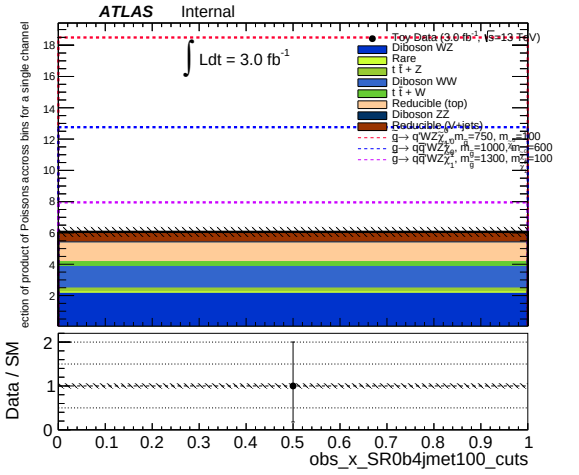

(d)$E_{\mathrm{T}}^{\mathrm{miss}} > 100$, ≥ 4 jets ($p_T > 40$)

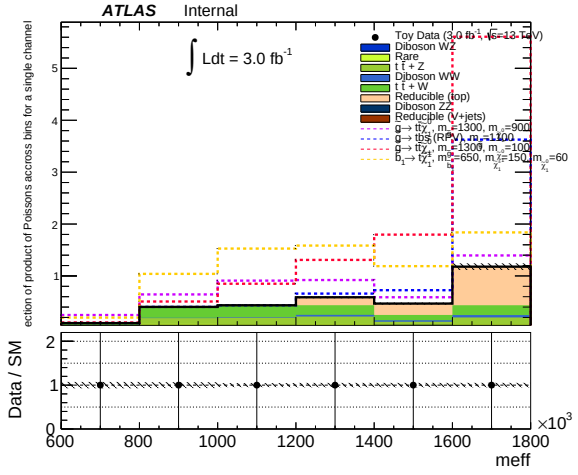

(e)$E_{\mathrm{T}}^{\mathrm{miss}} > 200$, ≥ 4 jets ($p_T > 50$

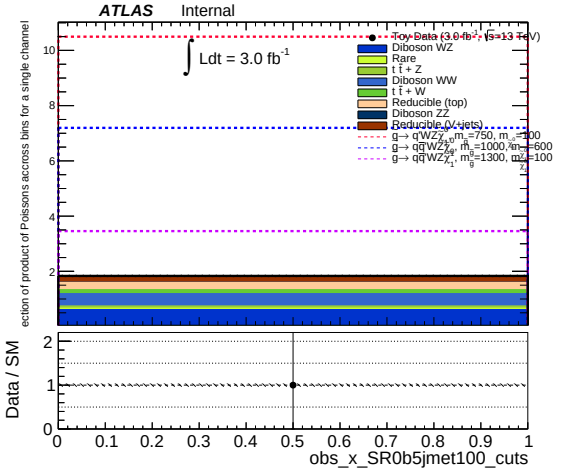

(f)$E_{\mathrm{T}}^{\mathrm{miss}} > 100$, ≥ 5 jets ($p_T > 40$)

Figure 21: Expected yields for Standard Model processes and a few characteristic signal scenarios, in selections with at least two same-sign leptons, at least one (left) or no b-jet (right), and the other cuts that define each of these signal region candidates.

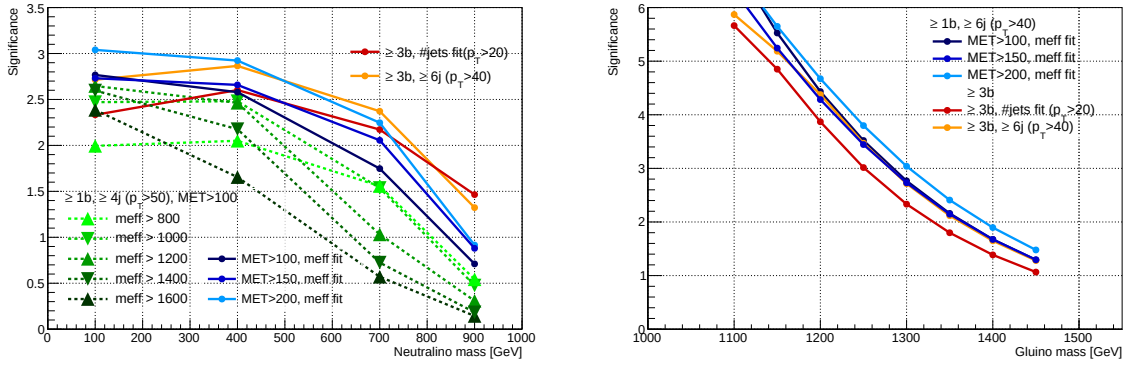

Figure 22: Expected signal significance for 3 fb^{-1} for the gluino offshell stop model $\tilde{g} \to t\bar{t}\tilde{\chi}_1^0$, varying the neutralino mass with a fixed gluino mass of 1300 GeV (left) or extrapolating to different gluino masses from a reference point with gluino and neutralino masses of 1300 and 100 GeV respectively (right).

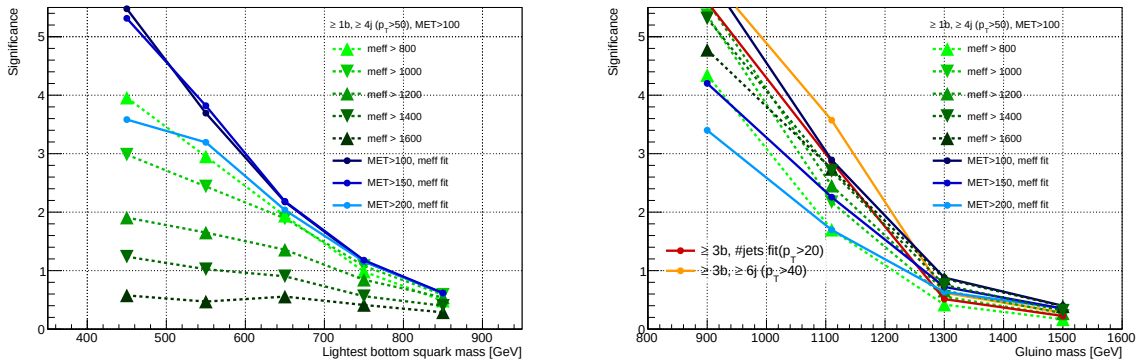

Figure 23: Expected signal significance for 3 fb^{-1} for the direct sbottom $\tilde{b}_1 \to t\tilde{\chi}_1^{\pm}$ (left) or the gluino RPV $\tilde{g} \to tbs$ (right) models. The neutralino mass is fixed to 100 GeV in the sbottom scenario.

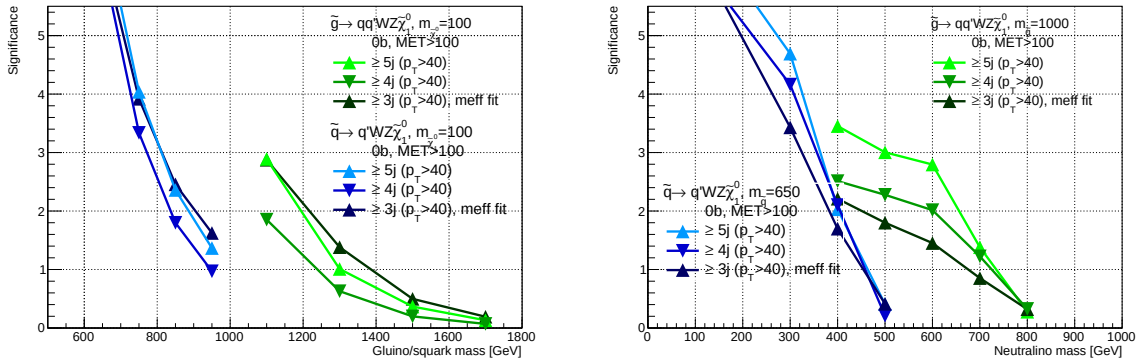

Figure 24: Expected signal significance for 3 fb^{-1} for the gluino and squark 2-step decay models $\tilde{g}/\tilde{q} \to q(q')WZ\tilde{\chi}_1^0$, varying the gluino or squark masses for a fixed neutralino mass of 100 GeV (left), or varying the neutralino mass for fixed gluino and squark masses of respectively 1000 and 650 GeV.

References

[1] H. Miyazawa, *Baryon Number Changing Currents*, Prog. Theor. Phys. **36 (6)** (1966) 1266.

[2] P. Ramond, *Dual Theory for Free Fermions*, Phys. Rev. **D 3** (1971) 2415.

[3] Y. A. Golfand and E. P. Likhtman, *Extension of the Algebra of Poincare Group Generators and Violation of p Invariance*, JETP Lett. **13** (1971) 323. [Pisma Zh.Eksp.Teor.Fiz.13:452-455,1971].

[4] A. Neveu and J. H. Schwarz, *Factorizable dual model of pions*, Nucl. Phys. **B 31** (1971) 86.

[5] A. Neveu and J. H. Schwarz, *Quark Model of Dual Pions*, Phys. Rev. **D 4** (1971) 1109.

[6] J. Gervais and B. Sakita, *Field theory interpretation of supergauges in dual models*, Nucl. Phys. **B 34** (1971) 632.

[7] D. V. Volkov and V. P. Akulov, *Is the Neutrino a Goldstone Particle?*, Phys. Lett. **B 46** (1973) 109.

[8] J. Wess and B. Zumino, *A Lagrangian Model Invariant Under Supergauge Transformations*, Phys. Lett. **B 49** (1974) 52.

[9] J. Wess and B. Zumino, *Supergauge Transformations in Four-Dimensions*, Nucl. Phys. **B 70** (1974) 39.

[10] P. Fayet, *Supersymmetry and Weak, Electromagnetic and Strong Interactions*, Phys. Lett. **B 64** (1976) 159.

[11] P. Fayet, *Spontaneously Broken Supersymmetric Theories of Weak, Electromagnetic and Strong Interactions*, Phys. Lett. **B 69** (1977) 489.

[12] G. R. Farrar and P. Fayet, *Phenomenology of the Production, Decay, and Detection of New Hadronic States Associated with Supersymmetry*, Phys. Lett. **B 76** (1978) 575.

[13] P. Fayet, *Relations Between the Masses of the Superpartners of Leptons and Quarks, the Goldstino Couplings and the Neutral Currents*, Phys. Lett. **B84** (1979) 416.

[14] ATLAS Collaboration, *Search for supersymmetry at $\sqrt{s}$=8 TeV in final states with jets and two same-sign leptons or three leptons with the ATLAS detector*, JHEP **1406** (2014) 035, arXiv:1404.2500 [hep-ex].

[15] J.-F. Arguin et al., *Search for strongly-produced superpartners in final states with two same-sign leptons or three leptons at $\sqrt{s}$ = 8 TeV*, Tech. Rep. ATL-COM-PHYS-2013-887, CERN, Geneva, Jun, 2013. https://cds.cern.ch/record/1558979.

[16] G. Herten, M. Vranjes Milosavljevic, J.-F. Arguin, N. Makovec, and B. Petersen, *Summary of the Searches for Inclusive Squarks and Gluinos with Run I LHC data at ATLAS*, Tech. Rep. ATL-COM-PHYS-2014-929, CERN, Geneva, Jul, 2014. https://cds.cern.ch/record/1746381.

[17] E. Nikolidakis and C. Smith, *Minimal Flavor Violation, Seesaw, and R-parity*, Phys.Rev. **D77** (2008) 015021, arXiv:0710.3129 [hep-ph].

[18] C. Csaki, Y. Grossman, and B. Heidenreich, *MFV SUSY: A Natural Theory for R-Parity Violation*, Phys.Rev. **D85** (2012) 095009, arXiv:1111.1239 [hep-ph].

[19] G. Durieux and C. Smith, *The same-sign top signature of R-parity violation*, JHEP **1310** (2013) 068, arXiv:1307.1355 [hep-ph].

[20] G. Durieux, J.-M. Gerard, F. Maltoni, and C. Smith, *Three-generation baryon and lepton number violation at the LHC*, Phys.Lett. **B721** (2013) 82–85, arXiv:1210.6598 [hep-ph].

[21] ATLAS Collaboration, G. Aad et al., *Search for supersymmetry at $\sqrt{s}$=8 TeV in final states with jets and two same-sign leptons or three leptons with the ATLAS detector*, JHEP **1406** (2014) 035, arXiv:1404.2500 [hep-ex].

[22] CMS Collaboration, S. Chatrchyan et al., *Search for new physics in events with same-sign dileptons and jets in pp collisions at $\sqrt{s}$ = 8 TeV*, JHEP **1401** (2014) 163, arXiv:1311.6736.

[23] ATLAS Collaboration, G. Aad et al., *Search for new phenomena in final states with large jet multiplicities and missing transverse momentum at $\sqrt{s}$=8 TeV proton-proton collisions using the ATLAS experiment*, JHEP **1310** (2013) 130, arXiv:1308.1841 [hep-ex].

[24] "DC14 Data and MC Sample Information." https://twiki.cern.ch/twiki/bin/view/AtlasProtected/DC14DataMCSampleInfo.

[25] G. Corcella et al., *HERWIG 6: An Event generator for hadron emission reactions with interfering gluons (including supersymmetric processes)*, JHEP **0101** (2001) 010, arXiv:hep-ph/0011363 [hep-ph].

[26] S. Gieseke, C. Rohr, and A. Siodmok, *Colour reconnections in Herwig++*, Eur.Phys.J. **C72** (2012) 2225, arXiv:1206.0041 [hep-ph].

[27] J. Alwall et al., *MadGraph/MadEvent v4: The New Web Generation*, JHEP **0709** (2007) 028, arXiv:0706.2334 [hep-ph].

[28] T. Sjostrand, S. Mrenna, and P. Z. Skands, *PYTHIA 6.4 Physics and Manual*, JHEP **0605** (2006) 026, arXiv:hep-ph/0603175 [hep-ph].

[29] ATLAS Collaboration, *ATLAS tunes of PYTHIA6 and Pythia8 for MC11*, ATL-PHYS-PUB-2011-009 (2011), https://cds.cern.ch/record/1363300.

[30] ATLAS Collaboration, *Further ATLAS tunes of PYTHIA6 and Pythia 8,*. http://cds.cern.ch/record/1400677.

[31] J. Pumplin et al., *New generation of parton distributions with uncertainties from global QCD analysis*, JHEP **0207** (2002) 012, arXiv:hep-ph/0201195 [hep-ph].

[32] C. Borschensky, M. Krmer, A. Kulesza, M. Mangano, S. Padhi, et al., *Squark and gluino production cross sections in pp collisions at $\sqrt{s}$ = 13, 14, 33 and 100 TeV*, Eur.Phys.J. **C74** no. 12, (2014) 3174, arXiv:1407.5066 [hep-ph].

[33] P. Nason, *A New method for combining NLO QCD with shower Monte Carlo algorithms*, JHEP **0411** (2004) 040, arXiv:hep-ph/0409146 [hep-ph].

[34] S. Frixione, P. Nason, and C. Oleari, *Matching NLO QCD computations with Parton Shower simulations: the POWHEG method*, JHEP **0711** (2007) 070, arXiv:0709.2092 [hep-ph].

[35] S. Alioli, P. Nason, C. Oleari, and E. Re, *A general framework for implementing NLO calculations in shower Monte Carlo programs: the POWHEG BOX*, JHEP **1006** (2010) 043, arXiv:1002.2581 [hep-ph].

[36] H.-L. Lai et al., *New parton distributions for collider physics*, Phys.Rev. **D82** (2010) 074024, arXiv:1007.2241 [hep-ph].

[37] P. Z. Skands, *Tuning Monte Carlo Generators: The Perugia Tunes*, Phys.Rev. **D82** (2010) 074018, arXiv:1005.3457 [hep-ph].

[38] M. Czakon and A. Mitov, *Top++: A Program for the Calculation of the Top-Pair Cross-Section at Hadron Colliders*, Comput.Phys.Commun. **185** (2014) 2930, arXiv:1112.5675 [hep-ph].

[39] T. Gleisberg et al., *Event generation with SHERPA 1.1*, **02** (2009) 007, arXiv:0811.4622.

[40] S. Catani, L. Cieri, G. Ferrera, D. de Florian, and M. Grazzini, *Vector boson production at hadron colliders: a fully exclusive QCD calculation at NNLO*, Phys.Rev.Lett. **103** (2009) 082001, arXiv:0903.2120 [hep-ph].

[41] J. M. Campbell and R. K. Ellis, $t\bar{t}W^{+-}$ *production and decay at NLO*, JHEP **1207** (2012) 052, arXiv:1204.5678 [hep-ph].

[42] A. Kardos, Z. Trocsanyi, and C. Papadopoulos, *Top quark pair production in association with a Z-boson at NLO accuracy*, Phys.Rev. **D85** (2012) 054015, arXiv:1111.0610 [hep-ph].

[43] N. Kauer, *Interference effects for $H \to WW/ZZ \to \ell\bar{\nu}_\ell\bar{\ell}\nu_\ell$ searches in gluon fusion at the LHC*, JHEP **1312** (2013) 082, arXiv:1310.7011 [hep-ph].

[44] N. Kauer and G. Passarino, *Inadequacy of zero-width approximation for a light Higgs boson signal*, JHEP **1208** (2012) 116, arXiv:1206.4803 [hep-ph].

[45] ATLAS Collaboration, G. Aad et al., *The ATLAS Simulation Infrastructure*, Eur.Phys.J. **C70** (2010) 823–874, arXiv:1005.4568 [physics.ins-det].

[46] GEANT4 Collaboration, S. Agostinelli et al., *GEANT4: A Simulation toolkit*, Nucl.Instrum.Meth. **A506** (2003) 250–303.

[47] T. Sjostrand, S. Mrenna, and P. Z. Skands, *A Brief Introduction to PYTHIA 8.1*, Comput.Phys.Commun. **178** (2008) 852–867, arXiv:0710.3820 [hep-ph].

[48] A. Sherstnev and R. Thorne, *Parton Distributions for LO Generators*, Eur.Phys.J. **C55** (2008) 553–575, arXiv:0711.2473 [hep-ph].

[49] M. Cacciari, G. P. Salam, and G. Soyez, *The Anti-k(t) jet clustering algorithm*, JHEP **0804** (2008) 063, arXiv:0802.1189 [hep-ph].

[50] ATLAS Collaboration, *Electron efficiency measurements with the ATLAS detector using the 2012 LHC proton–proton collision data*, ATLAS-CONF-2014-032, http://cdsweb.cern.ch/record/1706245.

[51] D. Adams and others, *Recommendations of the Physics Objects and Analysis Harmonisation Study Groups 2014*, Tech. Rep. ATL-PHYS-INT-2014-018, CERN, Geneva, Jul, 2014. https://cds.cern.ch/record/1743654.

[52] "JetEtmiss Group, How to clean jets." https://twiki.cern.ch/twiki/bin/viewauth/AtlasProtected/HowToCleanJets2011.

[53] "InDetTrackingPerformanceGuidelines, Pre-recommendations for Run-2." https://twiki.cern.ch/twiki/bin/view/AtlasProtected/InDetTrackingPerformanceGuidelines#Vertexing.

[54] J. Boyd et al., *Studies of events with three leptons and three b-tagged jets observed in the full 2012 ATLAS dataset*, Tech. Rep. ATL-PHYS-INT-2014-006, CERN, Geneva, May, 2014. https://cds.cern.ch/record/1698061.

[55] J. Maurer, O. A. Ducu, and T. Gillam, *Extension of the $\tilde{g} \to t\bar{t}\tilde{\chi}_1^0$ simplified model to include decays with off-shell tops, and exclusion limits from the SS/3 leptons + jets analysis*, Tech. Rep. ATL-COM-PHYS-2014-1422, CERN, Geneva, Oct, 2014. https://cds.cern.ch/record/1966089. One of the supporting documents for the inclusive squark/gluino summary paper.

[56] "CMS SUSY Summary Plots 8 TeV." https://twiki.cern.ch/twiki/pub/CMSPublic/SUSYSMSSummaryPlots8TeV/T1tttt_ICHEP2014.pdf.

[57] R. Bruneliere, M. DOnofrio, Y. Ming, J. Poveda, T. Sarangi, and S. Wu, *Search for gluinos with two same sign leptons, jets and missing transverse momentum at $\sqrt{s}$=7 TeV (supporting INT note)*, Tech. Rep. ATL-PHYS-INT-2012-042, CERN, Geneva, Apr, 2012. https://cds.cern.ch/record/1442562.

[58] "T. Gillam, PhD thesis chapter 4 on matrix method and beyond." https://bytebucket.org/tpgillam/bayesmm/raw/7e941bec4067b092c24ac2e23815cd08090d6d2c/docs/theory_extract.pdf.

[59] T. P. S. Gillam and C. G. Lester, *Improving estimates of the number of 'fake' leptons and other mis-reconstructed objects in hadron collider events: BoB's your UNCLE*, JHEP **1411** (2014) 031, arXiv:1407.5624 [hep-ph].

[60] ATLAS Collaboration, G. Aad et al., *Search for supersymmetry at $\sqrt{s}$=8 TeV in final states with jets and two same-sign leptons or three leptons with the ATLAS detector*, JHEP **1406** (2014) 035, arXiv:1404.2500 [hep-ex].

[61] "Flavour Tagging, Calibration Data Interface, Eigenvector method." https://twiki.cern.ch/twiki/bin/view/AtlasProtected/BTaggingCalibrationDataInterface#Eigenvector_variation_method.

[62] M. Garzelli, A. Kardos, C. Papadopoulos, and Z. Trocsanyi, *$t\bar{t}W^{\pm}$ and $t\bar{t}Z$ Hadroproduction at NLO accuracy in QCD with Parton Shower and Hadronization effects*, JHEP **11** (2012) 056, arXiv:1208.2665 [hep-ph].

[63] J. M. Campbell, R. K. Ellis, and C. Williams, *Vector boson pair production at the LHC*, JHEP **07** (2011) 018, arXiv:1105.0020 [hep-ph].

[64] M. Baak, G. Besjes, D. Cte, A. Koutsman, J. Lorenz, et al., *HistFitter software framework for statistical data analysis*, Eur.Phys.J. **C75** no. 4, (2015) 153, arXiv:1410.1280 [hep-ex].

A Details on the isolation optimization

For optimizing the isolation requirements in the analysis, and following the conclusions in Section 4.2.3 about which of the available isolation variables to use, the following benchmark isolation cuts are defined for electrons:

- `ELE Lose`: MediumLH, ptvarcone20/p_{T}<0.10, topoetcone20/p_{T}<0.10
- `ELE Medium`: MediumLH, ptvarcone20/p_{T}<0.06, topoetcone20/p_{T}<0.06
- `ELE Tight`: for p_{T}<60 GeV: MediumLH, ptvarcone20/p_{T}<0.06, topoetcone20/p_{T}<0.06; for p_{T}>60 GeV: TightLH, ptvarcone20/p_{T}<0.06, topoetcone20/p_{T}<0.06
- `ELE Very Tight`: TightLH, ptvarcone20/p_{T}<0.06, topoetcone20/p_{T}<0.06
- `ELE Very Very Tight`: TightLH, ptvarcone20/p_{T}<0.04, topoetcone20/p_{T}<0.04

Similarly, the following isolation cuts are defined for muons:

- `MUO Loose`: for p_{T}<40 GeV: ptvarcone30/p_{T}<0.12; for p_{T}>40 GeV: ptvarcone30/p_{T}<0.06
- `MUO Tight`: ptvarcone30/p_{T}<0.06
- `MUO Very Tight`: ptvarcone30/p_{T}<0.04

For each combination of the electron and muon isolation cuts, the signal significance is computed using RooStats::NumberCountingUtils::BinomialExpZ, assuming 30% background uncertainty and a luminosity of 3 fb^{-1}. For simplicity, only $t\bar{t}$ and $t\bar{t}+V$ is considered for the background. Four different signal points are used, covering mass spectra with large and also with small mass differences.

Table 20 shows the results obtained in a loose event selection, requiring either same-sign dilepton with 4 jets (p_{T}>40 GeV) and $E_{\mathrm{T}}^{\mathrm{miss}} > 100$ GeV, or ≥3 leptons, ≥3 b-jets ($p_{\mathrm{T}} > 40$ GeV). No m_{eff} requirement is applied. These results point to a preference for tight isolation cuts, with `ELE Very Very Tight` giving the maximum significance in the four signal models considered.

Since the signal and background composition can be different after the full signal region selection is applied, Table 21 shows the same numbers after applying the event selection requirements in Run-1 SR1b: same-sign dilepton, 3 jets (p_{T}>40 GeV), ≥1 b-jets, $E_{\mathrm{T}}^{\mathrm{miss}} > 150$ GeV and $m_{\mathrm{T}} > 100$ GeV. In this case, `MUO Tight` is preferred, with no strong preference between `ELE Very Very Tight` and `ELE Very Tight`.

As outcome of these studies, `MUO Tight` and `ELE Very Tight` was selected to be used for lepton isolation in the analysis.

Table 20: Number of background and signal events after the selection explained in the text normalized to 3fb^{-1} and corresponding signal significance for four signal models and different scenarios for the lepton isolation. The largest significance values is highlighted in bold.

			SMGG2WWZZ 1000_700_400		Gtt G1300_L100		SMGG2WWZZ 1000_900_800		Gtt G1300_L900	
ele	mu	BKG	n_{sig}	Signif	n_{sig}	Signif	n_{sig}	Signif	n_{sig}	Signif
L	L	27.04	16.76	1.319	5.09	0.307	2.48	0.052	2.63	0.068
M	L	24.22	16.11	1.392	4.91	0.335	2.19	0.045	2.46	0.074
T	L	23.45	15.94	1.415	4.81	0.338	2.15	0.047	2.41	0.075
VT	L	23.09	15.94	1.433	4.75	0.338	2.07	0.040	2.34	0.071
VVT	L	21.33	14.97	1.437	4.56	0.351	2.07	**0.056**	2.25	0.078
L	T	25.99	16.60	1.351	5.03	0.317	2.27	0.039	2.55	0.068
M	T	23.17	16.11	1.444	4.84	0.347	1.99	0.030	2.38	0.074
T	T	22.40	15.94	1.469	4.73	0.349	1.95	0.032	2.33	0.077
VT	T	22.04	15.94	1.489	4.67	0.350	1.87	0.025	2.27	0.073
VVT	T	19.85	14.97	1.522	4.48	0.373	1.87	0.045	2.18	**0.086**
L	VT	27.67	16.43	1.268	4.96	0.285	2.23	0.023	2.50	0.050
M	VT	24.13	15.94	1.382	4.77	0.322	1.95	0.018	2.32	0.059
T	VT	22.23	15.78	1.463	4.66	0.345	1.91	0.028	2.28	0.072
VT	VT	21.20	15.78	1.521	4.60	0.359	1.83	0.027	2.21	0.074
VVT	VT	19.20	14.81	**1.546**	4.42	**0.380**	1.83	0.046	2.12	0.085

Table 21: Number of background and signal events in the Run-1 SR1b normalized to 3fb^{-1} and corresponding signal significance for two signal models and different scenarios for the lepton isolation. The largest significance values is highlighted in bold.

			SMGG2WWZZ 1000_700_400		Gtt G1300_L100	
ele	mu	BKG	n_{sig}	Signif	n_{sig}	Signif
L	L	11.82	4.68	0.671	1.63	0.114
M	L	9.96	4.49	0.740	1.57	0.142
T	L	9.07	4.29	0.759	1.51	0.149
VT	L	8.97	4.29	0.766	1.49	0.149
VVT	L	8.37	3.90	0.724	1.42	0.147
L	T	10.90	4.68	0.721	1.61	0.130
M	T	9.04	4.49	0.801	1.56	0.162
T	T	8.15	4.29	0.827	1.49	0.171
VT	T	8.06	4.29	**0.834**	1.48	0.171
VVT	T	7.35	3.90	0.803	1.41	**0.174**
L	VT	13.46	4.49	0.565	1.57	0.076
M	VT	10.69	4.29	0.660	1.52	0.114
T	VT	9.01	4.10	0.723	1.45	0.138
VT	VT	8.24	4.10	0.777	1.44	0.155
VVT	VT	7.16	3.71	0.772	1.37	0.171

B Trigger efficiencies

Studies on performance and efficiency have been done for several single-lepton, dilepton and $E_{\mathrm{T}}^{\mathrm{miss}}$ triggers Results are shown here.

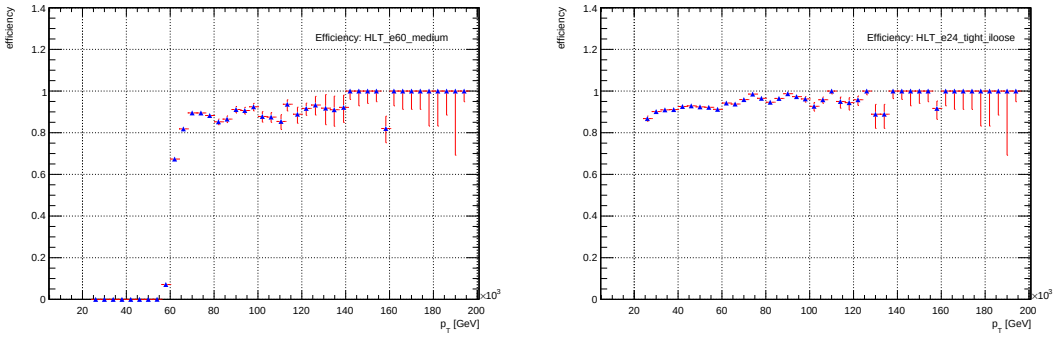

Figure 25: Trigger efficiencies for `HLT_e60_medium` and `HLT_e24_tight_iloose` versus p_{T} of the leading electron.

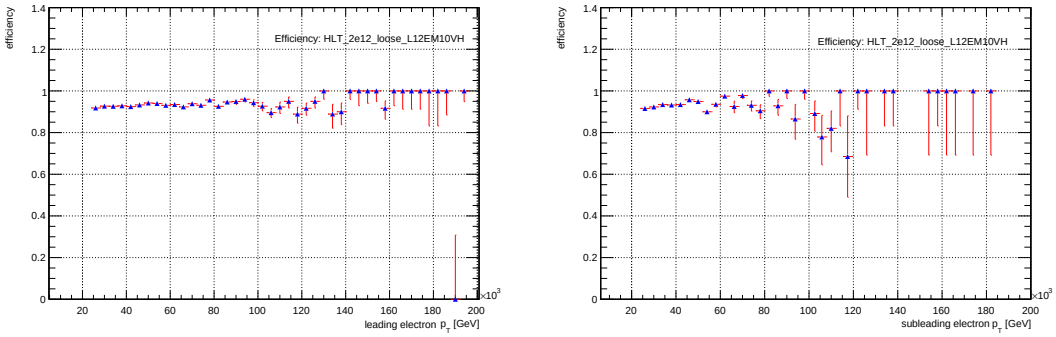

Figure 26: Trigger efficiency for `HLT_2e12_loose_L12EM10VH` plotted against p_{T} of the leading electron (left-hand side) and the subleading electron (right-hand side).

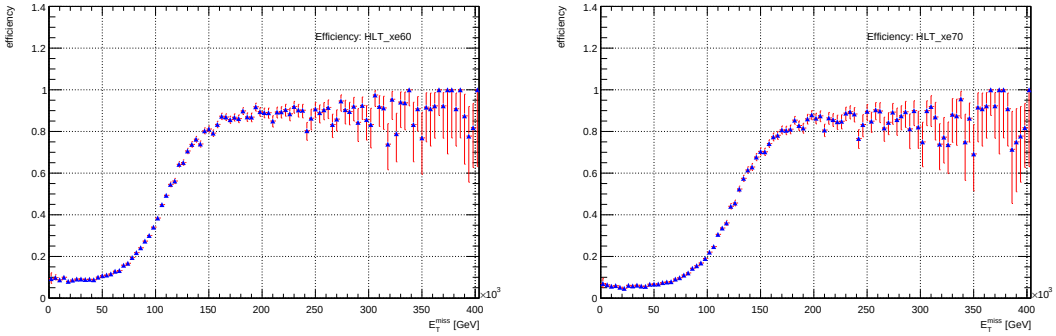

Figure 27: Trigger efficiencies for `HLT_xe60` and `HLT_xe70` versus the missing transverse energy.

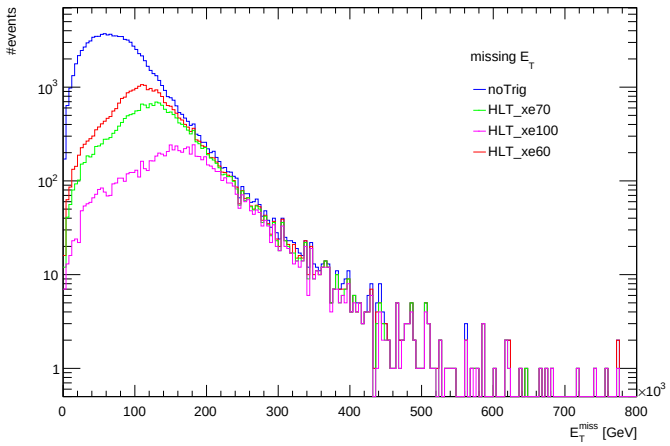

Figure 28: Events selected by different $E_{\mathrm{T}}^{\mathrm{miss}}$ triggers and without any trigger selection versus the missing transverse energy.

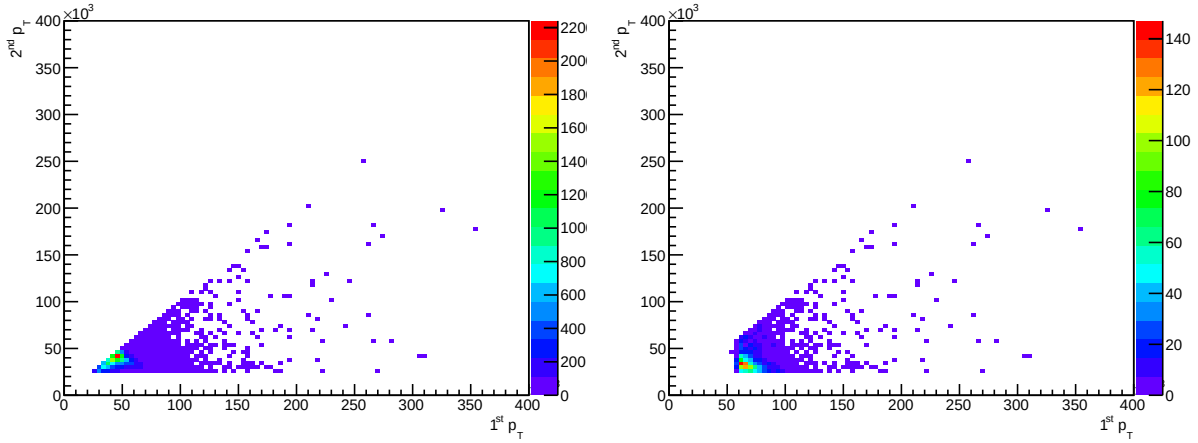

Figure 29: Leading electron versus subleading electron for events selected by `HLT_e20_medium` (left-hand side) and by `HLT_e60_medium` (right-hand side).

C Generated Samples for the Above the Diagonal Study

The samples for the above the diagonal study of Seciton 6.3 were generated at 8 TeV with detector simulation and reconstruction. The generated samples with the process id and the cross section for the different grid points considered in this study are shown below:

Table 22: Processes used in the current study with a derivation tag p1328.

Sample name	Process Id	Generated Events	Cross Section [fb]
G550_T2500_L285	204150	80000	1209.9
G650_T2500_L385	204151	80000	356.57
G700_T2500_L410	204153	80000	201.10
G750_T2500_L435	204154	80000	116.57
G750_T2500_L485	204155	80000	117.67
G800_T2500_L460	204156	80000	68.990
G800_T2500_L510	204157	80000	69.458
G850_T2500_L535	204158	80000	41.822
G850_T2500_L585	204159	80000	42.086
G900_T2500_L560	204160	80000	25.549
G900_T2500_L610	204161	80000	25.727
G950_T2500_L635	204162	80000	15.929
G950_T2500_L685	204163	80000	15.996
G1000_T2500_L660	204164	80000	9.9704
G1000_T2500_L710	204165	80000	1.0014
G1050_T2500_L735	204166	80000	6.3245
G1050_T2500_L785	204167	80000	6.3498
G1100_T2500_L760	204168	80000	4.0353
G1100_T2500_L810	204169	80000	4.0433
G1150_T2500_L885	204170	80000	2.6057
G1250_T2500_L985	204171	80000	1.0911